

**Indirect Structural Health Monitoring of Bridges:  
Mathematical Models and Laboratory Experiments**

**Fernando Alejandro Cerda Carrizo**

**A DISSERTATION  
SUBMITTED IN PARTIAL FULFILLMENT  
OF THE REQUIREMENTS  
FOR THE DEGREE OF  
Doctor of Philosophy  
In  
Civil and Environmental Engineering  
Carnegie Mellon University  
Pittsburgh, PA**

**September, 20, 2012**

## **Abstract**

An indirect approach is presented for determining the condition of model bridges based on data collected from instrumented vehicles that traverse the structure. The underlying idea behind this study is that vehicles traveling across bridges pick up dynamic characteristics of the structure which allow one to identify changes in the bridge condition. By using a fleet of vehicles and using a classification algorithm to discriminate between environmental factors and structural health, it would then become possible to examine efficiently the condition of a large stock of bridges using a smaller stock of vehicles. This research studies the indirect approach by means of mathematical and experimental models.

The feasibility of the indirect structural health monitoring (SHM) approach was first assessed by means of 1D and 3D mathematical models. A multiresolution classification algorithm was employed to detect the existence, severity, and location of changes in the bridge structure. Several classification experiments were run. The detection experiments, that is, classifying among “Damaged” of “Undamaged”, obtained on average 95% accuracy for the 1D models and 90% for the 3D models. It was observed a little dependence of the parameters of the moving vehicle. The damaged labels were defined as stiffness reduction of structural members

The detection capability of the approach was then tested in a laboratory setup for three different types of damage scenarios: changes in the support conditions (rotational restraint), additional damping, and an added mass at the midspan. A set of features based on discriminant frequencies was used in conjunction with a support vector machine classifier on data measured from a passing vehicle at the wheel and suspension levels, and directly from the bridge structure for comparison.

New sets of experiments were performed on the laboratory setup to explore the effects of variations of the vehicle-bridge interaction, the effect of roadway roughness and temperature

gradients. The experiments were also augmented by experimenting with a second model bridge, and including vehicle variations and damage at different locations.

Across all the different variations of vehicle mass, vehicle speed, roadway roughness and ambient temperature, it could be concluded that the indirect data obtained from sensors at the wheel level or at the suspension level, in general, performed just as well or better than the data from sensors on the bridge in terms of the classification accuracy obtained with the signal processing and classification methods used.

## Dedication

To my wife,  
and  
To my parents.

## Acknowledgements

I wish to express my gratitude for the extraordinary experience at Carnegie Mellon University while pursuing the Doctoral Degree. To my advisors in the Civil and Environmental Engineering Department (CEE), James Garrett and Jacobo Bielak, for their guidance, support and encouragement. To the committee members: Jelena Kovačević for her engagement and allowing this to be a truly interdisciplinary experience; Piervincenzo Rizzo, for all his inputs, advice and engagement. To all of them I give my deepest appreciation and gratitude.

I also would like to acknowledge the support of the different funding sources through the course of this work: Carnegie Mellon University through a Dean's fellowship; The National Science Foundation (Award No. CMMI1130616); Traffic 21 initiative at Carnegie Mellon University; Fulbright-MECESUP; and Universidad de Concepción.

Also the Pennsylvania Department of Transportation in the person of Wallace Stadfeld for his support providing practical knowledge about the current bridge inspection activities.

This thesis was also made possible through the contribution of several students: Graduate students from the Center for Bioimage informatics; Ramu Bhagavatula, Michael McCann and Siheng Chen; two visiting students; José Alberto Barrera and Eduard Romero; Undergraduate students from the Civil and Environmental Engineering Department; Ranny Zhao, Zhe Zhuang, Timothy Pianka and Madelyn Gioffre, who participated in the construction of the experimental setup and running of the experiments.

I would also like to acknowledge the staff members of the Civil and Environmental Engineering Department who were always very diligent and kind on their different roles: Ron Ripper, Maxine Leffard, Anne Fowler, Andrea Francioni Rooney and Cornelia Moore.

To all the friends I made and people I met along this journey; colleagues from CEE, staff from the Robotics Institute, friends from the Chilean community. I greatly appreciate your advice, companionship and support.

# Table of Contents

Abstract.....	II
Dedication .....	IV
Acknowledgements.....	V
List of Illustrations .....	IX
List of Tables.....	XIII
1 Chapter 1: Introduction .....	1
1.1 Problem statement .....	1
1.2 Proposed solution to the problem: an indirect approach .....	3
1.3 Hypothesis and research questions .....	7
1.4 Overview of the Research Approach.....	9
1.5 Dissertation overview .....	11
2 Chapter 2: Indirect SHM for Bridges by Image Classification of Transient Response: 1D and 3D Mathematical Models .....	12
2.1 Introduction.....	12
2.2 Experimental Approach .....	13
2.3 Multiresolution Classification .....	14
2.4 1D Model, Experiments and Results .....	19
2.4.1 1D Model Experimental Results .....	24
2.5 3D Numerical Model Description, Experiments and Results .....	27
2.5.1 3D Model Experimental Results for Setting 1.....	28
2.5.2 3D Model Experimental Results for Setting 2.....	34

2.6	Discussion .....	39
3	Chapter 3: Indirect structural health monitoring of a simplified laboratory-scale bridge model	42
3.1	Introduction.....	42
3.2	Experimental Setup and Protocol .....	44
3.2.1	Details of the Bridge and Vehicle Models.....	46
3.2.2	Motion Control and Data Acquisition Equipment.....	48
3.2.3	Protocol .....	48
3.3	Signal Analysis and Classification .....	50
3.3.1	Preprocessing .....	51
3.3.2	Feature extraction .....	52
3.3.3	Classification .....	56
3.4	Classification Results .....	57
3.5	Discussion .....	62
4	Chapter 4: Effect of temperature and boundary condition on the indirect health monitoring of a bridge model .....	64
4.1	Introduction.....	64
4.2	Experimental setup and protocol .....	65
4.3	Classification Experiments and Results .....	73
4.3.1	Effect on Classification Accuracy of Variations of Vehicles, Bridges, Vehicle Speeds and Severity of Change .....	73
4.3.2	Effect of Roughness and Damage Location.....	80
4.3.3	The Effect of Different Locations of Damage .....	82

4.3.4	Effect of Temperature gradient scenarios. ....	85
4.4	Discussion .....	87
5	Chapter 5: Summary, Contributions and Future Work.....	90
5.1	Summary .....	90
5.2	Contributions of this research .....	92
5.3	Future work.....	99
6	References .....	102



# List of Illustrations

Figure 1: Direct and indirect SHM different in terms of sensor location.....	4
Figure 2: Acceleration response of an oscillator compiled in an image representation constructed from 100 scaled response signals at a particular bridge condition.....	14
Figure 3: Multiresolution classification system for Damaged and Undamaged labels.....	15
Figure 4: Single level multiresolution decomposition. (a) Original image (Level 0) is split into (b)- (e) four subbands (Level 1). .....	17
Figure 5: Oscillator-beam interaction model. ....	20
Figure 6: Graphic experiment definition for 1D data. ....	21
Figure 7: Vehicle model degrees of freedom, parameter notation and corresponding values....	27
Figure 8: 3D Bridge model with corresponding beam groups for simulation Setting 1. ....	29
Figure 9: Graphic representation of experiment definition for 3D data Setting 1. ....	30
Figure 10: Images of vehicle response at center of gravity in 3D Model (a) Undamaged scenario, (b) 20% inertia reduction at G2, (c) 50% Inertia reduction at G2.....	33
Figure 11: 3D Bridge model with corresponding beam groups for simulation Setting 2. ....	35
Figure 12: Graphic representation of experiment definition for simulation Setting 2. ....	36
Figure 13: Experimental setup. a) General lateral view. b) Bridge bottom view. c) Bridge cross section.....	46
Figure 14: Experimental vehicle CAD drawings. (a) Parametric view. (b) Top view. (c) Vehicle picture. ....	48
Figure 15: Detail 1 – Roller support - Rotational restraint (a) technical drawing and (b) picture.	49
Figure 16: General classification system. ....	51
Figure 17: Time-domain signals.....	52
Figure 18: Discrete Fourier transform of the signal.....	53
Figure 19: Mean energy distribution (normalized to unit energy).....	53

Figure 20: Discriminant power (normalized to unit discriminant power).....	54
Figure 21: Summary of feature extraction process. ....	55
Figure 22: Clustering of two scenarios.....	56
Figure 23: Classification accuracy results (a) Average by damage types. (b) Average by speeds. .....	58
Figure 24: Classification results for rotational restraint scenarios (a,d) Bridge sensors, (b,e) Suspension sensors (c,f) Wheel sensors. ....	59
Figure 25: Classification results for damping increase scenarios. (a,d) Bridge sensors, (b,e) Suspension sensors (c,f) Wheel sensors. ....	60
Figure 26: Classification results for concentrated mass scenarios. (a,d) Bridge sensors, (b,e) Suspension sensors (c,f) Wheel sensors. ....	61
Figure 27: Experimental setup. a) General angle photo of experimental setup, b) Vehicle picture. W.A.V. is the wheel level on the A axle, and S.A.V is the suspension level on the A axle. W.B.V. and S.B.V. are the corresponding wheel and suspension levels on the B axle. .	66
Figure 28: Introduced modifications to the bridge structure. (a) Rotational restraints (b) Additional damping and (c) Roadway roughness profile built on top of guide rail (d) Measured additional roughness (e) Scheme for Heat Sheet locations. A.and B are reference points for the forward travelling direction. ....	68
Figure 29: Bridge longitudinal view; normal and Infrared images. ....	71
Figure 30: Bridge 1: (a-c) Damage detection accuracy for different vehicles averaged across different speeds and severity scenarios of the same damage type: (a) Rotational Restraint; (b) Damping Increase and (c) Mass Increase. (d-f) Damage detection accuracy for different speeds averaged across the different damage scenarios of the same vehicle: (d) Vehicle 1; (e) Vehicle 2 and (f) Vehicle 3.....	75
Figure 31: Bridge 2: (a-c) Damage detection accuracy for different vehicles averaged across different speeds and severity scenario of the same type: (a) Rotational Restraint; (b)	

Damping Increase; and (c) Mass Increase. (d-f) Damage detection accuracy for different speeds averaged across the different damage scenarios: (a) Vehicle 1; (b) Vehicle 2; and (c) Vehicle 3. ....	76
Figure 32 Bridge 1: (a-c) Damage severity classification accuracy for different vehicles averaged across different speeds and severity scenario of the same damage type: (a) Rotational Restraint; (b) Damping Increase; and (c) Mass Increase. (d-f) Damage severity classification accuracy for different speeds averaged across the different damage scenarios of the same vehicle: (d) Vehicle 1; (e) Vehicle 2; and (f) Vehicle 3. ....	78
Figure 33: Bridge 2: (a-c) Damage severity classification accuracy for different vehicles averaged across different speeds and severity scenario of the same damage type: (a) Rotational Restraint; (b) Damping Increase; and (c) Mass Increase. (d-f) Damage severity classification accuracy for different speeds averaged across the different damage scenarios of the same vehicle: (d) Vehicle 1; (e) Vehicle 2; and (f) Vehicle 3. .	79
Figure 34: Rotational restraints scenarios cluster analysis. Vehicle 1, Bridge 1, Speed 1 m/s, R1 (Roughness from accidental imperfections).....	80
Figure 35: Damage detection comparison among bridges with two different roughness profiles. (a-d) two Rotational Restraints scenarios: (a-b) Bridge 1 and(c-d) Bridge 2; (e-h) two Additional Damping scenarios: (e-f) Bridge 1 and (g-h) Bridge 2; (i-l) two Additional Mass scenarios: (i-j) Bridge 1 and (k-l) Bridge 2.....	81
Figure 36: Damage detection comparison among scenarios with different damage locations: Bridge 1 (a,b,e,f,i,j), Bridge 2 (c,d,g,h,k,l).....	83
Figure 37: Location classification comparison among scenarios with different damage location: (a) Bridge 1, (b) Bridge 2.....	85
Figure 38: Classification accuracy of damage scenarios for specific temperature gradient scenario.....	86

Figure 39: Classification accuracy of damage scenarios regardless temperature scenario for training and testing.....	87
--	----

## List of Tables

Table 1: Damage cases. ....	20
Table 2: 1D classification experiment definition. ....	24
Table 3: 1D Model, 2-class damage detection classification accuracy [%].....	25
Table 4: 1D Model, 5-class damage severity classification accuracy [%]. ....	25
Table 5: 1D model, Experiments 3 to 5 damage classification accuracy [%].....	26
Table 6: 3D setting 1 classification experiment definition. ....	31
Table 7: 3D model, 2-class detection of damage classification accuracy results, Setting 1. G1-8 group of beams where damage was inflicted. ....	31
Table 8: 3D model, 5-class severity of damage classification accuracy [%], Setting 1.....	32
Table 9: 3D model, 5-class severity of damage classification accuracy [%], Setting 1.....	33
Table 10: Vehicle properties for 3D experimental Setting 2.....	34
Table 11: Classification Experiment 1 classification accuracy [%], simulation Setting 2. ....	37
Table 12: Classification Experiment 2 classification accuracy [%], simulation Setting 2. ....	38
Table 13: Classification experiment 3-5 classification accuracy [%], simulation Setting 2.....	39
Table 14: Vehicle properties. ....	48
Table 15: Damage scenarios. ....	50
Table 16: Vehicle properties. ....	66
Table 17: Damage scenarios: types and severity. ....	69
Table 18: Damage scenarios: locations and roadway roughness ....	70
Table 19: Damage scenarios: temperature B1 R2.....	72

# Chapter 1: Introduction

Bridge structural health monitoring (SHM) has been an active research field for over 30 years. It is a multidisciplinary problem that involves: sensors, data acquisition systems, data analysis and data interpretation. In general terms, the objective of bridge SHM is the early detection and characterization of damage conditions before they pose a threat to the structural integrity of a bridge and the public it serves. An analogy can be made with the medical field where the early detection of pathology allows for several treatment options to be undertaken to restore health. A late diagnosis might lead to chronic illness or death. If diagnosed properly, prognosis and treatment follow diagnosis.

## ***1.1 Problem statement***

The current state of the aging bridge infrastructure in the USA and around the world requires more accurate diagnostic tools for a large stock of bridges. There has been an increase in public, as well as political, awareness of the current state of the bridge infrastructure. Old and new bridges are now under public scrutiny after catastrophic collapses. The collapse of the I-35 bridge over the Mississippi River on Aug. 1, 2007 is a noticeable example, as well as the collapse of other bridges around the globe (e.g., Shershan Bridge, Pakistan, Sep. 1 2007; Harp Road Bridge, USA, Aug 15 2007; Loncomilla Bridge, Chile, Nov 18, 2004.).

The research community has been developing structural health monitoring (SHM) techniques to aid in the ongoing bridge management efforts of local bridge authorities. The current standard bridge inspection practice is based on biannual visual inspections, which are subjective by nature. Sensor-based SHM is perceived as the technology that could improve the current visual inspection process (FHWA-2001). Monitoring bridge structural systems helps in planning different bridge intervention strategies, such as maintenance actions, repair or

replacement (Frangopol et al. 2008). Moreover, the life-span of the bridge structure can be extended even though it might not look sound if based on sensed physical data.

Traditional bridge SHM techniques entail the placement of sensors on the structure for measuring physical parameters that are then used as indicators of the structural behavior. SHM and damage assessment have been very active research areas, and have motivated several excellent review and overview papers, which highlight some of the most relevant approaches (e.g., Van der Auweraer and Peeters 2003; Farrar and Worden 2007). Brownjohn (2006) describes some general and fundamental objectives for monitoring civil infrastructure and points out some historical applications. More specific review topics include wireless, structural health monitoring, design of devices, and the trend for localized processing (Lynch, 2007); vibration-based condition monitoring (Doebling et al. 1998, Carden and Fanning 2004); damage identification using inverse methods (Friswell 2006); unsupervised learning (Fulgate et al. 2000, Worden and Dulieu-Barton 2004, Worden and Manson 2007); and vibration-based condition monitoring methods (Carden and Fanning 2004).

Two main approaches of this type have been pursued in recent years. One is a global vibrational approach and the other is the local approach (Mal et al 2005). The first looks at the vibration of the whole structure, while the latter focuses on the wave propagation along structural elements. We refer to these two approaches based on sensors placed on the structure as *direct* approaches. The direct approaches are especially useful when monitoring progression of damage of a particular known damage condition, or monitoring a critical member of a bridge structure.

However, the transition of the traditional SHM techniques from the research community to the practical field implementation still needs to overcome difficult challenges due mainly to technical and economic considerations (Farhey 2005, 2007). Considering the cost of a direct monitoring approach, a real world application of a monitoring program on the Lehigh River Bridge SR-33, it was reported that during the three year monitoring program, the direct cost

amounted to about 40% of the total cost. For a long term monitoring program, this direct cost must be addressed several times during the lifetime of the structure, due to software or equipment obsolescence. The other 60% indirect cost is related to labor and other related items (Frangopol et al. 2008). Some of the challenges of the *direct* approach include: labor intensive sensor deployment and maintenance, sensor system cost, powering the sensors system, data transmission and data interpretation.

Some of these challenges are currently being addressed by the research community. With respect to the power supply of the sensor systems, some of the proposed solutions for direct monitoring consider complex energy harvesting solutions to make the systems self-reliant for their power source. Among the power options, one can consider solar energy (Alippi and Galperti 2008) and vibration-based approaches (Beeby et al. 2006). However, other challenges, such as the lifespan of the sensor systems with respect to the lifespan of the sensed structure and deployment and maintenance costs, are unlikely to be solved with the same approach. Electrical systems and electronics are far more vulnerable to ambient conditions than structural elements and therefore less reliable than the system they are sensing. The threat of atmospheric conditions can also be extended to involuntary damage and vandalism. Depending on the socio-economic condition of a particular country, leaving electronic equipment unsupervised has to be carefully planned for and designed to prevent theft of the equipment.

The direct approach remains impractical to this day as a first diagnostic scan, especially when one considers the large bridge population of buildings that needs to be inspected (e.g. 600,000 bridges over 20 ft.) in the US bridge inventory.

## ***1.2 Proposed solution to the problem: an indirect approach***

The need for more efficient techniques for the SHM of bridges has led to the development of additional approaches to the direct method. One such approach is the *indirect SHM*, so-called



because it makes use of vibration data collected from sensors installed on vehicles crossing the bridge, rather than from sensors installed on the bridge itself (Lin and Yang 2005).

Figure 1 depicts the direct and the indirect SHM approaches. In principle, the vehicle-bridge interaction data captured by the moving vehicle provides information about the bridge, which can be used for diagnostic purposes. In other words, the indirect approach uses vehicle vibration data  $q_{vi}(t)$  for diagnosing a bridge's condition rather than data  $q_b(t)$  collected directly from the bridge. The use of signal processing techniques and machine learning algorithms allow one to explore the feature space of the signals collected from the vehicle and extracting vehicle-response patterns for bridge SHM. The indirect SHM approach was conceived only in the last decade, and is currently being actively researched.

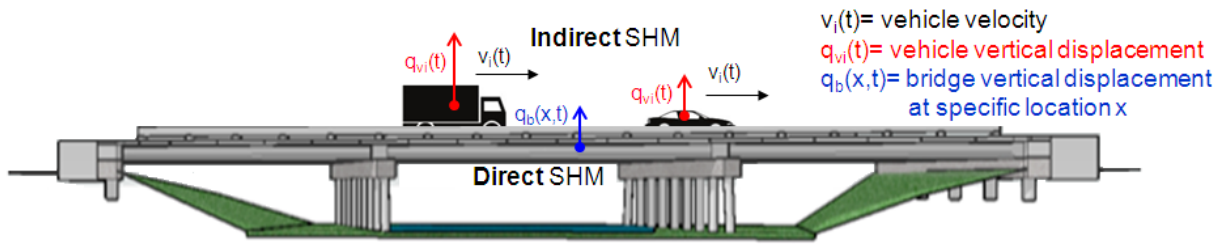


Figure 1: Direct and indirect SHM different in terms of sensor location.

The indirect approach can be viewed as being complementary to the *direct approach*. However, it has several conceptual advantages over the direct approach. The *indirect approach* allows the interrogation of a large bridge stock; it can be powered by the vehicle electrical system; it has no need to stop traffic for initial instrumentation of the structure or on-site maintenance actions; it can leverage the fleets of smart vehicles that communicate among themselves for other purposes such as: collision avoidance, traffic optimization, emergency localization or autonomous driving. The indirect approach is a data-based approach that can capture patterns of complex phenomena from large amounts of data. It takes advantage of advances in signal processing and pattern recognition algorithms.

Considering the practical future implementation of this approach, two possible scenarios might be feasible to obtain instrumented vehicle data. The first scenario that could be implemented over the medium-term considers the instrumentation of a specific fleet of vehicles that interrogate bridge structures as they go about their daily business. In this scenario, possible candidate fleets would be utility trucks or other type of public vehicles, such as transportation buses or mail trucks. They would be equipped with accelerometers, GPS, data acquisition systems and data transmission systems in order to determine their precise location and to collect their dynamic interaction data. The second scenario can be considered as a long-term vision. In the future, commercial vehicles will be readily equipped with a great number of sensors for different purposes. Some of the instrumentation that vehicles already have today are tire pressure sensors, accelerometers for adaptive suspension systems, GPS, front and rear cameras, internet connection and onboard computers. Akinci et al. envisioned taking full advantage of the opportunities that arise from having on-line vehicles making their data accessible for public interests (Akinci et al. 2003).

In the following paragraphs, we briefly review recent research efforts related to indirect SHM.

The indirect SHM was introduced by Yang et al. (2004), to extract the fundamental natural frequency of a bridge. Yang and his colleagues derived a closed-form solution for a single-degree-of-freedom oscillator moving over a single-span, simply supported beam by assuming that the beam vibrates only in its fundamental mode. The obtained solution allowed for the identification of the two main dimensionless parameters that affected the bridge response. These parameters were  $S$  and  $\mu$ ,  $S = \pi v / L \omega_b$ , a normalized vehicle velocity, where  $v$  = vehicle velocity,  $L$  = length of beam, and  $\omega_b$  = bridge's natural fundamental frequency; and  $\mu = \omega_b / \omega_v$ , where  $\omega_v$  is the vehicle (oscillator) vertical natural frequency. Yang et al. (2005) then expanded

the closed-form solution presented in 2004, to include several mode shapes as the basis for the dynamic response of the beam.

An experimental validation of the vehicle-based approach for extracting the natural frequencies of a bridge was conducted using an instrumented two-wheeled cart attached to a vehicle traveling over a simply-supported girder bridge; a heavy load truck was used to act as oncoming traffic (Lin and Yang 2005). The authors were able to identify the fundamental frequency of the bridge from the cart data, even with the simulated oncoming traffic. Toshinami et al (2010) also aimed at extracting bridge frequencies from vehicle response.

McGetrick et al. (2009) developed a numerical 1D model and studied the variations of dynamic parameters using the data derived from the numerical model. The authors report high sensitivity in the peak magnitude frequencies of the acceleration power spectral density to slight changes in the bridge structural damping. The same authors used laboratory model data (McGetrick et al. 2010) to identify the predominant frequencies of bridges and found good agreement between the signals acquired directly from the bridge and those from the vehicle as the vehicle travels over the bridge.

Kim and Kawatani (2008) presented an approach for accurately identifying damage on a bridge structure. This approach requires data from both the vehicle and the bridge. It was first explored with numerically simulated data and later through experiments (Kim et al. 2010). A hypothesis-testing scheme that looks for patterns in the bridge response from a laboratory experiment identified successfully only severe damage conditions on the bridge structure (Isemoto et al 2010).

Based on these studies, it is reasonable to conclude that vehicle responses collected from a vehicle while travelling over a bridge contain useful information of the structural condition of the bridge. However, past studies of the indirect approach concentrated mainly on identifying certain interaction properties and indexes, such as the fundamental frequency of the bridge, power spectral density magnitude variations from vehicle data, the agreement between vehicle

and bridge data predominant frequencies or the identification of severe structural changes. Thus, there is a need to complement the ongoing efforts with more robust signal processing and machine learning techniques that will allow one to detect small variations in the vehicle signature response and, therefore, allow exploration of the use of the indirect approach for diagnostic purposes.

The main objective of this work is to explore the use of the indirect method for developing a practical bridge SHM approach enhanced by signal processing and pattern recognition.

### ***1.3 Hypothesis and research questions***

This research was driven by the hypothesis that the dynamic response of a vehicle, as it traverses a bridge structure, contains dynamic information of the bridge that is useful for detecting and characterizing a damaged bridge condition. Applying novel signal processing techniques and pattern recognition approaches, that information can be mined so as to establish a sound bridge base line and detecting outliers to flag a bridge for a more precise inspection, or furthermore, recognize some damage in terms of location and severity for different types of damage scenarios.

The stated hypothesis lead to the following main research questions (RQ) and the corresponding subquestions and tasks to answer them.

**RQ1.-** *How well is the indirect approach able to detect and characterize different damage states from vehicle response data generated from a simplified 1D mathematical model and a more complex 3D mathematical model?*

To address the first research question one can pose the following related more specific questions:

RQ 1.1 *How are the mathematical models implemented?*

RQ 1.2 *Is there a classification algorithm that could be used for classifying vehicle responses into different damage classes?*

*RQ 1.3 How should the classification experiments be defined so that they would allow testing of the indirect approach?*

The research tasks for answering the first research question involved developing 1D and 3D mathematical models and implementing them into computer code models simulating the vehicle-bridge interaction and determining which classification experiments, using these models, would adequately test the indirect approach. An existing multiresolution image classification algorithm was used for running different classification experiments on the data generated by these models.

**RQ2.-** *How well is the indirect approach able to detect different scenarios of bridge damage using vehicle data collected using an experimental model?*

To address the second research question, one can pose the following related questions.

RQ 2.1 How and which types of damage to a bridge damage should be able to be simulated in the laboratory model to represent most likely bridge variations?

RQ 2.2 *How much does the speed of the vehicle influence the diagnostic capability of the indirect approach?*

RQ 2.3 *How different is the classification accuracy of the sensors placed on the vehicle compared to the classification accuracy obtained with data from sensors placed on the bridge?*

The main research tasks for answering the second research question involved constructing a laboratory experimental setup and developing a signal processing approach for classifying unidimensional time response signals. Several classification experiments were run for damage detection of different types of change imposed to the bridge structure. The results obtained from sensors at different locations allowed the comparison of the indirect and direct approaches in terms of the classification accuracy.

**RQ3.-** *How consistent are the classification results when the classification approach is applied to experimental data collected for four types of variation: 1) varying vehicle-bridge interaction*

*parameters; 2) varying roadway roughness; 3) changing the location of damage; 4) and varying atmospheric conditions?*

RQ 3.1 Would the results obtained for a particular bridge be consistent to another bridge with a different fundamental frequency?

RQ 3.2 How would variations of the vehicle affect the classification results?

RQ 3.3 How accurately can the approach locate the damage on the bridge?

RQ 3.4 Is the surface roadway roughness detrimental for detecting a damage condition on the bridge structure?

RQ 3.5 How significant is the effect of atmospheric conditions when classifying among damage scenarios?

The research tasks for answering the third research question involved constructing a second bridge structure with a lower fundamental frequency. Free vibration experiments were performed for characterizing the structures and the variations observed when introducing several changes as damage scenarios. New sets of vehicle-bridge interaction experiments were run at different speeds and for each scenario. Roadway roughness was introduced into the two bridge structures. Classification experiments were run with added roughness to the rails on which they ride. Another modification to the experimental setup included installing electrical heat sheets to produce temperature gradient scenarios. Another set of experiments combined damage scenarios with temperature gradients. The effect of atmospheric conditions on damage detection accuracy was tested with new sets of classification experiments.

## ***1.4 Overview of the Research Approach***

In this research we used and adapted signal processing techniques to capture frequency and time-dependent signal signatures from signals collected from many vehicles to detect the existence, location and extent of damage based on 1D and 3D mathematical model data. In particular, a multiresolution signal processing algorithm was used, as it allows for zooming in to

the frequency and time-dependent signatures. 1D and 3D computational models were used to generate image representations of a vehicle response for a specific bridge damage condition. Various classification experiments were performed with the multiresolution algorithm on the image representation data. The classification experiments were defined to test the indirect approach in terms of four aspects: 1) the detection of damage; 2) the classification among different severity levels of damage; 3) the classification among different locations of damage; and 4) the classification among both, severity and location of damage.

A particular signal processing methodology was developed for exploring the effectiveness of the indirect approach compared to the direct approach on experimental data from a laboratory vehicle-bridge interaction model. The setup consisted of a vehicle equipped with sensors at different locations that could repeatedly traverse a bridge structure at a prescribed speed. The bridge structure was also equipped with sensors so as to compare the indirect and direct approaches. Different classification experiments were run with data from sensors placed on the vehicle and sensors placed on the bridge. The classification results were then analyzed and interpreted.

The repeatability of the previous classification results were explored with a second bridge. Free vibration experiments on the two bridge structures using the first vehicle and an additional version of the vehicle with additional mass were performed to obtain the corresponding fundamental frequencies and critical damping ratios. Several vehicle-bridge interaction experiments were run for different speeds and scenarios. Additional roughness was fixed to the vehicle path on the two bridge structures to test and compare the classification results of the same types of damage scenarios with and without roughness. The effect of different ambient conditions was simulated with electrical heat sheets attached to the bridge deck. A circuit was built for discretely turning the heat sheets on producing different temperature gradient scenarios. Several vehicle-bridge interaction experiments were run under different temperature gradient conditions. Several classification experiments were designed and performed for

detecting damage scenarios. Some of these experiments aimed at detecting changes to the movement of supports, changes to the amount of damping and changes to the amount of concentrated mass placed on the bridge. Some other classification experiments were aimed at classifying among damage scenarios at different locations. Others were aimed at classifying among damage scenarios with different severities. Finally, two sets of classification experiments were performed to explore the effect of temperature gradients on the detection accuracy. The first set consisted of classifying among different damage scenarios in the same temperature gradient condition. The second set consisted of classifying among different damage scenarios in different temperature gradient conditions.

## ***1.5 Dissertation overview***

This dissertation is divided into three main parts. The first, presented in Chapter 2, is an exploration of the indirect approach via 1D and 3D mathematical models and a ready multiresolution image classification algorithm. The second part, presented in Chapter 3, explores the indirect approach by means of a laboratory scale experimental setup. This section describes the details of the experimental setup and a classification algorithm that uses simple frequency-based features and a standard Support Vector Machine classifier. The third part, in Chapter 4, further expands the space of possible variations on the indirect approach by introducing several variations on the experimental setup. Some of these variations include: the use of two bridge structures, changes of the properties of the moving vehicle, introduction of roadway roughness, and temperature gradients on the bridge deck.

A summary of the main results and conclusions obtained during this research, insights and possible future work is contained in Chapter 5.



## **Chapter 2: Indirect SHM for Bridges by Image**

### **Classification of Transient Response: 1D and 3D**

#### **Mathematical Models**

##### ***2.1 Introduction***

In this chapter, a methodology is proposed to improve the damage detection capabilities in bridges based on vehicle response. Numerical and experimental work shows that changes in modal shapes and other signal processing techniques, such as wavelet analysis, are good predictors of damage (Melhem and Kim 2003, Zhu and Law. 2006, Reda Taha et. Al 2006). These techniques are not only capable of capturing predominant frequencies, but also phase changes, shape and magnitude of the signals. A multiresolution classification algorithm developed in the Kovačević group (Chebira et al. 2007, Kellogg et al. 2007, Chebira and Kovačević 2008) is used to discriminate between different bridge conditions. This approach has produced good classification accuracies in several application domains. One example is the automated identification of the development stage of a *Drosophila* embryo, which has parallels to our problem of classifying the progression of bridge damage (Kellogg et al. 2007).

A well-established framework for describing the damage state of a structure involves determining: (1) presence; (2) location; (3) type; and (4) severity of damage (Rytter 1993). Researchers have also added prognosis as a fifth step (Farrar and Worden 2007). The effectiveness of the multiresolution classification algorithm for extracting relevant feature information is tested based on the previous progressive damage identification definition. Several classification experiments were conducted in the first four categories. The features were extracted from the dynamic responses of two different vehicle-bridge interaction mathematical models: a 1D and a 3D one.

This chapter is organized in the following manner. In Section 2.2, a general overview of our simulation and classification approach is presented. Section 2.3 describes the multiresolution classification system used for discriminating between bridge conditions. Section 2.4 presents in detail the 1D oscillator-beam model used to generate the vehicle-bridge interaction data followed by classification experiments. Section 2.5 describes the 3D vehicle-bridge model used to generate more realistic vehicle-bridge interaction data, followed by classification experiments. Finally, Section 2.6 presents a summary and discussion of the findings.

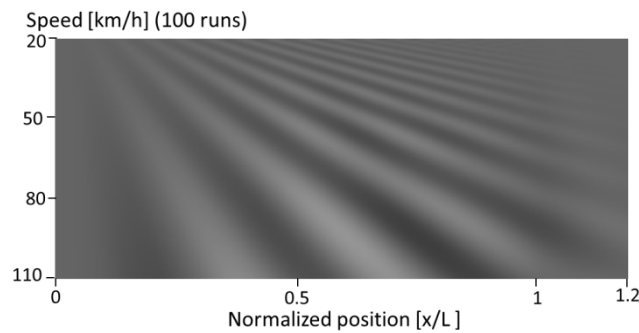
## ***2.2 Experimental Approach***

The experimental approach described in this chapter consists of the following steps: (1) the development of vehicle-bridge interaction mathematical models; (2) the development of an image generation procedure; (3) the definition of several classification experiments; (4) the application of the multiresolution classifier to conduct the experiments defined in step 3; and (5) the interpretation and analysis of the results. This section discusses the first two steps, the multiresolution classifier is explained in Section 2.3, and then Sections 2.4-2.5 cover the latter three steps in more detail where the corresponding model description follows the classification experiment definition and the corresponding results.

**Development of Vehicle-Bridge Interaction Models.** The numerical simulation experiments described in this chapter started with a simplified, 1D oscillator-beam interaction model to simulate data on vehicle-bridge interaction. This initial experiment was followed with a more complex 3D vehicle-bridge interaction model to simulate more realistic data on vehicle-bridge interaction, such as higher-mode and torsional dynamic effects from the vehicle motion and bridge response.

**Image Generation.** These mathematical models generate a 1D time response signal for a particular degree of freedom (DOF), e.g., the vertical motion of the oscillator in the 1D case, or any of the vertical DOFs of the vehicle in the 3D case, such as the acceleration time series.

Since the velocity of the vehicle is prescribed, the time can be directly related to the position of the vehicle on the bridge model. The vertical acceleration of the vehicle mass as it travels along the bridge from different simulations corresponding to different vehicle speeds were then collected and combined to form an image. The image captures all the responses of a particular vehicle travelling over a bridge structure at a particular condition. Figure 2 is an example of such an image, generated from a compilation of 100 runs of the 1D oscillator-beam numerical interaction model. The vertical axis represents the 100 different velocities (ranging from 20-110km/h) for which the acceleration response was simulated and collected for a specific damage scenario. The longitudinal axis refers to the location of the vehicle within the beam. Then, for a given abscissa and ordinate, the gray scale represents the magnitude of the vertical acceleration of the oscillator at a given location and vehicle velocity. A separate image is generated for each structural damage scenario considered in the study. Through this process, a set of images is generated each of which represents the response of a specific vehicle over a specific bridge and for a specific structural damage scenario on that bridge. These images will next be fed into the multiresolution classifier, which is described in the next section.

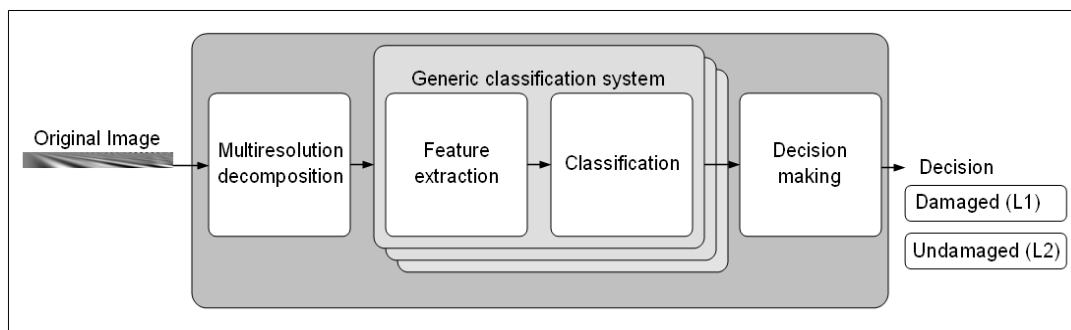


**Figure 2: Acceleration response of an oscillator compiled in an image representation constructed from 100 scaled response signals at a particular bridge condition.**

## **2.3 Multiresolution Classification**

To determine the bridge condition, whether for determining damage presence, severity, or location, the data obtained from passing vehicles needs to be classified into groups (for example, Damaged vs. Undamaged).

**Classification.** Classification is a standard machine learning/pattern recognition task whose goal is to assign a label to each of a given set of samples. For example, given an image as shown in Figure 2, we want to determine whether it belongs to a Damaged or Undamaged class of bridge. A generic classification system (see Figure 3) contains a *feature-extraction block*, which computes numerical features on the input to be used to discriminate among different classes. These features are computed on a set of training data, for which the labels are known. This is followed by a *classification block*, which assigns labels.



**Figure 3: Multiresolution classification system for Damaged and Undamaged labels.**

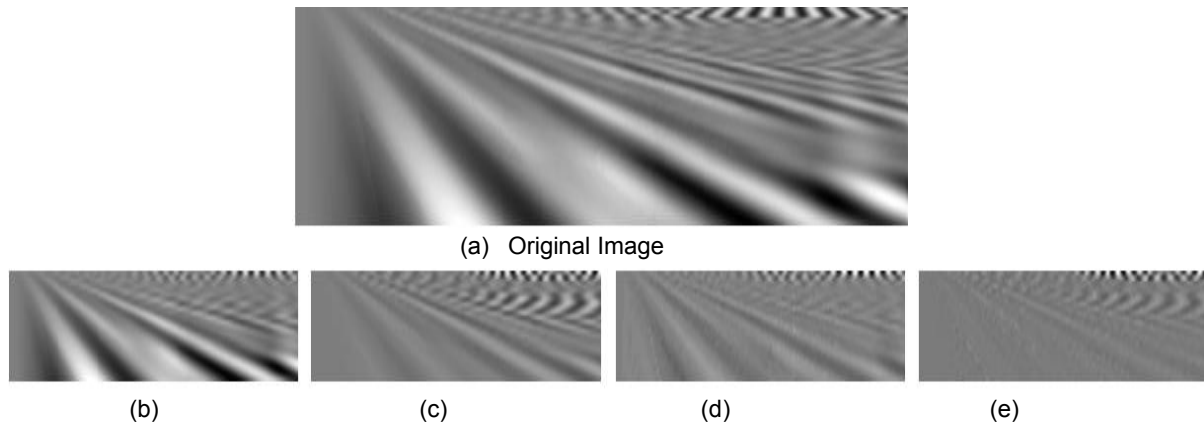
**Multiresolution Techniques.** These techniques have been developed to deal with nonstationary signals, which are signals whose behavior consists of a long-term component (for example, long-term deterioration of a bridge that affects the overall behavior of the structure) as well as short-term components (for example, localized damage and changes due to environmental variation). In such cases, the standard Fourier-type methods are not suitable as they are able to extract only global time trends. Local or Short-time Fourier methods were introduced as a step in the direction of providing some localization in both time and frequency. Additional multiresolution techniques offer varying degrees of time-frequency localization trade-offs that can be tailored to fit the task at hand. Kovačević and her group developed a multiresolution toolbox including a number of techniques such as wavelets and frames (Daubechies 1992, Vetterli & Kovačević 1995, Mallat 1999, Chebira and Kovačević 2008).

**Multiresolution Classifier.** In the biomedical arena, Kovačević and her group postulated classification not only based on original-signal domain information contained in the original signal, but also using information contained in corresponding multiresolution subspaces (at different scales and resolutions), would allow for better decision-making by leveraging both global and local signal characteristics. Based on this premise, they developed a multiresolution classifier, depicted in Figure 3 (Chebira et al. 2007). The idea was to first decompose the input signal into a series of children signals called subbands and subsequently classify each of these subbands using an appropriately trained subspace specific classifier. These subspace specific decisions will likely vary and thus must be rectified together (e.g., by voting) to provide a single global decision for the original input signal, a task accomplished by the decision-making block. The readers are referred to the publication by Chebira et al. (2007) for more details on their algorithm. This algorithm has been used with great success in several biomedical applications, with 96% accuracy on protein subcellular pattern classification (Chebira et al. 2007) and 98% accuracy in the determination of the developmental stage in *Drosophila* embryos (Kellogg et al. 2007).

Since bridge data are inherently nonstationary, these classification results published by Chebira et al. encouraged us to explore the use of this multiresolution classification method for the SHM of bridges. The system shown in Figure 3 is now described block by block.

**Multiresolution Decomposition.** A specific multiresolution decomposition is obtained as the decomposition of the original signal into different multiresolution spaces, and is implemented by a signal-processing device called a filter bank. Most of the well-known discrete transforms can be seen as subcases of multiresolution transforms, such as the discrete Fourier transform (DFT), the discrete cosine transform (DCT), the discrete wavelet transform (DWT) and the wavelet packet transforms (WPT). The specific application dictates which transform to use (Vetterli and Kovačević 1995).

The wavelet decomposition is explained in an example. Figure 4(a) shows the original image, or Level 0 image, of the decomposition. The bottom four images, (b)-(e), correspond to the first level of the multiresolution decomposition. The images at Level 1 are all subbands of the original image that can be reconstructed from these four subbands, if needed. They are obtained through filtering and sampling operations which result in the localization of different time-frequency content of the original image. The same process can be performed on one or all of the images at Level 1, decomposing them further into even smaller images at Level 2 resulting in additional and different time-frequency content localization. In our classification experiments, two levels were used as just described. Typically, the first subband, shown in (b), is obtained by lowpass filtering in both directions and then sampling, and thus carries the global characteristics of the signal and looks similar to the original signal. The other three subbands are obtained by a combination of lowpass filtering in one dimension and highpass filtering in the other, or highpass filtering in both dimensions. These subbands carry details to reconstruct the original signal, which appear as edges in the images. The localization of different time-frequency content now allows us to extract features that can be used for classification.



**Figure 4: Single level multiresolution decomposition. (a) Original image (Level 0) is split into (b)-(e) four subbands (Level 1).**

**Feature Extraction.** In this block, the numerical features used were the well-known Haralick texture features (Haralick 1973). This choice was motivated by our own past success with these

features. Derived from gray-level co-occurrence matrices of a given image (or subimage) such as those shown in Figure 4, the Haralick features aim to characterize the texture of the image in a statistical sense. Gray-level co-occurrence matrices quantify the frequency with which certain pairs of pixel intensities occur in specified spatial configurations. As a result, these matrices already achieve some characterization of texture in an image, but further measures are computed to more robustly represent them. While the original formulation of the features put forth 13 different measures, a subset of four features was chosen for these experiments: contrast, correlation, energy, and homogeneity features.

**Classification Block.** For this block, many options were possible. Neural networks built into the Matlab® toolbox were chosen for the research described in this Chapter because they are a simple, yet powerful nonlinear classifier; future work will evaluate whether one classifier or another works better. A two layer neural network (no hidden layers) was used, where the number of input layer nodes is equal to the number of features and the number of output layer nodes is equal to the number of classes. The Input Layer activation function was a Tangential Sigmoid function and the Output Layer activation function were Linear Target vectors, specifically one-hot/binary vectors (i.e., vectors of zeros except for the position corresponding to true class).

**Decision-Making Block.** This block makes a global classification decision for the original signal based on the local ones from all the subbands. The aim is to find the appropriate weights, so that more reliable subbands are more heavily weighted, and *vice versa*. To do that, an iterative algorithm was used. The weights were initialized uniformly, and a global classification decision was computed for each image in the training set. Since we know the ground truth for those images, if the decision is correct we go onto the next one. If not, we punish those subbands that made an incorrect decision by reducing their weights, and similarly, reward those that made a correct decision by increasing their weights. We continue until there is no further increase in accuracy in the training set.

**Training and Testing.** For the bridge problem, knowing the classification and the accuracy with which a classification is performed is important for estimating the classification accuracy when the classifier is applied to new incoming data (i.e., data that the classifier has not been trained on). A technique called leave-one-out cross validation (LOOCV) was used for this purpose. The LOOCV technique trains on all the data samples but one, and then the classifier is tested with the data sample that was left out of the training set. In LOOCV, this training and testing procedure is repeated for each of the data samples. The overall accuracy of the classifier for the data set is estimated by calculating the average accuracy of the individual results.

## ***2.4 1D Model, Experiments and Results***

A simplified oscillator-beam interaction model (OBIM) was chosen to simulate the idealized case of a 1D vehicle-bridge interaction, as depicted in Figure 5.

To simulate different vehicles, 11 oscillators with vertical fundamental frequencies ranging from 1 Hz to 3.5 Hz were modeled. The oscillator frequency range represents a wide variety of vehicles including small city cars, large family vehicles and trucks. Thirty percent critical damping was assumed for the suspension system in all cases.

The bridge structure was modeled as an undamped, simply supported beam. The beam is an idealization of a 40-m bridge, with the following properties: a moment of inertia  $I$  of  $0.219 \text{ m}^4$ , and a unit weight  $\gamma$  of  $74.09 \text{ kN/m}$  (Kim and Kawatani 2008). The total length of the beam was discretized into 10 finite elements as in Figure 5.



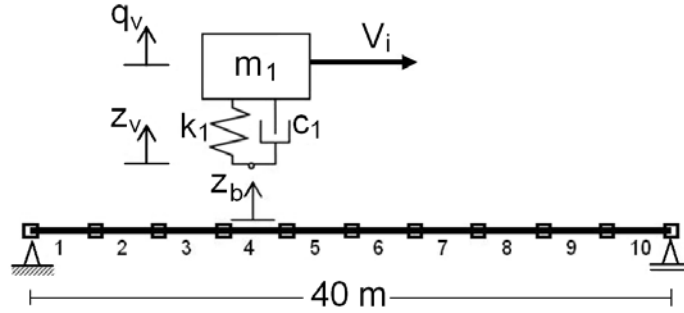


Figure 5: Oscillator-beam interaction model.

The interaction in the model was implemented as a decoupled iterative process consisting of three multiply applied steps. First, a constant load, corresponding to the oscillator's dead load, is placed over the bridge. Then, the bridge response at the point of the applied load is recorded. Next, the model uses the bridge displacement as input to the damped oscillator. These three steps are performed at each time step until the internal force between the vehicle and the bridge converges. Results for the undamaged model were verified against the analytical results reported by Yang et al. (2004) and those from previous models (Cerdeira et al. 2010).

The damaged cases were implemented using a reduction of the moment of inertia that ranged from 0% to 50% at 1% intervals, at a specific segment of the span. A total of 10 segments of moment of inertia reduction were considered, each segment corresponding to a beam finite element. Four different levels of severity were defined according to the range of reduction of the moment of inertia, as shown in Table 1. The beam was considered to be undamaged for reductions smaller than 5 percent.

Table 1: Damage cases.	
Damage labels	Inertia reduction [%]
Undamaged	0-5
Severity 1	6-15
Severity 2	16-25
Severity 3	26-35
Severity 4	36-50

The classification experiments were designed according to the SHM classification framework described earlier in Section 2.1 as: (1) presence; (2) location; (3) type; and (4) severity of damage. The first step (Experiment 1) is to identify whether the image constructed

from the data (i.e., the vehicle acceleration at different locations along the bridge and for 100 different vehicle speeds that ranged from 20 to 110 km/h as shown in Figure 2) indicates that a damage condition exists within the entire structure (i.e., determining whether the class is either Damaged or Undamaged). Successive experiments were conducted (Experiments 2 – 5) to determine the multiresolution classifier’s efficacy in classifying the severity, location, and type of damage from these same images. Figure 6 graphically depicts the five 1D experiments conducted.

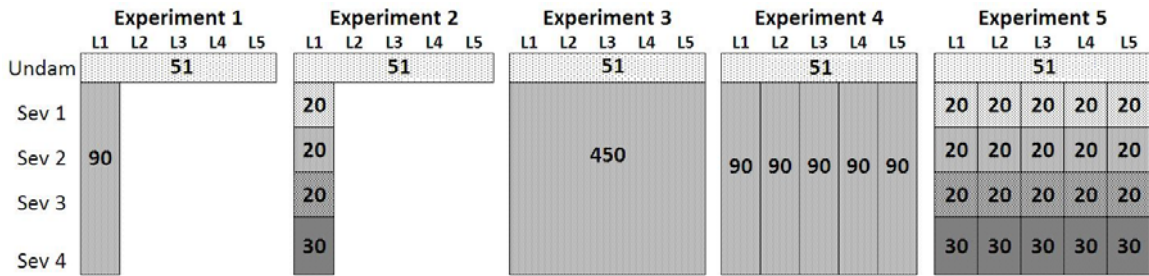


Figure 6: Graphic experiment definition for 1D data.

For each of the five experiments shown in Figure 6, the number of labels considered varied from two (e.g., in Experiment 1, the classes were Damaged and Undamaged) to 21 (e.g., in Experiment 5, the classes were Undamaged, and Damaged at five locations, L1-L5, at four levels of severity, Sev1-Sev4), Figure 6 presents the location of the inflicted damage (L1 to L5) horizontally and presents the amount of damage inflicted vertically. For each experiment, each label considered is represented by a rectangle. The numbers shown in each rectangle represent the total number of images for the respective label generated and available to be used to train and test the classifier (using LOOCV) in each fold (different selections of training and testing images) of that experiment. The images were generated as described in Section 2.2, each representing the interaction response of an oscillator for a particular structural condition. A 1% inertia reduction interval was arbitrarily chosen between each image. The number of images within each label depends on the inertia reduction interval as well as the number of elements that define the label. For example, the Undamaged label is defined to be within 0 to 5%

reduction of the moment of inertia and Locations L1-5, that is 1 image with 0% inertia reduction, and 5 images with 1-5% inertia reduction at a particular element, L1-5 in were modeled in total, by 10 beam finite elements and therefore 50 images giving a total of 51 images defining the undamaged label.

For each of the five experiments represented in Figure 6, an equal number of images were selected to represent each of the labels. For Experiments 1, 3 and 4, 50 images were randomly selected from each label. For Experiments 2 and 5, 20 images were randomly selected. Through this selection method, an LOOCV was evaluated by repeating folds where each fold's training set for a given label differed by one image. Each of the five experiments is described in more detail in the next five paragraphs.

**Experiment 1: Detection of damage classification.** This experiment evaluated the accuracy of the multiresolution-based approach for classifying a bridge into one of two labels: Undamaged or Damaged. The Undamaged label includes all the structural cases where the inertia was reduced less than 5% at a particular finite element beam. The Damaged label refers to the combination of Severity Levels 1-4, 6-50% inertia reduction, thus 45 images, one for each percent of reduction within that interval, related to some level of damage at each one of the two finite beam elements that define a particular location (L1 to L5 in Figure 6). Therefore 90 images were generated for the Damaged label out of which 50 images per label were randomly selected. This experiment was conducted 55 times: 5 different damage locations (L1-L5) and 11 different oscillators.

**Experiment 2: Severity of damage classification.** This experiment classified among five damage severity labels: the Undamaged label and four damage Severity Levels (Severity 1-4 as defined in Table 1). Similar to Experiment 1, the damage labels are also defined for a damage condition at a point located at one fifth of the total beam span from the left support. Each label is represented by 20 images randomly selected out of those available: 1) a total of 51 images

were available for the Undamaged case, 2) 20 images for each of the Severity 1 through 3, and 3) 30 total images for Severity case 4. This experiment was conducted 55 times.

**Experiment 3: Detection of damage classification.** Similar to Experiment 1, Experiment 3 uses only two labels: Damaged vs. Undamaged. However, the difference between Experiments 1 and 3 is that Experiment 3 uses data from all five damage locations to define a particular label. A total of 50 images per label were randomly selected: 50 out of the 51 images from the Undamaged label and 50 out of the 450 images from the Damaged label. Thus, in Experiment 3, the multiresolution classifier was used to take an image and determine if no damage is indicated or damage at any one of the five possible locations is indicated. This experiment was conducted 11 times, one for each of the 11 oscillators.

**Experiment 4: Detection and location of damage classification.** This experiment is a six-label experiment: Undamaged vs. Damaged at 5 different locations. Similar to Experiment 1, Experiment 4 has all the damage severities lumped together in a single Damaged label at a particular location. Each label is characterized by 50 images selected randomly. Thus, in Experiment 4, the multiresolution classifier is used to take an image and determine if no damage is indicated or damage at one of the five possible locations is indicated. This experiment was conducted 11 times.

**Experiment 5: Severity and location of damage classification.** This experiment is a 21-label experiment composed of an undamaged label, 4 severity levels (Severity 1-4) and 5 locations all combined. Each label is characterized by 20 images randomly selected. Thus, in Experiment 5, the multiresolution classifier was used to take an image and determine whether no damage is indicated or one of four severity levels of damage is indicated at one of the five possible locations is indicated. This experiment was conducted 11 times.

As indicated above, in each classification experiment a balanced number of images were defined for every label used in an experiment. Table 2 summarizes the number of labels that define each classification experiment, the number of images considered to define each label in

that experiment, and the number of folds of the experiment conducted for different combinations of oscillator type and damage location considered.

**Table 2: 1D classification experiment definition.**

	<b>Exp 1</b>	<b>Exp 2</b>	<b>Exp 3</b>	<b>Exp 4</b>	<b>Exp 5</b>
Number of Labels Considered	2	5	2	6	21
Number of images selected/label	50	20	50	50	20
Number of times experiment was run	55	55	11	11	11

## **2.4.1 1D Model Experimental Results**

To assess the effectiveness of decision-making using the multiresolution classification system, the classification accuracy was determined for the various cases. The results for the 1D Experiments are discussed in this section.

### **2.4.1.1 Damage Detection**

The results for Experiment 1, damage detection, are now discussed. Table 3 shows the overall classification accuracy for the Undamaged and Damaged labels for Experiment 1. Overall, an average accuracy of 94.6% was achieved when classifying between the two labels.

In general, a higher accuracy was achieved for damage inflicted near the midspan (Elements 5-6) than near the supports. When comparing the classification accuracy between the two supports, at Location 1 (Elements 1 and 2) the classification accuracy is 5.2% higher than at Location 5 (Elements 9 and 10). This difference may be related to the travelling direction of the oscillator. A variation in the bridge at the beginning of the recorded vehicle's response will have a greater influence than when the variation is located at the end of the bridge.

<b>Table 3: 1D Model, 2-class damage detection classification accuracy [%].</b>						
<b>Oscillator</b>	<b>Locations</b>					<b>Mean</b>
<b>frequency [Hz]</b>	<b>L1</b>	<b>L2</b>	<b>L3</b>	<b>L4</b>	<b>L5</b>	<b>accuracy [%]</b>
1.00	93	98	99	95	96	96.2
1.25	96	100	98	100	93	97.4
1.50	97	99	99	96	96	97.4
1.75	93	96	98	97	90	94.8
2.00	93	95	99	93	90	94.0
2.25	90	95	98	89	87	91.8
2.50	96	95	97	98	87	94.6
2.75	95	94	98	91	75	90.6
3.00	97	94	96	97	89	94.6
3.25	93	97	97	93	90	94.0
3.50	97	95	97	96	89	94.8
Mean	94.5	96.2	97.8	95.0	89.3	<b>94.6</b>

#### 2.4.1.2 Assessment of Damage Severity

The results for Experiment 2, assessment of damage severity, are now discussed. For the 1D model classification experiment with five severity labels (Undamaged and four damage levels), the accuracies obtained are lower (Table 4) compared to the previous Experiment 1. The mean classification accuracy is 77.3%. This decrease in the classification accuracy wrt Experiment 1 is to be expected, since this experiment discriminates between different level of damage, rather than just performing a binary classification as in Experiment 1.

<b>Table 4: 1D Model, 5-class damage severity classification accuracy [%].</b>						
<b>Oscillator</b>	<b>Locations</b>					<b>Mean</b>
<b>frequency [Hz]</b>	<b>L1</b>	<b>L2</b>	<b>L3</b>	<b>L4</b>	<b>L5</b>	<b>accuracy [%]</b>
1.00	89	91	82	79	90	86.2
1.25	92	84	93	91	84	88.8
1.50	83	86	75	74	80	79.6
1.75	89	80	82	71	84	81.2
2.00	80	67	75	66	73	72.2
2.25	80	63	76	63	78	72.0
2.50	64	73	71	71	70	69.8
2.75	80	67	74	70	68	71.8
3.00	76	77	83	76	62	74.8
3.25	79	84	78	70	68	75.8
3.50	86	82	83	71	70	78.4
Mean	81.6	77.6	79.3	72.9	75.2	<b>77.3</b>

### 2.4.1.3 Damage Localization and Assessment

The results for Experiments 3-5 shown in Table 5, are now discussed. As was the case for Experiments 1 and 2 (Table 3 and Table 4), a classification accuracy result was obtained for each of the 11 oscillators. However, for Experiments 3, 4 and 5, all the data regarding the different locations of damage is used in a single execution of the experiment, as shown in Figure 6. Therefore, each experiment is conducted only 11 times, once for each of the 11 oscillators considered, but not for the different locations as in Experiments 1 and 2. The two-label problem defined in Experiment 3 shows an approximate decrease of classification accuracy of 6.5% in the result from the mean accuracy of Experiment 1. This decrease is attributed to the added difficulty of determining a common response pattern for the Damaged label that now includes data from different locations. In Experiment 3, the Damaged label is defined by randomly selecting 50 images from a total of 450 to represent changes at all the different locations. Despite the decrease, 88% classification accuracy can still be considered a high classification result. The mean 85% classification accuracy obtained for Experiment 4 demonstrates the ability of the classifier to differentiate between states of damage at different locations. For Experiment 5, the 77% classification accuracy is very high for this 26-label problem, especially if one considers that the direct probability of randomly assigning the correct label is approximately 4%.

**Table 5: 1D model, Experiments 3 to 5 damage classification accuracy [%].**

<b>Oscillator frequency [Hz]</b>	<b>Exp 3</b>	<b>Exp 4</b>	<b>Exp 5</b>	<b>Mean accuracy [%]</b>
1.00	90	85	82	86
1.25	90	92	86	89
1.50	90	86	78	85
1.75	88	82	79	83
2.00	84	83	71	79
2.25	86	85	73	81
2.50	91	79	77	82
2.75	83	89	73	82
3.00	85	86	79	83
3.25	93	88	76	86
3.50	88	84	76	83
Mean	88	85	77	83

## 2.5 3D Numerical Model Description, Experiments and Results

A 3D vehicle-bridge interaction model was implemented after the 1D oscillator-beam model. This model is richer, capturing dynamic effects, such as torsion in the bridge structure and pitching and rolling on the vehicle model.

Similarly to the oscillator in the 1D case, in the 3D models, a vehicle was simulated to travel over the bridge at the same velocity range and a 100 times as in the 1D case. The simulated response of the speed range was compiled into an image using the process that was previously described.

Figure 7 depicts the 5 vertical degrees of freedom (DOF) of the vehicle model and the parameters used in the simulations. In 3D settings, the suspension and dimension parameters from the vehicle were made to be the same as those described by Ikenaga et al. (2000) and are summarized in Figure 7. The bouncing frequency of the vehicle is 1.41 Hz for the parameters shown in the Figure 7. The classification experiments in the 3D Model were conducted with three different degrees of freedom: the vertical degree of freedom at the center of gravity  $Z_{CG}$ , and the unsprung mass vertical degrees of freedom at the left ( $Z_{fl}$ , and at the right side ( $Z_{fr}$ ) of the vehicle front suspension.

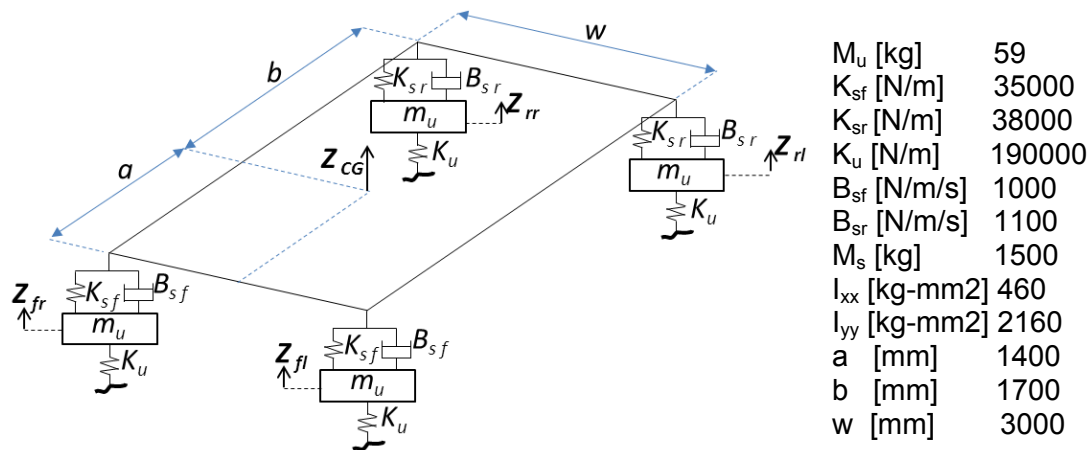


Figure 7: Vehicle model degrees of freedom, parameter notation and corresponding values.

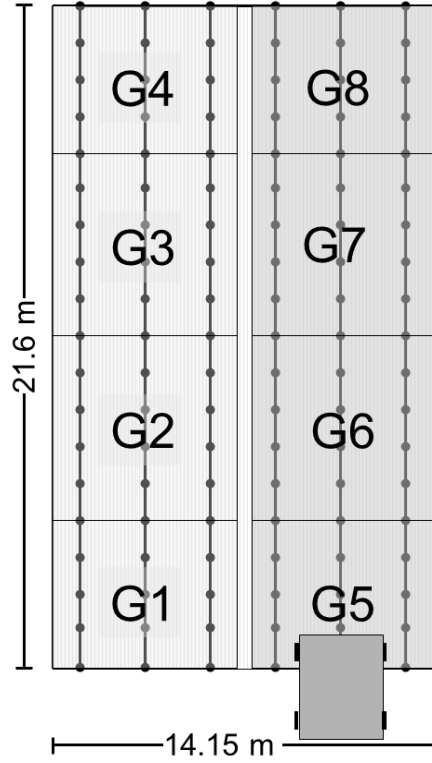


The 3D bridge modeled is a 21.6m long, 14.15m wide girder bridge (Li et al. 2008). The bridge model consists of bending plate elements for the deck and beam elements for the 6 girders.

For the 3D case, two experimental settings were explored to test the classification capability of the multiresolution algorithm. The two settings are later referred Setting 1 and Setting 2 in separate sections that also show the corresponding results. The 3D simulation settings treated the damage as a simultaneous moment of inertia reduction on a group of beams. The damage was represented by a moment of inertia reduction that ranged from 0 to 50% on a group of beam elements simultaneously. The two *settings* differ in terms of the amount of simulated change inflicted into the bridge structure and the vehicle parameters.

### **2.5.1 3D Model Experimental Results for Setting 1**

Figure 8 shows a view of the girder beam axis and the finite beam elements, on top of which are the eight groups of beams for which the inertia was reduced for simulation Setting 1. The bridge model consists of a total of 8 groups of beams: G1 to G4 at the left lane that includes the leftmost 3 rows of beam elements, and groups G5 to G8 at the right which include the 3 rightmost rows of beam elements. Groups near the supports, G1, G4, G5 and G8 are 12 beam elements each, and groups G2, G3, G6 and G7 are 15 beam elements each. This arbitrary definition has double symmetry with respect to the midspan, and the midline of the bridge. G1-G4 are not in the travelling path of the vehicle while G5-G8 are on the travelling path of the vehicle as shown in Figure 8.



**Figure 8: 3D Bridge model with corresponding beam groups for simulation Setting 1.**

Classification experiments were performed on the vehicle data simulated with the 3D model that were similar to the previous five experiments performed on the 1D data as described in Section 4. Figure 9 shows the graphical representation of these experiments for 3D data simulation Setting 1. The location data of these experiments are labeled in terms of the groups previously defined on the 3D model Setting 1. These 5 classification experiments on the 3D model data differ from the experiments on the 1D model in terms of the amounts of data on each of the defined labels and the selected amounts of data for each experiment. The numbers on the labels represent the total number of images on each label.

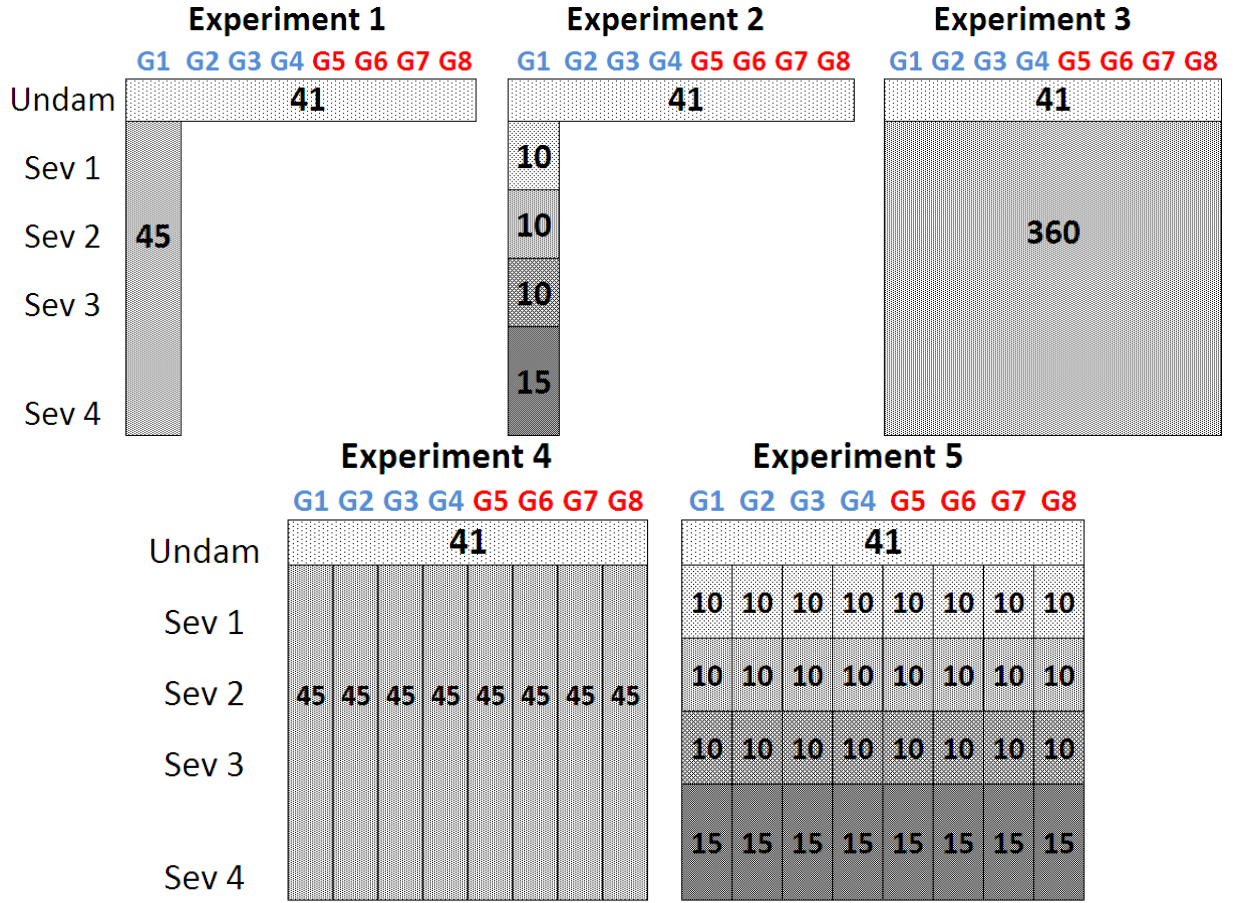


Figure 9: Graphic representation of experiment definition for 3D data Setting 1.

Just as in the 1D case, a balanced number of images were defined for every label in a specific run of an experiment. Table 6 shows the number of labels that define each classification experiment, the number of images considered to define each label, and the number times the experiment was conducted. In Setting 1 for the 3D Model data, Experiment 4 has 9 labels that distinguish among the different locations. Experiment 5 has a total of 33 labels that consider location and severity of the moment of inertia reduction. In the 3D case, one can choose several degrees of freedom from which to collect data and perform the corresponding classification experiments. Each classification experiment is repeated three times because of the different DOFs, and in the case of Exp1 and Exp2, each of those three experiments are conducted for the 8 different possible locations of the damage, which means that 24 instances of Experiments 1 and 2 were conducted.

**Table 6: 3D setting 1 classification experiment definition.**

	<b>Exp 1</b>	<b>Exp 2</b>	<b>Exp 3</b>	<b>Exp 4</b>	<b>Exp 5</b>
Number of Labels Considered	2	5	2	9	33
Number of images selected/label	40	10	40	40	10
Number of times experiment was run	24	24	3	3	3

### 2.5.1.1 Damage Detection

The results for Experiment 1, damage detection, are now discussed. Experimental Setting 1 evaluated the accuracy of the multiresolution classification approach when applied to distinguish between Damaged and Undamaged labels. The classification accuracy results for Experiment 1 are presented in Table 7. The leftmost column is the degree of freedom from the vehicle used for a particular classification experiment. Over the three DOFs,  $Z_{fl}$  and  $Z_{fr}$  at the axle level and  $Z_{CG}$  at the center of gravity, an average classification of 96.7% was obtained (Table 7). Compared to the 1D model (Table 3), we can see that the 3D simulated model data was able to be more accurately classified (by about 2%) than the data from the 1D model.

**Table 7: 3D model, 2-class detection of damage classification accuracy results, Setting 1. G1-8 group of beams where damage was inflicted.**

	<b>Left lane</b>				<b>Right lane</b>				
<b>DOF</b>	<b>G1</b>	<b>G2</b>	<b>G3</b>	<b>G4</b>	<b>G5</b>	<b>G6</b>	<b>G7</b>	<b>G8</b>	<b>Mean</b>
$Z_{CG}$	95	98	98	85	96	98	99	95	95
$Z_{fl}$	98	98	99	94	99	99	99	95	97
$Z_{fr}$	99	100	99	90	99	99	100	94	97
Mean	97	98	98	90	98	98	99	95	96.7

Considering each DOF individually, the accuracy is higher for the data at the axle level ( $Z_{fl}$  and  $Z_{fr}$ ) than for the degree of freedom located at the center of gravity of the vehicle ( $Z_{CG}$ ). For the different locations of damage, the obtained accuracies are similar except for G4. One explanation for this decrease may be related to the traveling path and direction of the vehicle. The vehicle's traveling path is not symmetric as shown in Figure 8. The prescribed travelling path is on the right lane of the bridge and passes over G5 to G8, not over G4 which is in the left lane. Just as in the 1D experiment, the moment of inertia variation for locations at the end of the bridge in the traveling direction has lower influence on the response than for locations at the beginning. Thus, the difference in accuracy between G4 and G8 is attributed to the chosen

traveling path. For G4, there is also a difference in classification accuracy between the DOFs. A 4% difference in classification accuracy between the left and right DOFs at the axle level for G4 can be attributed to this asymmetry of the travelling path. The right DOF ( $Z_{fr}$ ) is further away from G4 and, therefore, less influenced by the inertia reduction of G4 than the left DOF ( $Z_{fl}$ ).

These results suggest that, when considering a more complex system where torsion is introduced by the asymmetric loading path of the travelling vehicle, the classification algorithm is able to find even more robust patterns from which to classify damaged and undamaged cases.

### 2.5.1.2 Assessment of Damage Severity

The results for Experiment 2, damage severity classification, are now discussed. The results for this experiment are shown in Table 8. Overall, a 90% accuracy was achieved for severity classification. This classification accuracy is significantly higher than the 77.3% obtained when running the experiment on the 1D model generated data, and higher than the 20% direct probability of randomly assigning one of the five Labels to any image  $P=1/5$ .

**Table 8: 3D model, 5-class severity of damage classification accuracy [%], Setting 1.**

DOF	Left lane				Right lane				Mean
	G1	G2	G3	G4	G5	G6	G7	G8	
$Z_{CG}$	88	86	98	84	96	94	88	88	90
$Z_{fl}$	94	98	90	80	88	92	88	86	90
$Z_{fr}$	90	90	94	90	94	94	90	90	92
Mean	91	91	94	85	93	93	89	88	90

### 2.5.1.3 Damage Localization and Assessment

The results for Experiments 3-5, are now discussed. Results from the 3D Model (Table 9) are consistent in terms of the classification accuracy achieved, with respect to the results from the 1D Model (Table 5), especially when comparing the mean accuracy results of Experiments 3 and 4 with 5% difference for the final Mean accuracy. For example, the 3D case of Experiment 4, is a 9-label experiment (i.e., Undamaged and eight labels corresponding to the eight damage locations), while Experiment 4 in the 1D case had 6 labels (i.e., Undamaged and five damage

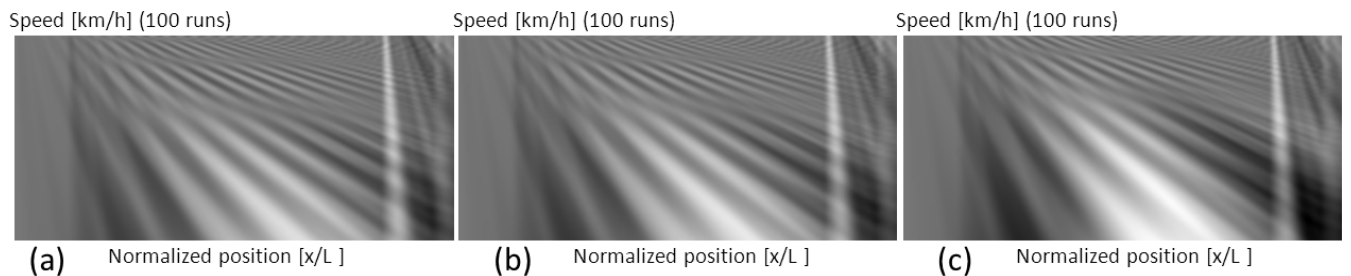
locations) and achieved 87% and 88% classification accuracy, respectively. Experiment 5 in the 3D case is a 33 label experiment, and for the 1D case is a 21-label experiment. In Experiment 5, the most complex experiment, classification accuracies of over 85% were obtained for the unsprung DOFs ( $Z_{fr}$  and  $Z_{fl}$ ) and an average of 83% for all three vehicle DOFs.

In general, the results obtained with the response data of the unsprung mass are more accurate than those obtained for the degree of freedom at the center of gravity at the chassis level.

**Table 9: 3D model, 5-class severity of damage classification accuracy [%], Setting 1.**

DOF	Experiment #		
	3	4	5
$Z_{CG}$	85	85	79
$Z_{fl}$	94	91	86
$Z_{fr}$	83	90	85
Mean	87	89	83

In light of the previous results, it is important to illustrate the complexity of the damage classification task. Figure 10 shows a set of three images that represent very different levels of damage in the 3D bridge structure model for simulation Setting 1. Although the three images appear to be identical, they represent three different damage severity scenarios at the location defined as G2 (Figure 9). The first image represents the undamaged case, the second image results from a 20% moment of inertia reduction at G2, and the third image is obtained with a 50% moment of inertia reduction. Expecting accurate manual classification of these three images by human visual inspection is not realistic. However, the multiresolution classifier can perform the classification task using data taken from either the 1D Model or the 3D Model.



**Figure 10: Images of vehicle response at center of gravity in 3D Model (a) Undamaged scenario, (b) 20% inertia reduction at G2, (c) 50% Inertia reduction at G2.**

## 2.5.2 3D Model Experimental Results for Setting 2

A total of 6 different vehicles were considered in this second simulation setting. The properties of the vehicles are listed in Table 10. Note that Vehicle #3 is the same as the one from the 3D model Setting 1.

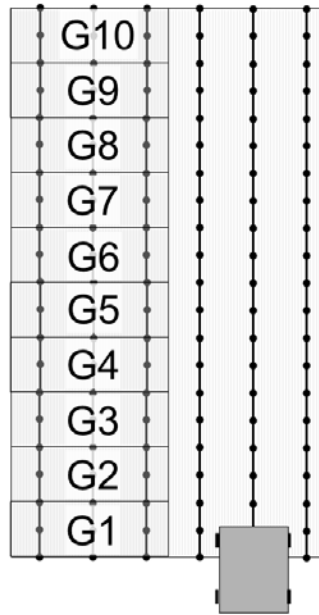
The vehicle properties were selected to represent a range of possible vehicles. Some of the properties are similar to each other in pairs. The distinct values are italicized. For example, Vehicles 1 and 2 are a stiffer variation of Vehicle 3 (see  $K_{sf}$  and  $K_{sr}$  in Table 10). Vehicle 1 is lighter than Vehicle 2 ( $M_s$ ) while Vehicle 4 is a heavier version of Vehicle 3. Vehicles 5 and 6 are dimensionally larger ( $a$  and  $b$ ), and one order of magnitude heavier than the other vehicles ( $M_s$ ). The corresponding bouncing frequency for each vehicle is also shown in Table 10.

**Table 10: Vehicle properties for 3D experimental Setting 2.**  
**Vehicle#**

<b>Property</b>	<b>1</b>	<b>2</b>	<b>3</b>	<b>4</b>	<b>5</b>	<b>6</b>
Freq [Hz]	2	1.68	1.41	1.09	1.72	1.66
$M_u$ [kg]	59	59	59	59	59	59
$K_{sf}$ [N/m]	<i>55000</i>	<i>55000</i>	35000	35000	350000	<i>450000</i>
$K_{sr}$ [N/m]	<i>58000</i>	<i>58000</i>	38000	38000	350000	<i>500000</i>
$K_u$ [N/m]	190000	190000	190000	190000	2500000	<i>3500000</i>
$B_{sf}$ [N/m/s]	1000	1000	1000	1000	4000	4000
$B_{sr}$ [N/m/s]	1100	1100	1100	1100	4100	4100
$M_s$ [kg]	<i>1000</i>	1500	1500	<i>2500</i>	10000	<i>15000</i>
$I_{xx}$ [kg-mm <sup>2</sup> ]	460	460	460	460	500	500
$I_{yy}$ [kg-mm <sup>2</sup> ]	2160	2160	2160	2160	<i>10160</i>	<i>10160</i>
$a$ [mm]	1400	1400	1400	1400	3600	3600
$b$ [mm]	1700	1700	1700	1700	2400	2400
$w$ [mm]	3000	3000	3000	3000	3000	3000

The same bridge parameters from Setting 1 were used in Setting 2. However, regarding the simulated damage, for Setting 2 the magnitude of the applied change in the structure was decreased by reducing the area of the simulated damage and defining ten groups of beams: Groups 1 to 10 on the left lane with 6 beams each as shown in Figure 11. This is less than half the area from groups G1, G4, G5 and G8 from the previous setting, increasing the classification difficulty of the experiments performed on this setting for the same number of levels of the

damage states. Moreover, note that the groups in Setting 2 are not directly on the travelling path of the vehicle but on the adjacent lane for the purpose of testing an adverse identification condition.



**Figure 11: 3D Bridge model with corresponding beam groups for simulation Setting 2.**

Figure 12 is the graphical representation of the experiments for simulation Setting 2. As in Setting 1, the moment of inertia reduction groups define the locations of the damage. For Setting 2, Experiments 4 and 5 consider more labels than for Setting 1. Experiment 4 now has 11 Labels, while Experiment 5 has 41 different labels. As in the previous cases, the number of images that define a label are shown in each experiment graphical label definition. The results of these experiments follow.



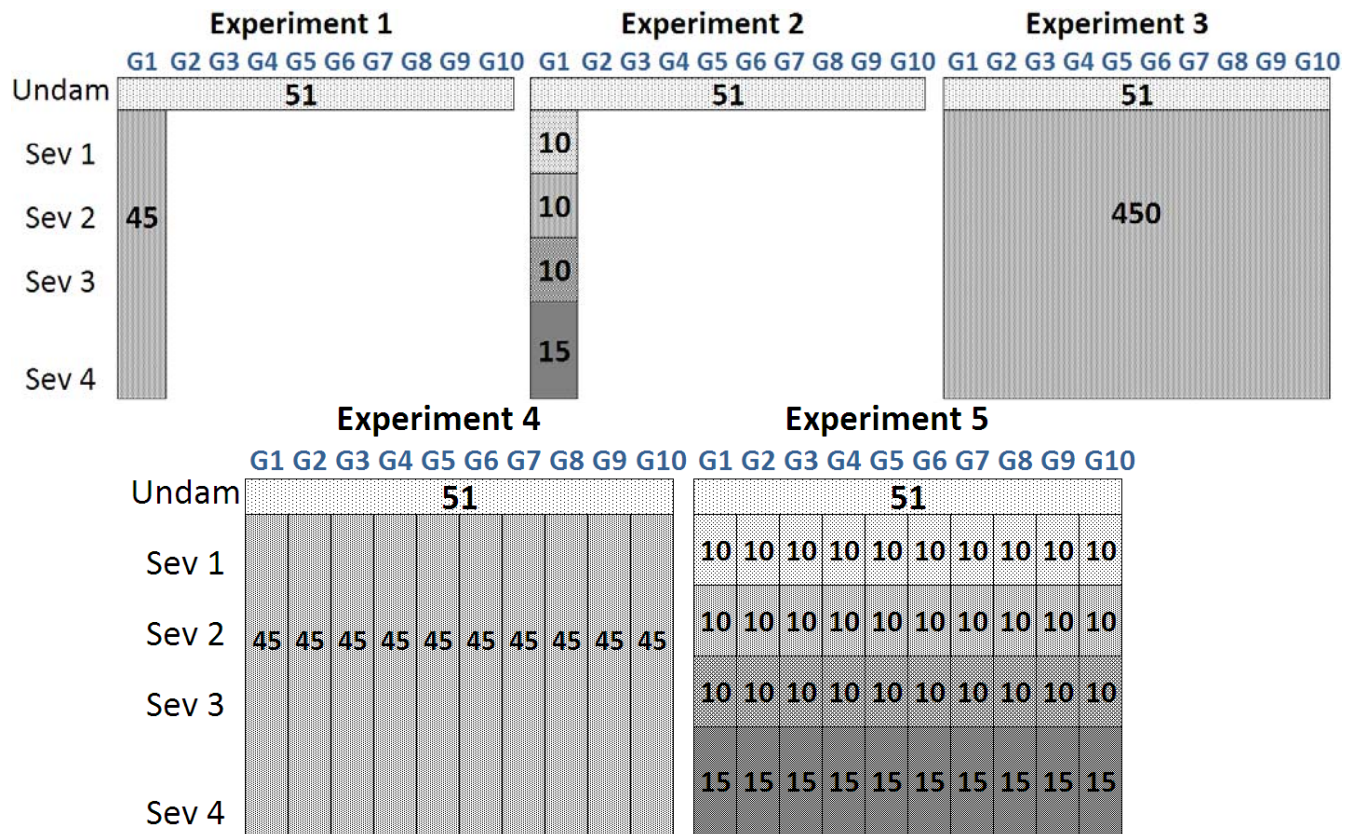


Figure 12: Graphic representation of experiment definition for simulation Setting 2.

### 2.5.2.1 Damage Detection

The results for Experiment 1, damage detection, are now discussed. Table 11 summarizes the results for the detection experiment for the 6 vehicles at the 10 locations and for the tree vertical degrees of freedom considered. For Vehicle 3, the classification accuracy decreased by about 7%, from an average of 96.7% in 3D Setting 1 to 90% in Setting 2. This reduction can be attributed to the decrease in the magnitude of the damage, as well as the location of the damage groups. The damage groups in Setting 2 reduce the magnitude of the total change in the structure and, therefore, the variation in the dynamic response. Moreover, these damage groups are not in the traveling path of the vehicle. Over all, there is a slightly better performance when using the data from Vehicles 1-4 than the two heavier Vehicles 5 and 6.

**Table 11: Classification Experiment 1 classification accuracy [%], simulation Setting 2.**  
**Vehicle** **Location**

DOF	#	G1	G2	G3	G4	G5	G6	G7	G8	G9	G10	Mean
$Z_{CG}$	1	91	87	88	88	84	90	88	84	89	99	89
	2	89	87	88	87	89	91	90	82	96	94	89
	3*	91	88	89	88	86	91	92	88	83	94	89
	4	94	88	87	91	89	90	90	84	86	98	90
	5	81	78	84	84	84	99	94	89	79	87	86
	6	90	81	84	84	89	96	92	89	83	90	88
	Mean	89	85	87	87	87	93	91	86	86	94	88
$Z_{fl}$	1	89	81	87	87	89	99	98	89	79	89	89
	2	88	80	86	88	88	96	98	90	77	87	88
	3*	93	83	88	88	88	94	99	93	84	84	90
	4	84	80	86	89	90	94	97	88	80	89	88
	5	88	86	88	83	81	93	96	87	81	86	87
	6	84	78	87	87	83	92	93	82	84	77	85
	Mean	88	81	87	87	86	95	97	88	81	85	87
$Z_{fr}$	1	91	87	87	88	89	97	98	94	87	96	91
	2	94	87	91	88	88	96	94	92	91	96	92
	3*	89	82	86	86	89	96	99	94	93	91	90
	4	86	84	88	88	89	97	96	97	88	92	90
	5	90	82	88	88	91	96	99	91	87	89	90
	6	88	86	87	86	89	98	96	90	89	88	89
	Mean	90	85	88	87	89	96	97	93	89	92	91
Total Mean		89	84	87	87	87	95	95	89	85	90	88.8

\*Vehicle 3 characteristics are identical to those used for 3D Model Setting 1.

### 2.5.2.2 Assessment of Damage Severity

The results for Experiment 2, damage severity, are now discussed. The results for assessment of different levels of damage severity are shown in Table 12. As in Experiment 1, there is a reduction in the classification accuracy with respect to the first setting. In this Experiment 2 Setting 2, the classification accuracy for Vehicle 3 is about 81%, less than 10% lower than Setting 1. As observed in Experiment 1, classification accuracies are slightly lower when using data from the heavier vehicles.

**Table 12: Classification Experiment 2 classification accuracy [%], simulation Setting 2.**  
**Vehicle** **Location**

DOF	#	G1	G2	G3	G4	G5	G6	G7	G8	G9	G10	Mean
$Z_{CG}$	1	78	76	76	86	86	82	82	86	82	92	83
	2	86	82	74	76	76	82	84	76	84	90	81
	3*	82	78	78	72	82	86	80	90	84	88	82
	4	80	84	80	88	76	82	70	78	80	92	81
	5	78	76	84	74	78	90	90	80	70	82	80
	6	82	76	72	74	74	92	92	78	80	88	81
	Mean	81	79	77	78	79	86	83	81	80	89	81
$Z_{fl}$	1	86	88	78	76	78	80	92	76	72	84	81
	2	84	78	80	78	84	88	88	82	76	80	82
	3*	80	72	74	76	78	86	82	92	76	84	80
	4	82	74	82	76	86	90	86	82	74	76	81
	5	82	66	72	76	68	98	80	78	72	72	76
	6	78	74	70	74	76	84	92	84	70	70	77
	Mean	82	75	76	76	78	88	87	82	73	78	80
$Z_{fr}$	1	88	72	74	80	80	88	86	88	84	74	81
	2	88	78	74	76	76	92	88	88	84	82	83
	3*	82	76	70	86	82	90	78	78	82	84	81
	4	90	78	84	84	76	92	92	78	86	82	84
	5	68	76	74	74	76	90	84	78	88	82	79
	6	80	68	80	74	74	90	90	78	80	76	79
	Mean	83	75	76	79	77	90	86	81	84	80	81
Total Mean		82	76	76	78	78	88	85	82	79	82	80.

\*Vehicle 3 characteristics are identical to those used for 3D Model Setting 1

### 2.5.2.3 Damage Localization and Assessment

The results for Experiments 3-5, are now discussed. They are summarized in Table 13. In the case of Experiment 3, the classification accuracy for Vehicle 3 was about a 6% lower than for Experiment 3 in Setting 1. This reduction is consistent with the accuracy reductions observed in Experiments 1 and 2 from the previous 2 experiments and can be attributed to the same causes: magnitude and location of damage. However, in Experiments 4 and 5, Vehicle 3 shows a significant decrease in accuracy with respect to Setting 1. Experiment 4 has an average accuracy of 64%, while Experiment 5 has a 51% classification accuracy. On top of the more subtle changes inflicted in Setting 2 wrt Setting 1, this reduction in the classification accuracy can be attributed to the increased number of labels to which each image can be assigned. Experiment 4 has 11 labels in Setting 2 compared to 9 in Setting 1, and Experiment 5 has 41 labels in Setting 2 compared to 33 from Setting 1.

**Table 13: Classification experiment 3-5 classification accuracy [%], simulation Setting 2**

DOF	Vehicle	Experiment #		
	#	3	4	5
$Z_{CG}$	1	72	61	50
	2	84	59	50
	3*	87	63	54
	4	88	64	48
	5	57	58	45
	6	73	54	47
	Mean	77	60	49
$Z_{fl}$	1	78	65	49
	2	69	63	50
	3*	83	67	54
	4	73	65	53
	5	75	61	43
	6	67	64	50
	Mean	74	64	50
$Z_{fr}$	1	81	67	53
	2	89	70	54
	3*	74	71	54
	4	82	70	54
	5	78	66	54
	6	81	67	57
	Mean	81	68	54
Total Mean		77.3	64.2	51.1

\*Vehicle 3 characteristics are identical to those used for 3D Model Setting 1

## 2.6 Discussion

This chapter introduced the use of multiresolution analysis for classification of vehicle response data for indirect monitoring SHM approach of bridges. Five classification experiments were performed on data from 1D numerical models and two settings of 3D models. The models simulate damage at various locations by reducing the moment of inertia of the main girders.

High classification accuracies were obtained with the different model data. In many cases, the classifier was able to differentiate the vehicle response with greater than 90% accuracy considering location and severity of inertia reduction of the modeled bridge structures.

Even though the severity definition considered very small moment of inertia changes between the different damage models (e.g., a 6% inertia reduction was arbitrarily defined as Damaged while a 5% as Undamaged), the classifier was able to characterize the severity of damage with high accuracy for Experiment 1 using 1D and 3D numerical model data.

Regarding the location of the damage conditions, in most cases, changes near the midspan of the bridge were more easily classified by the algorithm than damage near the supports. This result is consistent with a higher value at this location of the moment envelope due to a moving load on a simply supported bridge structure.

For the 3D model data, the classification results were consistent with respect to those obtained with the 1D models and differed by less than 10% for Experiments 1 through 3, where the number of labels were the same. In 3D model Setting 1, the overall classification accuracy was higher than that obtained for the 1D model data. However, under Setting 2, the classification accuracy results were lower than those obtained for the 1D Model. This variation can be attributed mainly to the relative magnitude and location of the damage applied to the 3D model with respect to the 1D model and the parameters of the 3D setting. In 3D model Setting 1, the moment of inertia reduction to the group of beams is more significant than when applied to a single element as was done using the data from 1D model. In contrast, for 3D model Setting 2 this relative significance is lower and, therefore, the classification accuracy was lower. Nevertheless, the classification accuracy obtained for 3D model Setting 2, was on average, higher than an 88% for Experiment 1, 80% for Experiment 2 and 77% for Experiment 3.

Damage scenarios for 3D model Setting 2 considered groups of elements that were not on the driving path of the vehicle, while for the 1D model, the damage was always in the loading path of the oscillators. The consistently high classification accuracy of this setting for Experiments 1 through 3 can be attributed to the increase in complexity of the system when compared with the 1D model. By adding 3D effects, such as torsion and asymmetric loading, the response of the passing vehicles becomes much richer. Consequently, the algorithm is able to better capture the changes in response images and determine more significant classification patterns.

A significant decrease in the classification accuracy for Experiments 4 and 5 was observed between 3D model Setting 1 and 3D model Setting 2. These results illustrate the increased complexity that occurs when classifying among a higher number of labels.

For Setting 2, different vehicles were modeled. The results do not show great variation on the classification accuracy results depending on the vehicle, however, there is a slight decrease on the classification accuracy when using data from heavier vehicles.

The overall effectiveness of the classification algorithm is dependent on the complexity of the task as reflected by the number of labels defined for any given experiment. As one would expect, a coarser assignment of labels (e.g., no damage localization) to a set of data generally allows for more leeway in what is considered an accurate result. Additionally, more refined/finer labeling of data generally reduces the amount of data available for training the algorithm and thus reduces its robustness. However, the use of overly coarse labels requires that the classifier learn a given label from data that spans a wide range. While our experiments do not demonstrate this latter concern, it must be considered in future work. Design of an effective system requires finding a reasonable balance of type and fidelity of labels.

These results were obtained with data from highly idealized models under perfect operating conditions without considering possible sources of data variation such as: sensor noise, roadway roughness or environmental variations. These results serve as a reference for the expected variation on the classification accuracy for different experiments. For example, a two label damage detection experiment such as Experiment 1 will have higher classification accuracy than a five label severity classification or a six label, nine or eleven label damage location classification as defined in Sections 2.4.1 for the 1D model and Sections 2.5.1 and 2.5.2 for the 3D models. These results will allow defining classification experiments for damage conditions on more realistic experimental data from other numerical models, physical laboratory experiments or full-scale tests.

## **Chapter 3: Indirect structural health monitoring of a simplified laboratory-scale bridge model**

### **3.1 Introduction**

In this chapter, the hypothesis that an array of sensors, mounted on moving vehicles that travel across the bridge of interest, can be helpful in identifying structural damage and thus serve as an indicator for more detailed analysis is experimentally investigated using a physical model. As discussed in Chapter 1, this approach is referred to as *indirect health monitoring*.

Yang and Chang (2009) reported results associated with field experiments where the first two natural frequencies of a bridge were extracted from the vehicle response by using empirical mode decomposition. Bu et al. (2006) measured the dynamic response of a vehicle moving on top of a simply supported Euler–Bernoulli beam. The vehicle served as a sensor and force transducer to detect damage defined in terms of the reduction of flexural stiffness. The model incorporated noise measurements, road surface roughness, and model errors such as underestimating vehicle parameters or bridge flexural stiffness.

Kim and Kawatani (2008) developed a pseudo-static damage detection method that makes use of the coupled vibration of a vehicle-bridge system. It requires data collected from both the bridge and the vehicle to characterize the damage. A numerical model that included the roadway roughness effect was used to test the approach. It was subsequently validated experimentally for different vehicle speeds and different amounts of reduction of the moment of inertia of the girders. McGetrick et al. (2009) modeled a simplified quarter car-bridge interaction to extract the fundamental natural frequency and corresponding damping of the bridge from the spectra of the vehicle accelerations. They found that better accuracy was achieved at lower speeds and smoother road profiles. Moreover, the magnitude of the acceleration power spectral density's peaks decreased with increasing bridge damping and this decrease was easier to

detect with a smoother road profile. This work was validated experimentally by observing the effects of a vehicle moving across a steel girder that included a road surface profile. The effects of varying vehicle model mass and speed were investigated as well (McGetrick et al. 2010).

Isemoto et al. (2010) developed a hypothesis-testing scheme for damage detection based on the bridge vertical acceleration data induced by a passing vehicle. An experimental vehicle-bridge model, including roadway roughness, was used and only severe damage scenarios were identified. Miyamoto and Yabe (2011) exploited the vibration induced by a public bus for the indirect health monitoring of existing short- and medium-span reinforced/prestressed concrete bridges. The tests demonstrated a correlation between the vehicle vertical acceleration and the bridge vibration at midspan. By means of a numerical 3D finite element model, the distribution of characteristic deflection values was found for a particular driving speed and two severe damage scenarios.

Yin and Tang (2011) proposed a finite-element method to simulate the interaction of a vehicle and a cable-stayed bridge. The vertical displacement from the vehicle was used to identify tension loss and deck damage. The relative displacement of a passing vehicle of a bridge with known damaged conditions is used to generate a vector basis. The proper orthogonal decomposition on the relative displacement of a vehicle passing a bridge with an unknown damage condition is optimized with the known basis, and parameters of the unknown damaged bridges are reconstructed. Finally, Sirigoringo and Fujino (2012) proposed an indirect approach to estimate the fundamental natural frequency of a bridge using the response of a passing instrumented vehicle. The method was validated experimentally on a full-scale simply supported short span bridge by using a light commercial vehicle instrumented with accelerometers. The spectra of the vehicle's dynamic responses while crossing the bridge were analyzed to reveal the first natural frequency of the bridge when the vehicle moved with constant velocity. The experimental study considered traveling speed ranging from 10 to 30 m/s.



All of the above indirect monitoring studies aimed at identifying the dynamic parameters of a bridge by either observing a single damage-sensitive feature or by optimizing model-based damaged sensitive vectors. The authors of these studies, however, did not report on detecting various types of damage conditions, the confidence with which the detection was ascertained, or the effects of different boundary conditions, weather patterns, traffic loads, and comprehensive inspection of the vehicle's speed on the structural diagnosis.

In this chapter, results are presented from a study that aims at bridging this gap. The long-term objective is to create a decentralized monitoring approach using fleets of vehicles that can continuously store or send data about the bridges over which they travel. In the laboratory, a bridge model is subjected to different vehicle speeds, damage scenarios, and structural boundary conditions. In addition to the indirect measurement of the bridge motion obtained through the vehicle vibration, other three sensors were directly on the bridge. Contrary to previous studies, the indirect and the direct data were used independently, and introduce a new detection algorithm. This allows comparing the indirect and the direct strategies and to evaluate the effectiveness of our indirect damage detection algorithm.

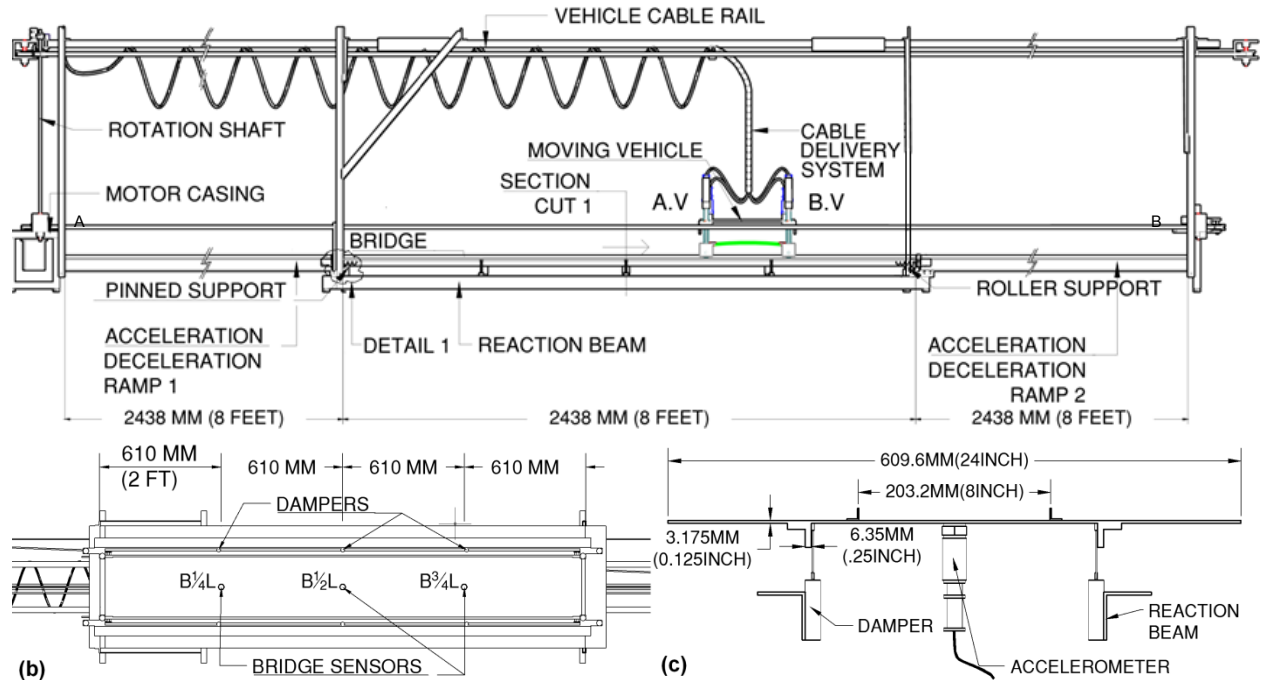
### ***3.2 Experimental Setup and Protocol***

A laboratory experimental setup was built to collect data from a vehicle, which could be used to detect changes in the condition of the bridge. Using this model, acceleration data from a bridge structure and a vehicle passing over it can be collected and later analyzed for characterizing vehicle-bridge interaction patterns. The complete experimental setup consists of mechanical components that make up the bridge and vehicle system, a vehicle motion control system, and data acquisition equipment. The different mechanical components resemble a simply supported bridge structure and a four-wheeled vehicle with an independent suspension system at each wheel. The motion control equipment is able to move the vehicle over an acceleration ramp, a bridge and a deceleration ramp, causing the vehicle to reach a target

speed before the end of the acceleration ramp, then maintain that velocity over the bridge, followed by a deceleration of the vehicle so that it stops at the end of the deceleration ramp. The data acquisition system records accelerations at different locations on the vehicle and the bridge, as well as the position of the vehicle. This experimental setup was inspired by the work of Kim et al. (2010).

An overview of the setup is shown in Figure 13. The vehicle, approximately in the middle of the figure, is pulled by a belt system. The vehicle was instrumented with Vibra-metrics accelerometers (Model 5102) powered by cables supported by a cable delivery system that moves parallel to the vehicle. The cables and the vehicle are propelled by a motor at the leftmost part of the experimental setup.

The travelling path of the vehicle corresponds to the acceleration/deceleration ramps and the bridge as labeled in Figure 13 a. The simply supported bridge structure is in the middle of the travelling path. Below the simply supported bridge there are two reaction beams that are used to support the bridge reactions and the added dampers.



**Figure 13: Experimental setup.**  
 a) General lateral view. b) Bridge bottom view. c) Bridge cross section.

### 3.2.1 Details of the Bridge and Vehicle Models

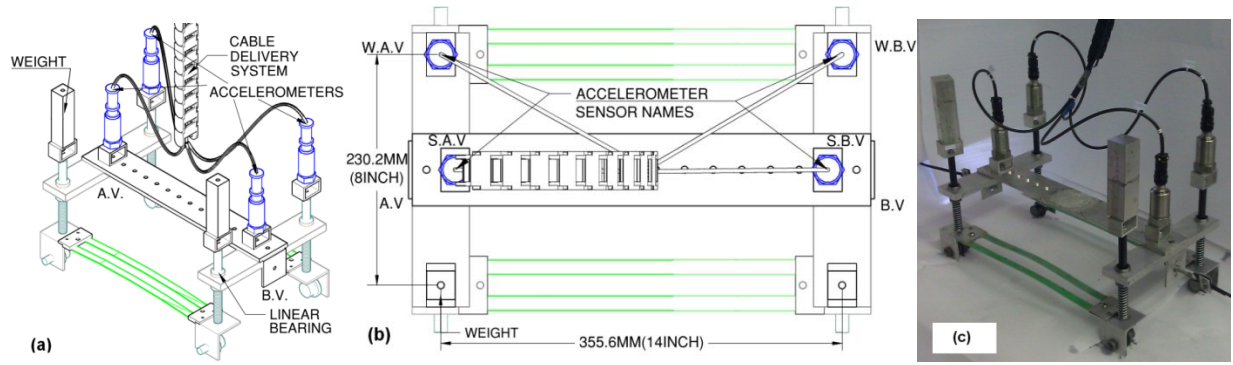
The bridge is simply supported by a roller support at the left and a pinned support at the right. The vehicle enters the bridge from the left. The whole system is constructed to act as a closed force loop system. The longitudinal forces generated by the motor to move the vehicle are transmitted between the two supports by two connecting beams labeled as “reaction beams” in Figure 13a. The bridge structure is instrumented with three 5102 Vibra-metrics accelerometers as in Figure 13b. The sensors are equally spaced along the longitudinal direction of the bridge and named accordingly as B1/4L, B1/2L and B3/4L where L=2438 mm. The reaction beams act as a support for localized dampers that connect to the bridge structure as in Figure 13c. The bridge deck consists of an aluminum plate, and two angle beams act as the bridge girders. On top of the plate two angle beams serve as rails for the travel path of the vehicle. Detailed dimensions of the bridge section are shown in Figure 13c.

The bridge has a total mass of 18.3 kg, a fundamental natural frequency of 7.23 Hz, a fraction of critical damping of 3.6 percent. These are the properties of the bridge in the pristine condition, later referred to as Scenario 1.

Figure 14a shows a 3D view of the vehicle constructed for the experimental setup with the main components labeled. The vehicle was instrumented with two accelerometers connected to the suspension shafts in order to record the acceleration at the wheel level and with two accelerometers placed on the suspension to acquire data filtered by the suspension system. To keep the symmetry of the vehicle, two calibrated weights were placed on top of the un-sensed wheel shafts. Similarly to the bridge structure, the vehicle was built mainly with aluminum parts.

Two reference points are labeled on the longitudinal direction of the vehicle as points A Vehicle (A.V) and B Vehicle (B.V). A top view of the vehicle is shown in Figure 14b. The length and width of the vehicle as well as the labels assigned to the four sensors are also indicated. The sensor labels are defined by their position and location to the reference point. Suspension A.V and Suspension B.V are labeled S.A.V and S.B.V, respectively, and the two wheel level sensor locations are labeled W.A.V and W.B.V. A picture of the model vehicle is shown in Figure 14c.

The frequency of the A.V and B.V axles of the vehicle were determined through free vibration experiments on the suspension. These experiments were performed on the vehicle when separated from the belt of the vehicle motion control system. The frequencies were obtained by averaging the power spectra of five free vibration experiments; the results are summarized in Table 14. Damping in both axles was observed to be equal to the critical damping; that is, at the limit between vibration and non-vibration.



**Figure 14: Experimental vehicle CAD drawings. (a) Parametric view. (b) Top view. (c) Vehicle picture.**

**Table 14: Vehicle properties.**

Vehicle weight [kg]	4.8
A.V axle frequency[Hz]	5.0
B.V axle frequency[Hz]	5.5

### 3.2.2 Motion Control and Data Acquisition Equipment

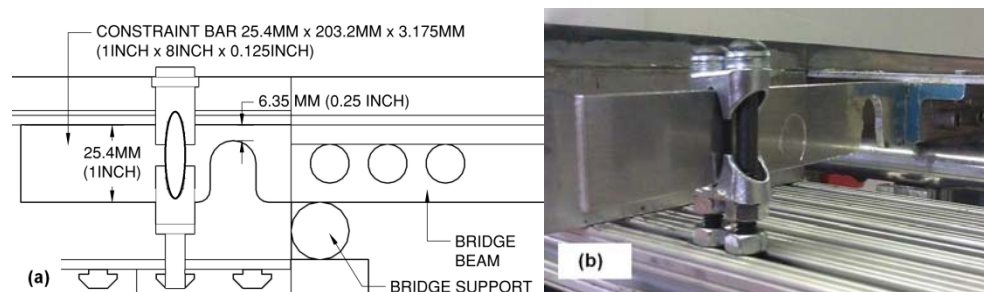
A National Instruments® PXI system running in LabView® was assembled to operate the instrumented vehicle and to allow for data acquisition and storage. The system consisted of a PXI Chassis (NI PXI 1031) with a motion control card (NI PXI 7342), a motion interface (UMI 7772), a stepper drive (P70360) and a dual shaft stepper motor (NEMA 34). A feedback loop for position was achieved with an encoder. The acceleration data were digitized and stored for post-processing using two digitizers (NI 9234).

### 3.2.3 Protocol

Three different types of “damage” scenarios were designed: 1) variations on the support condition by imposing rotational restraints, 2) increase of damping at different locations, and 3) a mass increase at the midspan. For each kind, four levels of severity were devised in order to obtain a total of 12 different damage scenarios. Table 15 shows the twelve conditions of damage. For each case the resonance frequency and the critical damping are reported and compared to the baseline, i.e. Scenario 1. For all cases, the fundamental natural frequency of

vibration and the damping coefficient are determined by means of conventional free-vibration experiments.







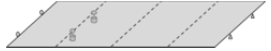
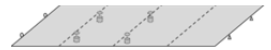





The rotational restraint mechanism was built into each of the four beam supports of the bridge model. As shown in Figure 15a, an aluminum bar (12x1x1/8 inch) was attached to the main girder of the bridge at one extreme and connected to the support at the other extreme to provide vertical restraint. The plate was drilled down to 6.35 mm [1/4 in] with 12.7 mm radius [1/2 in] to provide only a partial restraint.



**Figure 15: Detail 1 – Roller support - Rotational restraint (a) technical drawing and (b) picture.**

Variation of the rotational restraints simulates the case of rubber bearings becoming stiffer in time or steel corrosion occurring on rocker supports. This condition is denoted as frozen bearings and it is a common cause of undesired stress in the structure, and, therefore, a reduction in the load capacity. In Table 15, the variations of the rotational restraints are described as scenarios 2 to SC5. In Scenarios 2-5, one, two, three and all four supports are restrained, respectively. As expected, the greater the number of rotational restraints, the higher the fundamental frequency, which provides an indicator of change to the bridge structure.

The variation of localized damping is achieved by adding dampers to the bridge at those locations schematized in Table 15 (Scenarios 6 to 9) according to the scheme presented in Figure 13c. A set of AIRPOT adjustable dampers were used. They were calibrated to provide the same damping coefficient. In Scenarios 6-9, one, two, four and six dampers, respectively were attached to the bridge structure as depicted in the schematics of Table 15.

Table 15: Damage scenarios.					
Schematics	SC	f [Hz]	% f shift	% $z_{crit}$	% $z$ shift
	1	7.23	-	3.63	-
	2	7.46	3.17	6.34	74.9
	3	7.66	6.00	6.45	77.8
	4	8.11	12.2	7.97	119
	5	8.56	18.4	9.43	158
	6	7.24	0.17	8.52	134
	7	7.25	0.28	11.3	211
	8	7.28	0.73	26.4	629
	9	7.30	0.98	31.4	766
	10	7.19	0.56	4.44	22.4
	11	7.18	0.66	4.34	19.5
	12	7.14	1.29	4.07	12.2
	13	7.09	1.85	4.37	20.5

Finally, the concentrated mass at the midspan of the structure consisted of weights equal to 50 g, 100 g , 200g and 300 g, and referred to as Scenarios 10 to 13, respectively, in Table 15. As expected, the presence of the mass, decreased the fundamental frequency of vibration of the structure.

Eight different vehicle speeds, varying from 1 m/s to 2.75 m/s, were considered for each damage scenario.

### 3.3 Signal Analysis and Classification

In general terms, the task of distinguishing various bridge conditions is a signal-processing task of classification. The classification task is first described in general, and then it is explained how it was used in our setting. Assume a real signal  $x$  of length  $N$ , i.e.,  $x \in R^N$  (see Original

signal in Figure 16). The problem, then, can be formulated as that of designing a map from the signal space of vibrational signals  $X \subset R^N$  to a response space of class labels  $Y \subset \{1, 2, \dots, C\}$  (in Figure 4 these are Damaged and Pristine labels). That is, the decision  $d : X \rightarrow Y$  is the map that associates an input signal with a class label.

A general classification system consists of a feature extractor and a classifier (see Figure 16). Since the dimensionality of the input space is typically large, the feature extractor is introduced to reduce this dimensionality by setting up a feature space  $F \subset R^k$  where  $k \leq N$  between the input space and the response space. The feature extractor is the map defined as  $f : X \rightarrow F$  and the classifier as a map  $g : F \rightarrow Y$ .

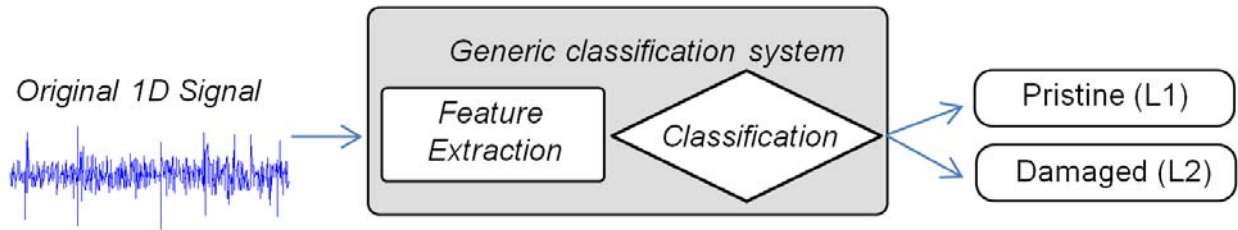


Figure 16: General classification system.

### 3.3.1 Preprocessing

Figure 17 shows the signal obtained from the vibration of the vehicle, from the time when it starts moving, through its motion across the bridge, until it is brought to a stop. The only relevant information for the bridge characterization, however, is that of the vehicle moving across the bridge. The reference start time was chosen as the moment when the rear wheels enter the bridge and as the end time the instant when the front wheels exit the bridge. That portion of the signal is highlighted in Figure 17a-d by the two vertical lines. The extracted portions of the signals are then normalized to have zero mean and unit variance.



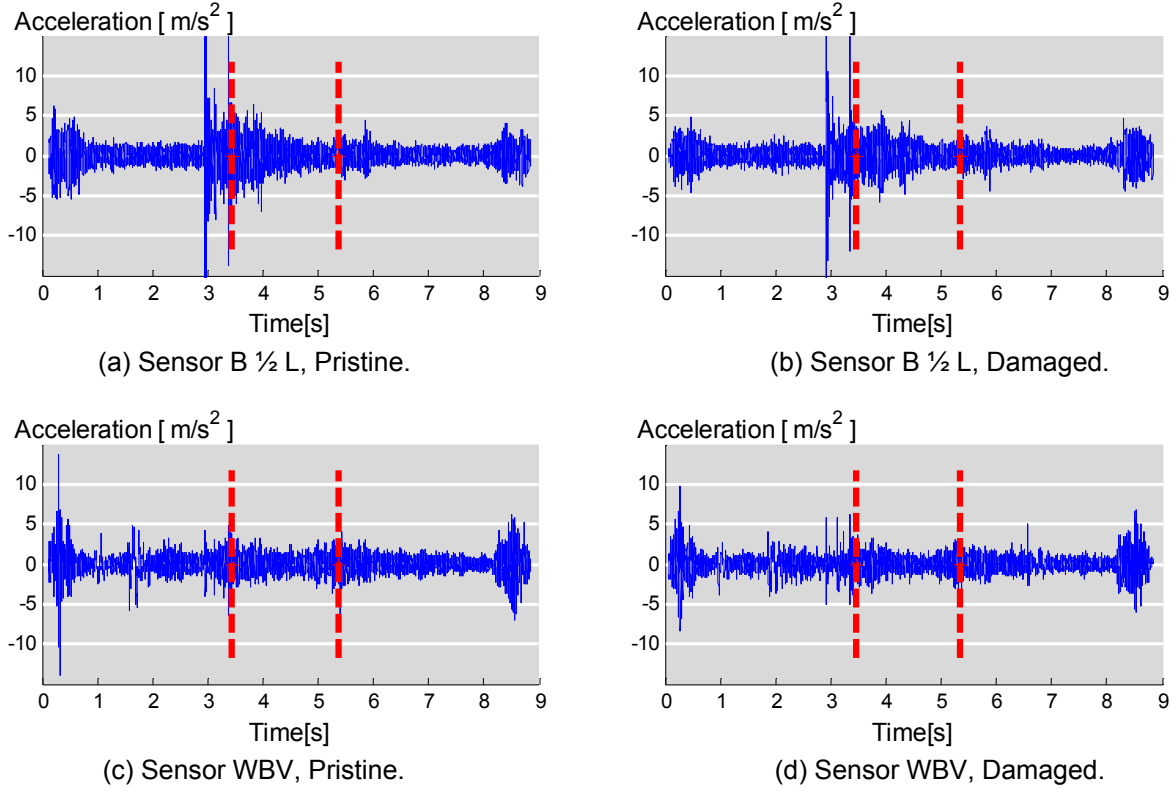
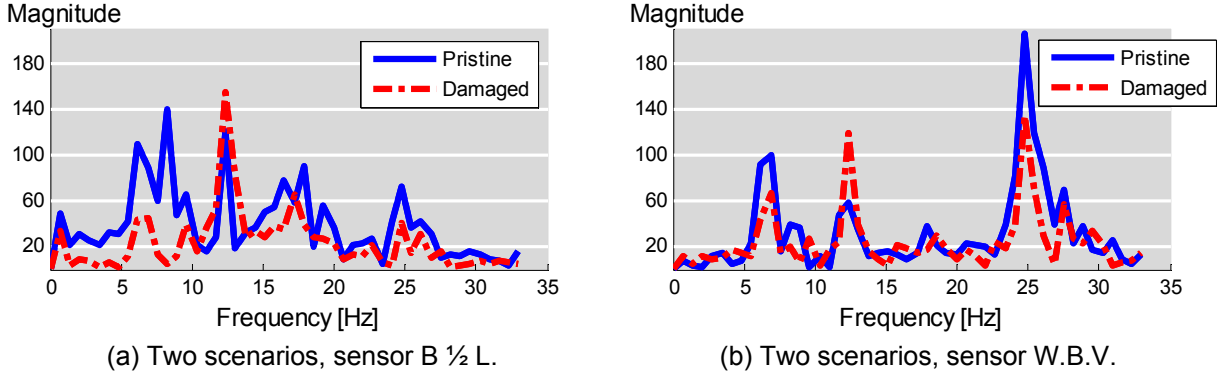


Figure 17: Time-domain signals.

### 3.3.2 Feature extraction

A linear structural system can be characterized in the frequency domain by its predominant natural frequencies, and their corresponding mode shapes and damping values. We explore therefore the use of frequency spectra characteristics for damage detection.

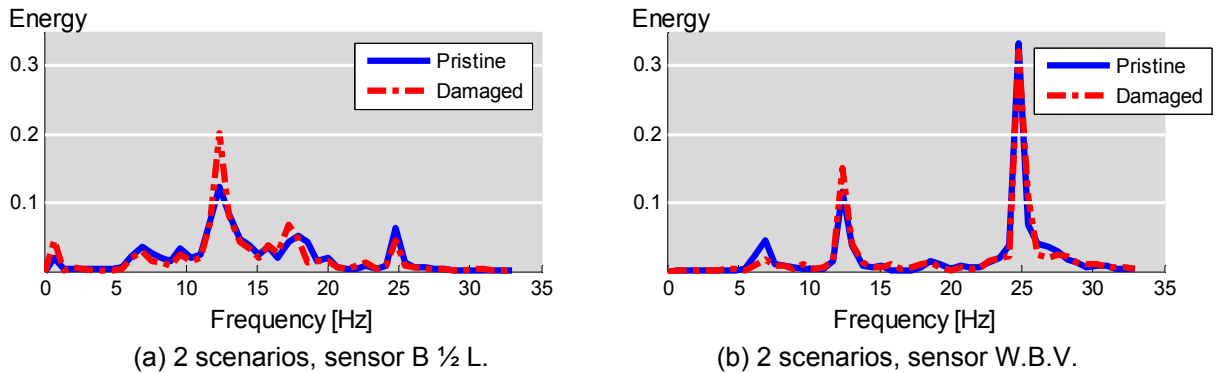
Considering the fundamental natural frequencies of the damage scenarios and the vehicle main bouncing frequency, we limited the analysis frequency spectrum to up to 33 Hz. For example, looking at the spectrum of the signal in Figure 18 for signals from two different scenarios, a pristine and a damaged one, we see that potentially we could tell responses apart from separate sensors by looking at magnitudes at certain characteristic frequencies. We thus decided to use frequencies as features, hoping to distinguish among different scenarios. Our task is then to find a set of features to maximize differentiation between classes.



**Figure 18: Discrete Fourier transform of the signal.**

Since the acceleration signal contains a large number of spikes and other transient signals, the spectra are noisy with little consistency between runs. To reduce noise and keep non-transient frequencies of interest, a typical approach is to average the spectra across frequency. Averaging the frequency spectra is a well-known technique used in noisy signal processing. For example, on radar signal analysis, a redundant number of antennas capture noisy signals from the same source and average them to increase the signal to noise ratio.

After averaging, we calculate the frequency-domain energy distribution for each scenario. This technique relies on the assumption that each scenario has its unique energy distribution in the frequency domain. Since we wish to tell classes apart and not individual runs, we average all the energy distributions from the same class and use the mean energy distribution as the representative member of that class (see Figure 19).



**Figure 19: Mean energy distribution (normalized to unit energy).**

Let  $\{x_i^{(c)}\}_{i=1}^{N_c}$  be a set of signals with  $N_c$  samples belonging to Class  $c$ . The Fourier energy map is

$$\Gamma_c(j) = \frac{\sum_{i=1}^{N_c} \|w_j^T x_i^{(c)}\|^2}{\sum_{i=1}^{N_c} \|x_i^{(c)}\|^2} \quad (1)$$

where  $w$  denotes Fourier basis vector and  $j$  denotes the frequency band. To evaluate the power of discrimination of every Fourier basis vector, we need a discriminant measure  $D$  to evaluate the power of discrimination. We will assume that higher discriminant power provides higher discrimination between classes.

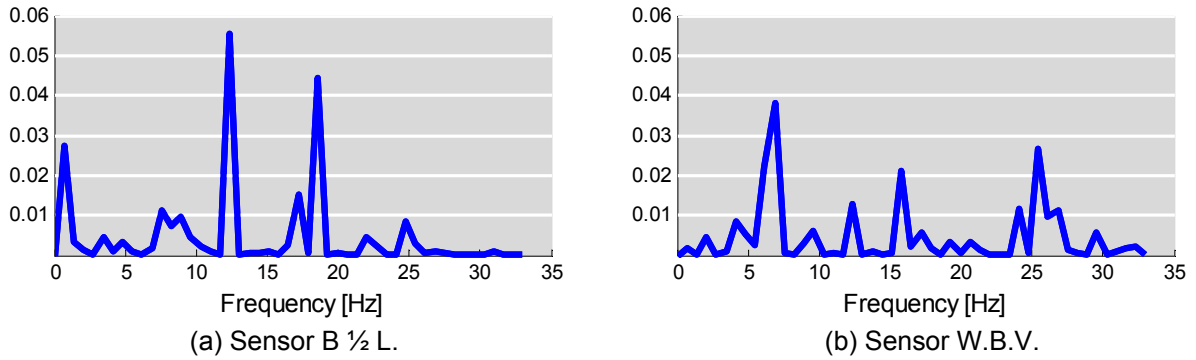
For the  $j$ th Fourier basis vector, the power of discrimination  $\Delta$  is denoted by

$$\Delta_j = D(\{\Gamma_c(j)\}_{c=1}^C). \quad (2)$$

There exist numerous choices for the discriminant measure; we use J-divergence (Kullback and Leibler 1951). Let  $p = \{p_i\}_{i=1}^n$ ,  $q = \{q_i\}_{i=1}^n$  be two nonnegative sequences with  $\sum p_i = \sum q_i = 1$ , J-divergence between  $p$  and  $q$ ,

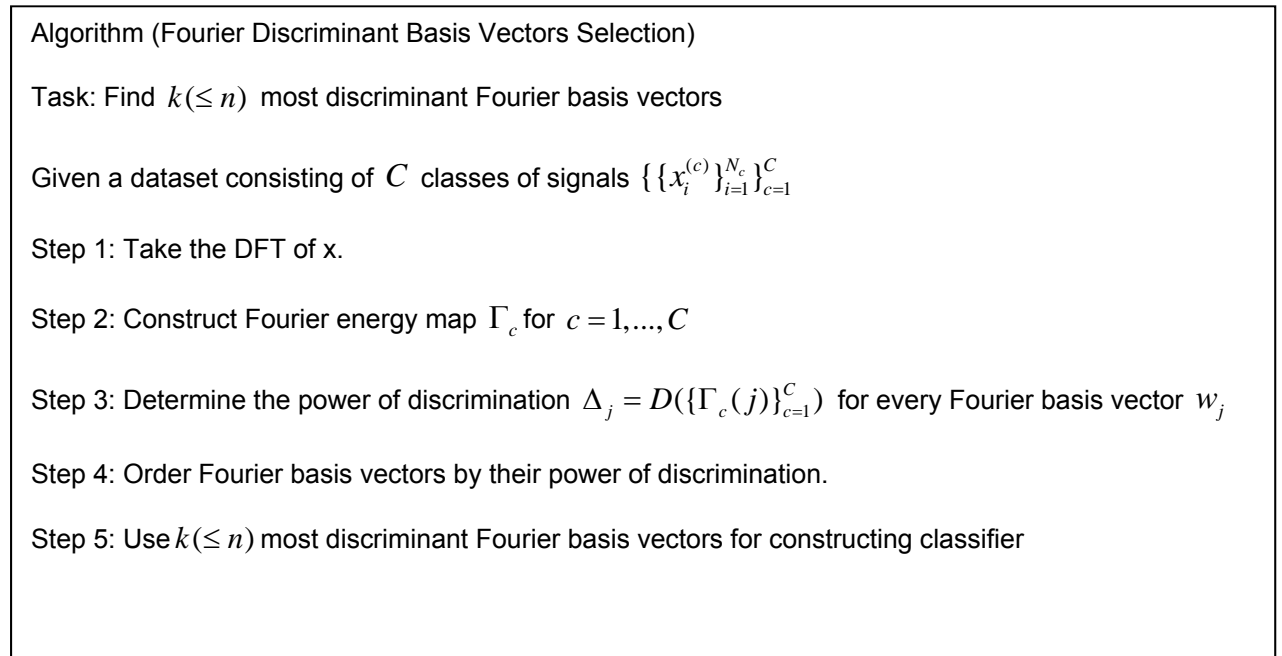
$$J(p, q) = \sum_{i=1}^n p_i \log \frac{p_i}{q_i} + \sum_{i=1}^n q_i \log \frac{q_i}{p_i} \quad (3)$$

Figure 20 shows a graph of the discriminant power between the frequency signals previously depicted in Figure 19.



**Figure 20: Discriminant power (normalized to unit discriminant power).**

To help understand the feature selection method, we summarize our assumptions and conclusions thus far: 1) to differentiate signals from different scenarios, we use frequencies as features. 2) if the discriminant power is higher, it is easier to discriminate between classes. The discriminant power will thus predict how well a feature will perform during classification; 3) a small number of frequencies provide most of the discriminative power; in other words, the frequency feature set is sparse. Only those frequencies that have large discriminative power are selected (this is called nonlinear approximation); see Figure 21.



**Figure 21: Summary of feature extraction process.**

This selection method performs nonlinear approximation in the Fourier domain and is data adaptive. Different data may give different frequency information and different discriminant powers. Since this method learns from the data and always chooses the frequencies with large discriminant power, it is more robust than traditional linear approximation.

Figure 22 shows the first 3D feature space. Blue circles denote the pristine scenario and red asterisks the damaged scenario. We see that with just three Fourier discriminant basis vectors, it is easy to separate the two classes.

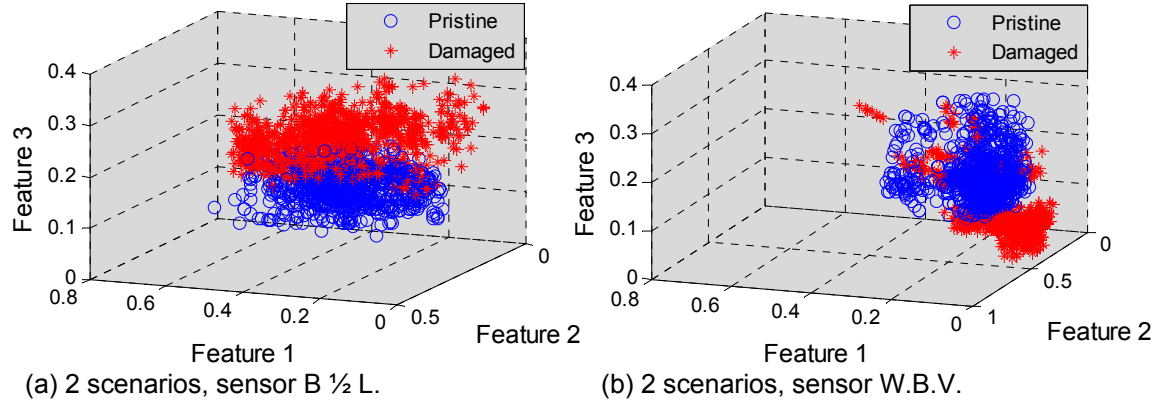


Figure 22: Clustering of two scenarios.

### 3.3.3 Classification

The second part of a classification system is the classifier itself. It takes as input a feature vector and outputs a class label. The classification problem here is called supervised learning, as a labeled training set is given. Many different classifiers are available, such as naïve Bayes, neural networks and many others (Duda et al 2000). In this work the support vector machine (SVM) was chose, which is described next.

When looking for the best boundary between classes, it is desired to achieve two things: 1) find the boundary that gives high classification accuracy; 2) avoid overfitting. To satisfy these two requirements, SVM maximizes the margin, which means the distance between a decision boundary and a data point, and expresses it as a function of the weight vector and bias of the separating hyperplane, which is used to separate the space into two half spaces.

In each scenario, data for 32 runs was collected, out of which 3 were averaged, yielding  $C_{32}^3=4960$  available samples for each scenario. As our dataset, 1000 out of 4960 samples were chosen for each scenario. 20-fold cross validation was performed. Each time, 2000 data samples, consisting of 1900 training samples and 100 testing samples, were used to create and test the SVM-based classifier. A Fourier discriminant basis search algorithm was used and the top 5 frequencies that provide the largest discriminant power were selected as features. Then a kernel SVM was used as the classifier.

### **3.4 Classification Results**

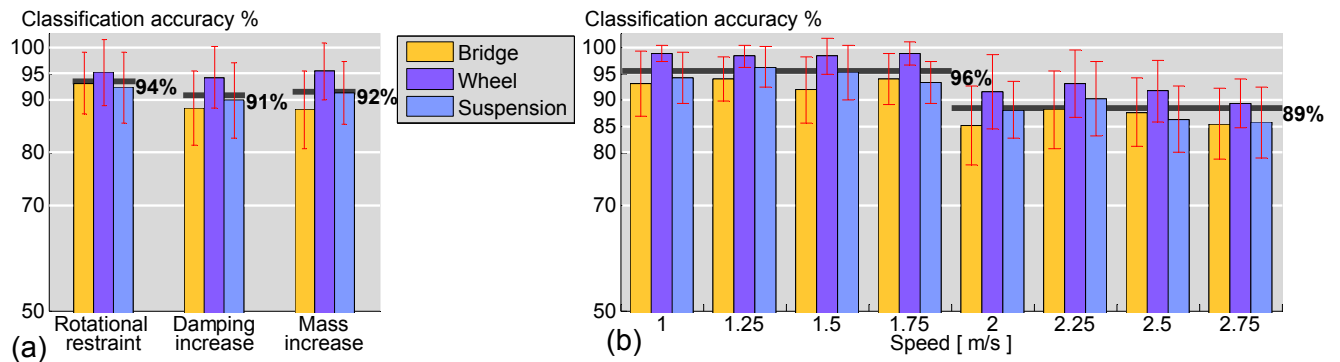
The results of the classification experiments are presented and discussed in terms of the classification accuracy, which is defined as the number of test samples correctly classified divided by the total number of test samples.

For the two classes defined, pristine and damaged, scenarios 2-13 belonged to the latter class. The data collected from all seven accelerometers were used.

Figure 23 shows the variation of the average classification accuracy for different variables. Figure 23a shows the average across the different severities, speeds and sensor locations for each damage type. The three bridge sensors, B1/4L, B1/2L and B3/4L, are averaged and referred to as “Bridge”, the two sensors at the wheel level, (W.A.V and W.B.V) are averaged and referred to as “Wheel” and the two sensors at the suspension level, (S.A.V and S.B.V) are averaged and referred to as “Suspension”. The standard deviation across the averaged variables is shown at the top of each bar. An average classification accuracy for all the sensors for each damage type is depicted with a black line and corresponding percentage. The baseline in Figure 23a and b is 50%, which is the expected probability of randomly choosing between two labels (pristine or damaged). Classification accuracy values of over 90% are obtained despite the subtle changes introduced in the bridge structure. The amount of change inflicted was deliberately small to test the detection capability of the combined indirect approach using the signal processing techniques described in Section 3.3. The signals from the sensors located at the wheel level were classified consistently across the different damage types, and more accurately than those from the sensors located on the bridge or on the vehicle at the suspension level.

The classification results in Figure 23b show how the average classification accuracy for all damage scenarios varies for different vehicle speeds. Similarly to Figure 23a, each bar represents the mean accuracy classification across the different damage scenarios. At the top

of each bar, the corresponding standard deviation is shown. Looking at Figure 23b, one can see that there is a jump between the first four speeds, between 1 and 1.75 m/s and the four higher speeds from 2 to 2.75 m/s. The average across the two groups of speeds is shown by a black line and corresponding percentage. There is about a 7% difference in classification accuracy between these two speed ranges. This classification accuracy difference is consistent for the average classification accuracy of the sensors at the different locations (i.e., Bridge, Wheel and Suspension).

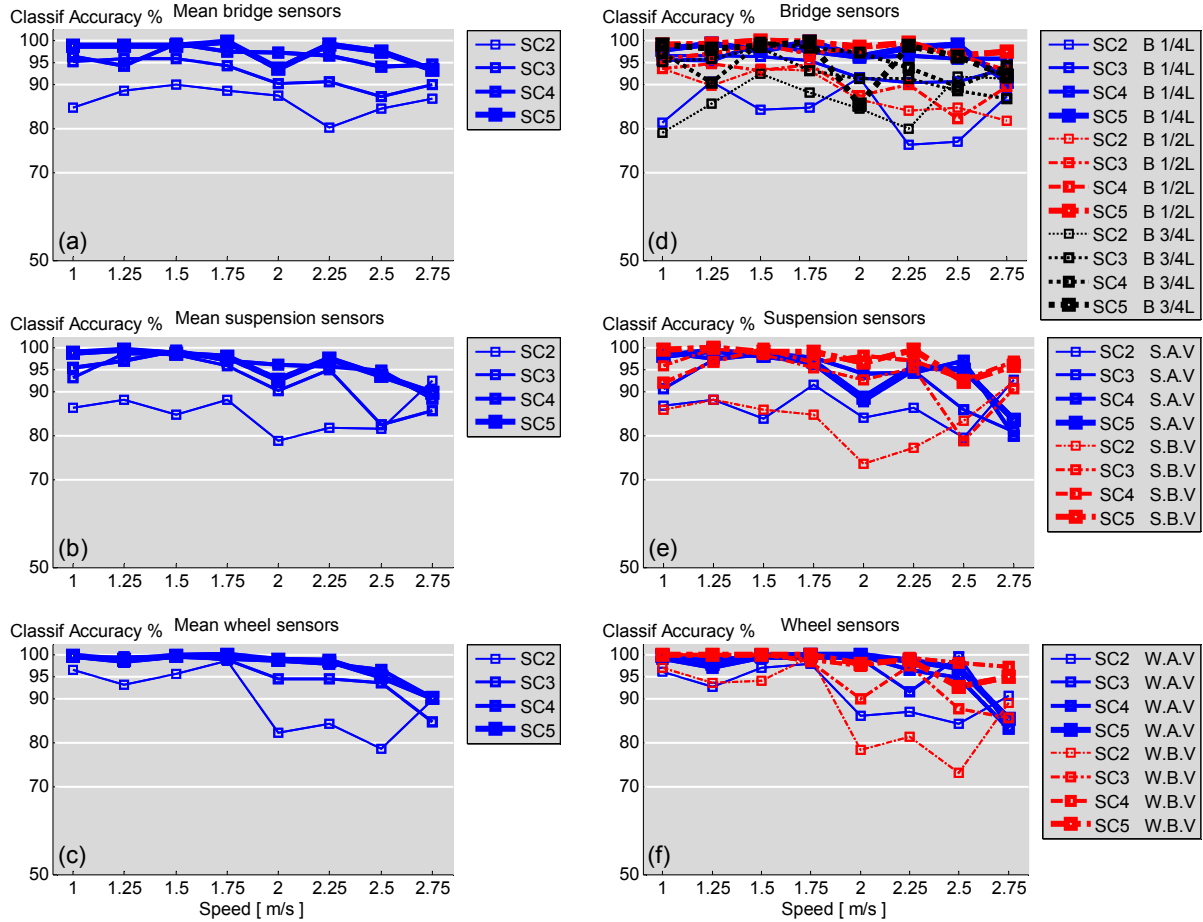


**Figure 23: Classification accuracy results (a) Average by damage types. (b) Average by speeds.**

Figure 24 illustrates the sensitivity of the classification method to different levels of severity of the different damage types inflicted in the damage scenarios. Figure 24a, b and c shows the average classification for the different damage severity levels for the rotational restraint damage type for different vehicle speeds. For all of these graphs, the thickness of the line depicts the level of damage, with the thinnest line indicating the least amount of damage inflicted (e.g., only one of four rotational restraints invoked in SC2) and the thickest line indicating the maximum amount of damage inflicted (e.g., all four rotational restraints invoked in SC5).

Figure 24a, b and c shows the average classification accuracy for each rotational restraint damage severity level for the signals from all the sensors on the bridge, all the sensors on the suspension, and all the sensors on the wheel, respectively. Figure 24d, e, and f break the results down for each sensor and show the average classification accuracy for each rotational

restraint damage severity level for each signal from the three sensors on the bridge, B1/4L, B1/2L and B3/4L, from the two sensors on the suspension, S.A.V and S.B.V, and from the two sensors on the wheel, W.A.V and W.B.V, respectively.

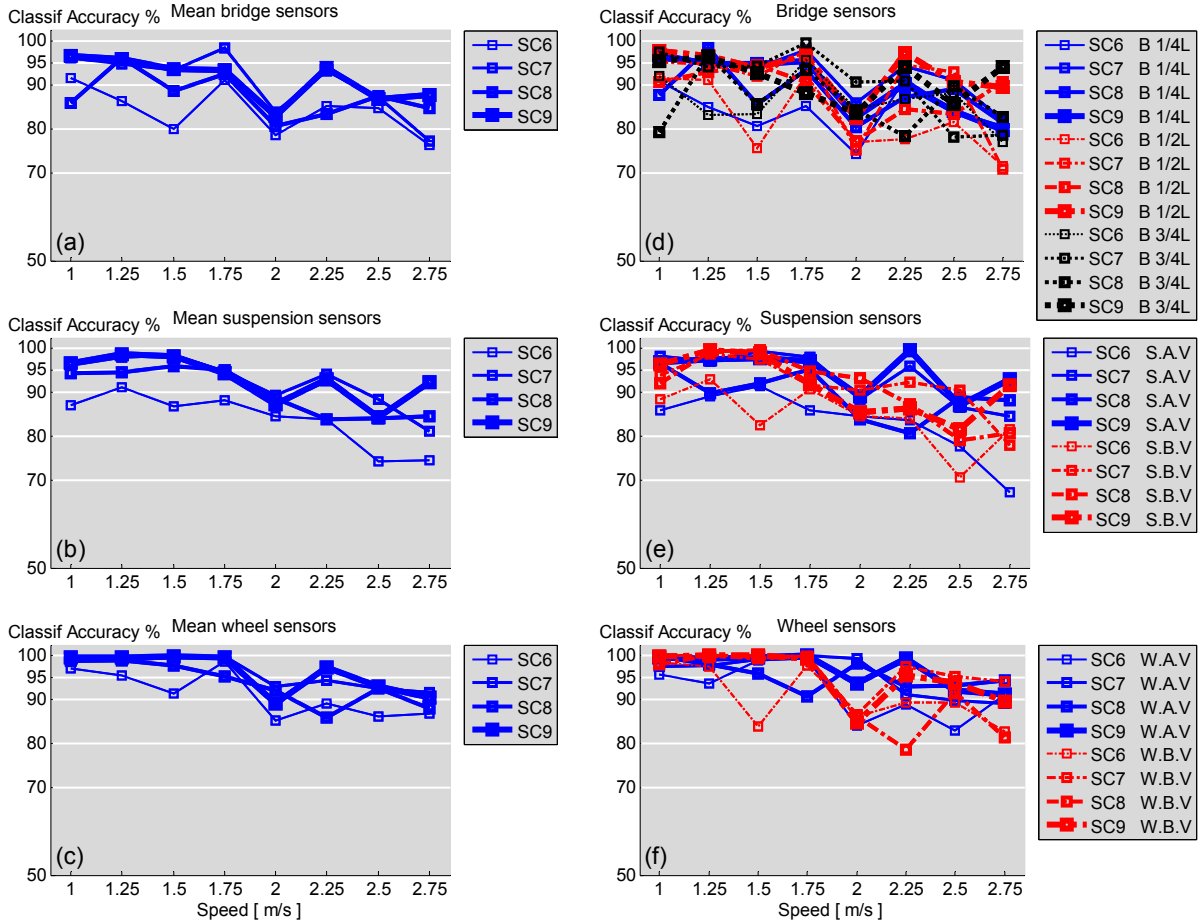


**Figure 24: Classification results for rotational restraint scenarios (a,d) Bridge sensors, (b,e) Suspension sensors (c,f) Wheel sensors.**

As can be seen from the graphs in Figure 24, the classification accuracy for SC2 is lower than for the other rotational restraint scenarios (SC3, SC4 and SC5), and increases as the severity of damage increases. For SC2, there is a variation in the classification accuracy with respect to the speed. However, the more severe rotational restraint scenarios seem to be more independent of the speed with high classification accuracy for low speeds and a slight parabolic decrease for higher speeds. No significant difference in the classification accuracy is apparent in Figure 24 regarding the sensor location. This shows that in terms of classification accuracy,



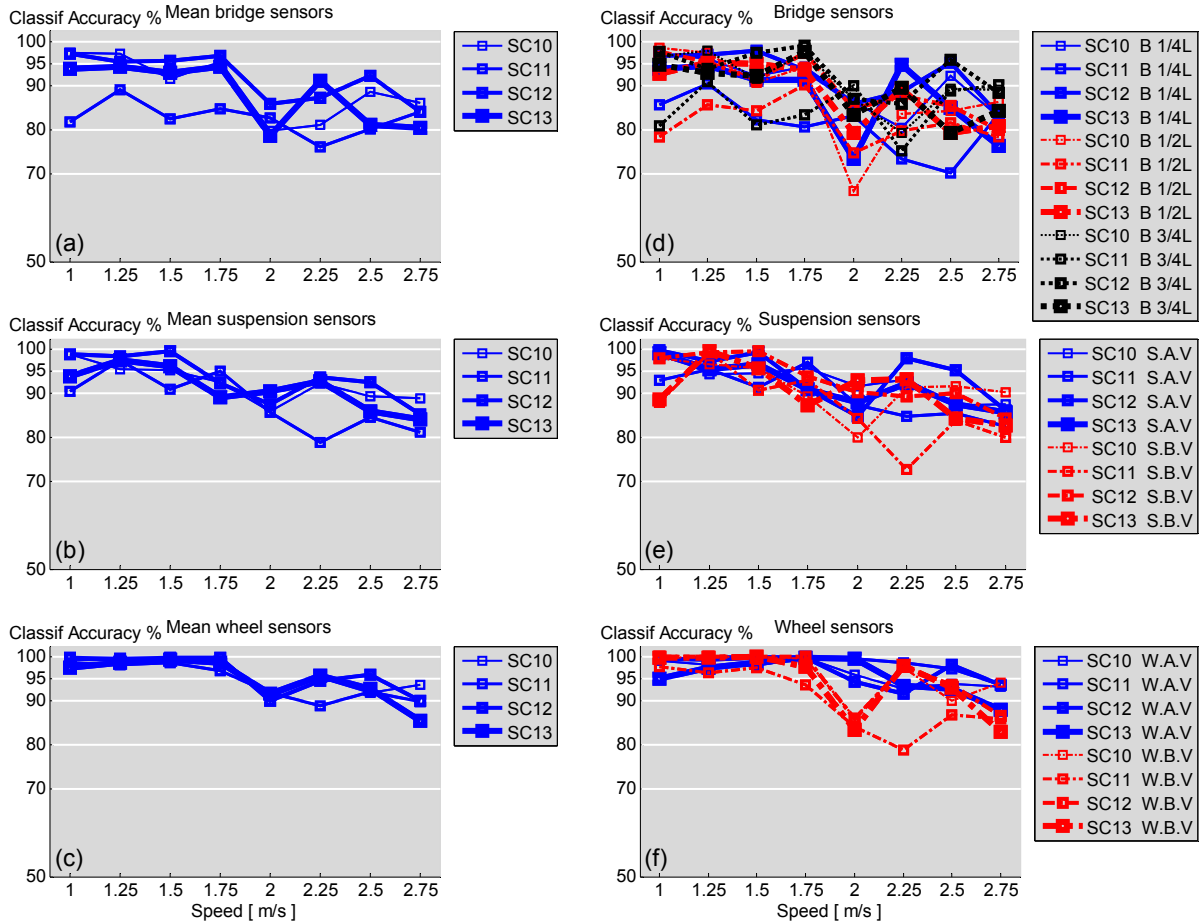
the signal processing approach performs as well with sensor data from the vehicle (sensor or wheel) as with sensor data directly measured on the bridge. In other words, the results would indicate that in this particular set of experiments, the indirect approach has a classification accuracy that is as good as that of the direct approach.



**Figure 25: Classification results for damping increase scenarios. (a,d) Bridge sensors, (b,e) Suspension sensors (c,f) Wheel sensors.**

Figure 25 and Figure 26 are similar in nature to Figure 24, but display the classification accuracies for the two other damage types explored: the scenarios with increasing amounts of damping and with increasing amounts of mass. Figure 25a b and c shows Scenario 6, the scenario with the single damper, as the one with the least classification accuracy across all speeds. In terms of effects due to changes of vehicle speed, a decrease in the classification accuracy appears to occur when the vehicle velocity is 2 m/s as shown in Figure 25a. In general

terms, the same observations from Figure 24 apply to Figure 25. There is a slight decrease of the classification accuracy with higher speeds, and the classification accuracy seems to be independent of the sensor location; that is, there is little difference in the classification capability between the direct and the indirect approaches. Figure 26 shows the classification results for the scenarios with a mass increase at the midspan. Even though the inflicted change in the bridge structure is quite subtle, the classification accuracy is high, especially for the lower speeds. The same observations made for Figure 25 can be made for Figure 26 regarding the variation of classification accuracies with respect to the vehicle speed and the sensor locations.



**Figure 26: Classification results for concentrated mass scenarios. (a,d) Bridge sensors, (b,e) Suspension sensors (c,f) Wheel sensors.**

### 3.5 Discussion

The damage detection capability of an indirect monitoring approach based on data collected from moving vehicles was proposed and evaluated for bridge monitoring by applying classification to experimental data taken from a laboratory vehicle-bridge physical model.

To perform numerous test repetitions, a fully automatic vehicle-bridge model needed to be built. In this study, the amount of experimental data samples is significantly greater than that from previous experiments. Each scenario was run 32 times at eight different velocities. Three different damage types were built into the experimental setting, and each damage type had four different severity scenarios.

The synchronized acceleration data from the bridge and the vehicle, and the vehicle position data, allowed for the comparison of the *direct* and *indirect* approaches in terms of the accuracy with which each could classify the existence of damage for different extents of damage.

A feature extraction technique based on averaging the power spectrum from a set of data was used to achieve very high noise reduction. Then, features extracted from the Fourier domain were automatically chosen from the denoised data samples based on their significance and classified using an SVM classifier.

High classification accuracy was achieved across three *distinct types of changes* inflicted into the bridge structure: 1) a change in the support conditions obtained by introducing rotational restraints at the supports; 2) an increase in the damping of the bridge structure; and 3) a localized mass increase at the midspan of the bridge.

The *severity* of the changes inflicted in the bridge structure was consistent with higher classification accuracy. For example, SC3, SC4 and SC5 imposed more significant changes into the bridge structure than SC2, and consistently higher classification accuracy was obtained. Nonetheless, the classification accuracy achieved for the subtle change inflicted on SC2 is on average above 85%.

The detection of the various changes in the bridge structure was quite insensitive to the vehicle *speed*. This effect can be important for practical applications where vehicle speeds cannot be readily controlled. However, a small jump was observed between the lower and higher speeds, where the classification accuracy decreases by about 7 percent at the higher speeds.

Independent of the sensor *location*, high classification accuracy was achieved across all the sensors. The *indirect* and *direct* approaches seem to be equally effective for damage detection when applying the proposed signal processing techniques. Of the two sensor locations considered in the *indirect* approach, the wheel level and the suspension level, the sensors at the wheel level performed better than the sensors at the suspension level.

Given the simplicity of the model considered, the results presented are strictly applicable only to the particular experimental setup and cannot be generalized for full-scale structures at this time. On the other hand, we observed a high degree of consistency in the classification accuracies across the very different types and severity of damage and for different vehicle speeds. This gives us hope that our approach might be applicable to more general systems. Clearly, further research is needed to validate the robustness of these results for more realistic systems and conditions, including different roadway roughness profiles, atmospheric conditions and other bridge interaction variables such as different vehicle/bridge mass ratios, the effect of ongoing traffic and torsional effects on the bridge by non-symmetric loading from the vehicle path.

## **Chapter 4: Effect of temperature and boundary condition on the indirect health monitoring of a bridge model**

### ***4.1 Introduction***

The indirect approach to the health monitoring of bridge structures uses a smaller number of sensors, mounted on moving vehicles that travel across the bridge of interest, to collect data that may help in identifying structural damage and thus serve as an indicator for more detailed analysis.

Chapters 3 presented the initial results of a study that proposes to employ fleets of vehicles to routinely acquire and send data about the bridges over which they travel. A laboratory-scaled (i.e., 8 ft. (2438 mm) long) bridge model was subjected to different vehicle speeds, damage scenarios, and structural boundary conditions. In addition to the indirect measurement of the bridge motion obtained through the vehicle vibration, sensors were installed on the bridge to compare the effectiveness of the proposed indirect approach to a conventional direct SHM paradigm. The indirect and direct approaches seem to be at least equally effective for damage detection when applying the proposed signal processing techniques. The average damage detection accuracy obtained was over 90% for three different types of damage scenarios and four different severities of damage. Of the two sensor locations considered in the indirect approach, the wheel level and the suspension level, the sensors at the wheel level performed better than the sensors at the suspension level. However, the previous results were constrained to one vehicle and one bridge.

The present Chapter 4 builds upon the work in Chapter 3 (Cerdeira et al 2012) and presents a study where the effect of three instrumented moving vehicles was evaluated on two Bridges; the effect of temperature; and simulated road roughness were also considered. With respect to the previous work in the area of indirect bridge health monitoring, this paper presents

four new evaluations of the effectiveness of this indirect SHM approach: 1) the effect of temperature and roughness on the accuracy of the damage classification; 2) the generality of the approach when three different vehicles instead of one are used to collect data; 3) the generality of the approach when two slightly different bridge models are tested; and 4) how well classification of damage scenarios can be performed for different locations and severities.

Although the environmental and operating conditions have been addressed in the literature for direct SHM approaches (Farrar et al. 1998; Peeters and Roeck 2001; Cornwell et al. 1999; Sohn 2007; Meruane and Heylen 2011; Yan et al. 2005a-2005b, Deraemaeker et al. 2008, Serker Kamrujjaman et al 2010, Zhu and Rizzo 2011), this paper presents new insights concerning the effect of certain environmental conditions on the indirect SHM approach using vehicle accelerations.

This chapter is organized into 4 sections, with the first being the introduction. The second section presents a description of the experimental setup and protocol used for the experiments described in this paper. The third section presents the experimental results in four subsections: a discussion of the effects of vehicle and bridge variations; a discussion of the effects of roadway roughness; a discussion of the effect of varying the location of damage and the effects of temperature gradients. The fourth section presents the discussion to the chapter.

## ***4.2 Experimental setup and protocol***

The indirect SHM proposed in this study was tested on two bridge models. A picture of the bridge setup, hereafter designated as B1, is presented in Figure 27a. A picture of the vehicle is presented in Figure 27b. Details and technical drawings of the experimental setup were presented in Section 3.2 and shown in Figure 13. The model consisted of three segments of 8ft. (2438 mm) long each: an acceleration ramp made of 2 in. x 1 in. x 1/8 in. (50.8 mm. x 25.4 mm. x 3.175 mm.) 6063-T52 Aluminum Arch. Channel section, a bridge deck consisting of a simply supported aluminum plate with angle sections as girders as previously shown in Figure 13c, and

a deceleration ramp identical to the first segment. The deck was a 8 ft.x 2 ft. (2438 x 610 mm) aluminum plate with thickness equal to 1/8 in. (3.175 mm). The second bridge herein indicated as B2, differed from B1 by having smaller (3.175 mm instead of 6.35 mm) angle sections as longitudinal girders (See Figure 13c).



**Figure 27: Experimental setup. a) General angle photo of experimental setup, b) Vehicle picture. W.A.V. is the wheel level on the A axle, and S.A.V is the suspension level on the A axle. W.B.V. and S.B.V. are the corresponding wheel and suspension levels on the B axle.**

The bridges were travelled over (and thus sensed) by the moving vehicle shown in Figure 27b. The vehicle was instrumented with four commercial accelerometers, two located at the wheel level and two at the suspension level. Other details and technical drawings are presented in Section 3.2. Figure 27b shows the sensor locations named according to the referent axle.

To create three different vehicles for testing the generality of our concept for different vehicles, three different masses were placed at the midspan of the bar connecting the front and rear axle of the vehicle. As such three vehicles with different dynamic properties were able to be used in testing the indirect SHM approach. The fundamental frequencies of the three vehicles are summarized in Table 16.

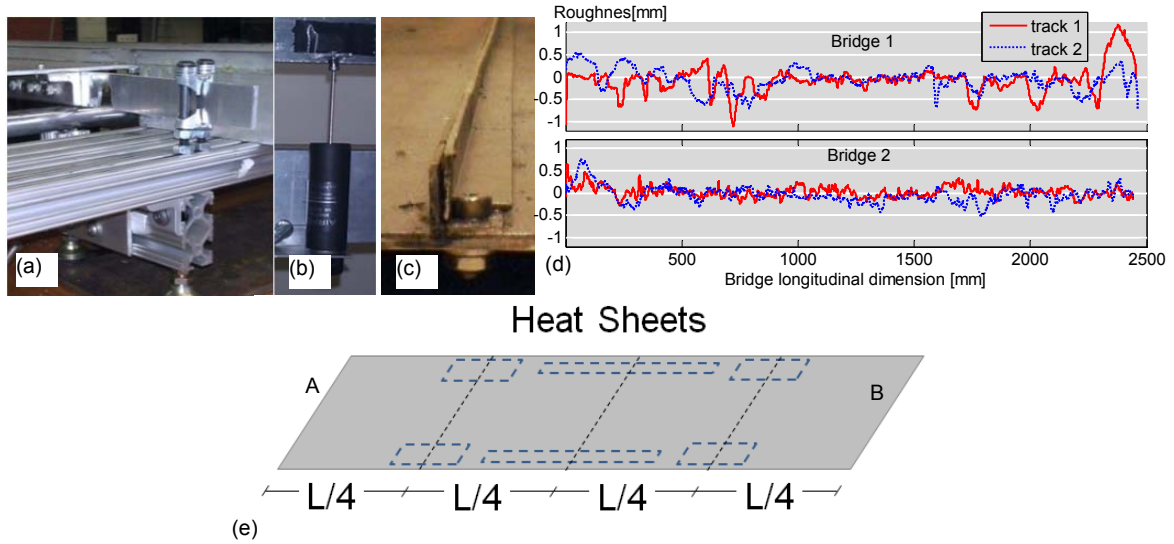
	<b>Table 16: Vehicle properties.</b>		
	<b>V1</b>	<b>V2</b>	<b>V3</b>
Vehicle weight [kg]	4.8	5.2	5.7
A.V axle frequency[Hz]	5.0	4.6	4.5
B.V axle frequency [Hz]	5.3	4.8	4.7

So as to compare the indirect SHM approach with a conventional SHM paradigm, both bridges were instrumented with three accelerometers located underneath the deck at equally spaced distances (see Figure 13b). All the sensors and the moving vehicles were controlled by a National Instruments® PXI system running LabView®. The motor control consisted of a PXI Chassis with a motion control card, a motion interface, a stepper drive and a dual shaft stepper motor. A feedback loop for position was achieved with an encoder. The acceleration data were digitized at 1650 Hz sampling rate and stored for post-processing.

In this study, the effect of damage scenarios, temperature variation, and surface roughness on the response of the sensors was evaluated. To simulate different damage scenarios, the following boundary conditions were varied: (a) rotational restraints, (b) damping and (c) mass. Rotational restraints were added to the bridge at the each of the four supports of the bridge girders as detailed in Figure 28a. Six dash-pot dampers (Figure 28b) were progressively connected to the deck to change the bridge damping characteristics. An additional mass (from 50g up to 300g) was positioned at different locations on the deck in order to simulate a change in the natural frequencies and mode shapes of the structure. Two roughness conditions, hereafter indicated as R1 and R2, were simulated when testing the indirect SHM approach for classifying each of the damage scenarios. R1 represents the case of accidental imperfections of nominally smooth guide rail over which the vehicle travels. R2 represents the case of a built-in roughness profile for a particular bridge. R2 was achieved by modifying the rail that guides the moving vehicle with an angle section that had been randomly filed down to generate a roughness profile as shown in Figure 28c. The roughness profile measured for B1R2 and B2R2 is shown in Figure 28d, where track 1 is the right rail on the A-B motion direction and track 2 the left rail on the A-B motion direction. Finally, six electric heat sheets were attached underneath the deck in order to model the effect of changes in temperature. The heat sheets location is shown in Figure 28e. A circuit was built to discretely turn on and off the heat sheets



and produce different temperature distribution. An infrared camera was used to record and report the bridge temperature scenarios.


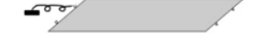


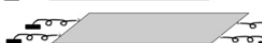

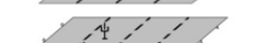
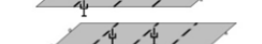
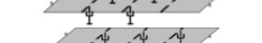
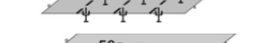
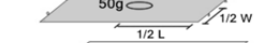
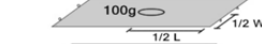



**Figure 28: Introduced modifications to the bridge structure. (a) Rotational restraints (b) Additional damping and (c) Roadway roughness profile built on top of guide rail (d) Measured additional roughness (e) Scheme for Heat Sheet locations. A and B are reference points for the forward travelling direction.**

Three sets of experiments were conducted. In the first set, 13 different boundary conditions were created and the three vehicles were used to monitor both bridges B1 and B2. Table 17 summarizes the location of the rotational restraints (scenarios SC020BiR1-SC050 BiR1), dashpots (SC060 BiR1-SC090 BiR1), and masses (SC100BiR1-SC130BiR1), where  $i=1$  for Bridge 1 and  $i=2$  for Bridge 2. The table also presents the corresponding fundamental frequency ( $f$  [Hz]) and % critical damping ( $\% \zeta_{crit}$ ) for both bridges. We used conventional free vibration testing to determine these dynamic parameters. The variation with respect to the baseline condition (SC010BiR1, the *undamaged* scenario) is presented as well in terms of % shift and  $\% \zeta_{crit}$  shift in Table 17. These dynamic parameters in Table 17 are shown to illustrate the magnitude of the change imposed to the bridge structure for the different damage scenarios. Then, classification analysis was performed with data collected from vehicle-bridge interaction experiments. Each of the three vehicles crossed the bridge at 8 different speeds ranging from 1 to 2.75m/s at 0.25 m/s increments. To assess repeatability, 32 iterations were performed for

each combination of vehicle, damage scenario and vehicle speed. Data was recorded when the vehicle was moving in both the forward (A-B) direction and backward (B-A) direction. As such, a total of 13 (scenarios) x 2 (bridges) x 3 (vehicles) x 8 (speeds) x 32 (iterations) x 2 (motion directions) = 39936 individual experiments were conducted. However, in this paper only the forward motion is considered from this point forward, which means that 19968 experiments composed the first set of interaction experiment data set.

**Table 17: Damage scenarios: types and severity.**

Schematics	B1 R1					B2 R1				
	SC	f [Hz]	% f shift	% $\mathfrak{z}_{crit}$	% $\mathfrak{z}_{crit}$ shift	SC	f [Hz]	% f shift	% $\mathfrak{z}_{crit}$	% $\mathfrak{z}_{crit}$ shift
	010B1R1	7.23	0.00	3.63	0.0	010B2R1	5.75	0.000	7.70	0.00
	020B1R1	7.46	3.17	6.34	74.9	020B2R1	6.07	5.56	8.59	11.6
	030B1R1	7.66	6.00	6.45	77.8	030B2R1	6.36	10.5	11.3	46.0
	040B1R1	8.11	12.2	7.97	120	040B2R1	6.72	16.8	13.9	79.9
	050B1R1	8.56	18.4	9.37	158	050B2R1	7.11	23.7	14.4	86.7
	060B1R1	7.24	0.17	8.52	135	060B2R1	5.80	0.87	14.3	86.3
	070B1R1	7.25	0.28	11.3	212	070B2R1	5.81	1.04	15.8	105
	080B1R1	7.28	0.73	26.4	629	080B2R1	5.96	3.66	30.2	293
	090B1R1	7.30	0.98	31.4	767	090B2R1	5.94	3.22	46.7	507
	100B1R1	7.19	-0.56	4.44	22.5	100B2R1	5.73	-0.43	6.97	-9.52
	110B1R1	7.18	-0.66	4.34	19.5	110B2R1	5.71	-0.72	6.60	-14.2
	120B1R1	7.14	-1.29	4.07	12.3	120B2R1	5.69	-1.02	6.42	-16.6
	130B1R1	7.09	-1.85	4.37	20.5	130B2R1	5.66	-1.60	6.41	-16.8

In the second set of experiments, the effect of roughness and location of damage was studied. The roughness condition R2 was compared to the smooth rail condition R1 for some scenarios and after only the roughness condition is used as it is a more realistic condition. Table 18 summarizes the configurations and dynamic characteristics of both bridges under roughness scenarios R2. The scenarios in Table 18 allowed comparing the effect of roughness on scenarios SC020BiR2, SC030BiR2, SC070BiR2, SC080BiR2, SC110BiR2 and SC120BiR2, with their corresponding SC020BiR1, SC030BiR1, SC070BiR1, SC080BiR1, SC110BiR1 and SC120BiR1, where i=1 for Bridge 1 and i=2 for Bridge 2.

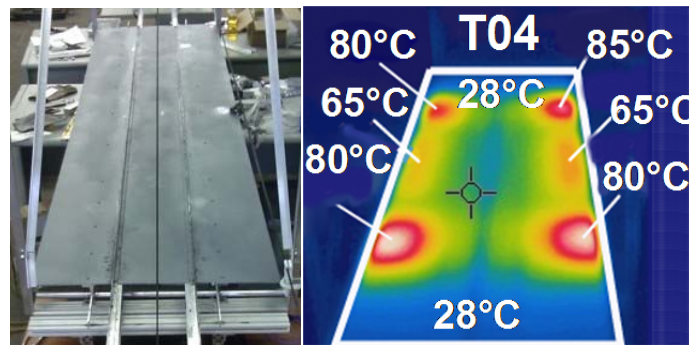
Table 18: Damage scenarios: locations and roadway roughness

Schematics	B1 R2					B2 R2				
	SC	f [Hz]	% f shift	% $\Delta_{crit}$	% $\Delta_{crit}$ shift	SC	f [Hz]	% f shift	% $\Delta_{crit}$	% $\Delta_{crit}$ shift
	010B1R2	7.77	0.00	13.04	0.00	010B2R2	5.80	0.00	5.81	0.00
	020B1R2	7.86	1.06	15.63	0.20	020B2R2	5.95	2.62	9.85	0.69
	021B1R2	7.87	1.30	19.64	0.51	021B2R2	5.95	6.10	8.53	0.47
	022B1R2	8.00	2.99	13.46	-0.03	022B2R2	6.15	6.90	13.55	1.33
	023B1R2	8.17	5.20	24.85	0.91	023B2R2	6.20	12.07	9.23	0.59
	030B1R2	8.10	4.27	16.17	-0.24	030B2R2	6.50	13.79	8.46	0.46
	031B1R2	8.30	4.27	21.05	0.61	031B2R2	6.60	8.62	11.61	1.00
	032B1R2	8.40	8.14	19.53	-0.5	032B2R2	6.30	6.90	9.32	0.60
	033B1R2	8.10	6.85	9.98	-0.23	033B2R2	6.20	-0.86	13.14	1.26
	070B1R2	7.77	0.00	18.93	0.45	070B2R2	5.75	-0.86	19.00	2.27
	071B1R2	7.77	0.00	27.06	1.08	071B2R2	5.75	-0.86	33.13	4.70
	072B1R2	7.77	0.00	18.54	-0.42	072B2R2	5.75	-0.86	18.82	2.24
	073B1R2	7.77	0.00	23.40	0.79	073B2R2	5.75	-0.86	23.42	3.03
	080B1R2	7.67	-1.30	34.52	1.65	080B2R2	5.75	-0.86	40.47	5.97
	081B1R2	7.67	-1.30	33.80	1.59	081B2R2	5.75	-0.86	37.91	5.52
	082B1R2	7.67	-1.30	35.51	1.72	082B2R2	5.75	-0.86	39.85	5.86
	083B1R2	7.70	-0.88	37.03	1.84	083B2R2	5.75	-0.86	40.36	5.95
	110B1R2	7.67	-1.30	11.82	-0.09	110B2R2	5.65	-2.59	10.16	0.75
	111B1R2	7.67	-1.30	12.28	-0.06	111B2R2	5.65	-2.59	10.87	0.87
	112B1R2	7.67	-1.30	11.70	-0.10	112B2R2	5.65	-2.59	9.64	0.66
	113B1R2	7.67	-1.30	13.81	0.06	113B2R2	5.65	-2.59	8.99	0.55
	120B1R2	7.60	-2.16	11.25	-0.14	120B2R2	5.60	-3.45	9.04	0.56
	121B1R2	7.70	-0.88	12.55	-0.04	121B2R2	5.65	-2.59	9.41	0.62
	122B1R2	7.77	0.00	12.62	-0.03	122B2R2	5.65	-2.59	8.86	0.52
	123B1R2	7.60	-2.16	11.28	-0.14	123B2R2	5.60	-3.45	8.17	0.41

To conduct experiments related to the effect of damage location, four cases for each damage scenario were conducted. For example, in the damage scenario where a single rotational restraint is applied (SC020BiR2), it is applied at four different locations; for these four locations, the labels SC020BiR2, SC021BiR2, SC022BiR2 and SC023BiR2 were used. The same was done for scenarios SC030 BiR2, SC070 BiR2, SC080 BiR2, SC110 BiR2 and SC120

BiR2 with corresponding scenarios where the location of damage was changed. Vehicle 1 (V1 from Table 16), operated at four speeds ranging from 1.5 to 2.25m/s in 0.25 m/s increments in the second experiment set. As such, 25 (scenarios) x 2 (bridges) x 1(vehicle) x 4 (speeds) x 32 (iterations) = 6400 experiments composed the second set of experiments.

In the third set of experiments, the effect of a temperature gradient on the bridge was investigated. The bridge B1 with roughness R2 was subjected to eleven different temperature patterns, as summarized in the leftmost column of Table 19. For illustrative purposes, Figure 29 shows one of these patterns. It must be noted that in order to make the infrared measurements accurate, the surface of the deck was painted using a standard gray paint. For each pattern four different damage scenarios were devised. One is the pristine condition and the other three represent one of each of the three damage types. Vehicle V1 was used at speeds ranging from 1.5 to 2.25m/s at 0.25 m/s increments. A total of 11 (temperature gradients) x 4 (bridge scenarios) x 4 (speeds) x 1 (vehicle) x 1 (bridge) x 32 (iterations) = 5632 experiments composed the third set of experiments.



**Figure 29: Bridge longitudinal view; normal and Infrared images.**

The different scenarios described in this section were processed for feature extraction and classified using the same methodology as described in Section 3.3. The Following describes the classification experiments performed results obtained.

Table 19: Damage scenarios: temperature B1 R2

Infrared Images	Schematics	SC	f [Hz]	% f shift wrt T00	% f shift wrt SC010	$\bar{z}$	% $\bar{z}_{crit}$ wrt T00	% $\bar{z}_{crit}$ wrt SC010
<b>T00</b> 		010B1R2	7.26	0.00	0.00	9.30	0.00	0.00
		020B1R2	7.40	0.00	1.92	6.32	0.00	-32.06
		070B1R2	7.16	0.00	-1.39	13.45	0.00	44.67
		110B1R2	7.16	0.00	-1.39	5.78	0.00	-37.85
<b>T01</b> 		010B1R2	7.63	4.98	0.00	13.06	40.48	0.00
		020B1R2	7.71	4.08	1.05	12.15	92.35	-6.98
		070B1R2	7.68	7.28	0.77	14.43	7.32	10.52
		110B1R2	7.61	6.22	-0.22	9.03	56.27	-30.86
<b>T02</b> 		010B1R2	7.46	2.66	0.00	14.49	55.90	0.00
		020B1R2	7.55	2.04	1.30	12.33	95.28	-14.90
		070B1R2	7.47	4.23	0.11	17.75	31.98	22.47
		110B1R2	7.44	3.87	-0.23	12.87	122.72	-11.21
<b>T03</b> 		010B1R2	7.59	4.51	0.00	9.54	2.66	0.00
		020B1R2	7.91	6.79	4.14	14.79	134.25	55.02
		070B1R2	7.67	7.04	1.00	17.17	27.67	79.92
		110B1R2	7.59	5.99	0.00	11.77	103.65	23.29
<b>T04</b> 		010B1R2	7.32	0.81	0.00	15.58	67.60	0.00
		020B1R2	7.50	1.35	2.46	19.0	200.86	21.95
		070B1R2	7.47	4.23	1.95	16.63	23.63	6.72
		110B1R2	7.38	3.05	0.80	12.39	114.49	-20.46
<b>T05</b> 		010B1R2	7.52	3.47	0.00	15.58	68.71	0.00
		020B1R2	7.60	2.72	1.17	11.45	81.25	-27.01
		070B1R2	7.57	5.63	0.67	16.26	20.91	3.68
		110B1R2	7.53	5.16	0.22	10.01	73.33	-36.15
<b>T06</b> 		010B1R2	7.67	5.56	0.00	13.35	43.60	0.00
		020B1R2	7.66	3.40	-0.16	13.46	113.15	0.84
		070B1R2	7.47	4.23	-2.63	22.23	65.33	66.57
		110B1R2	7.42	3.52	-3.29	17.0	194.25	27.35
<b>T07</b> 		010B1R2	7.71	6.13	0.00	12.84	38.10	0.00
		020B1R2	7.86	6.12	1.90	10.2	61.55	-20.53
		070B1R2	7.67	7.04	-0.55	16.19	20.41	26.14
		110B1R2	7.67	7.04	-0.55	11.11	92.28	-13.47
<b>T08</b> 		010B1R2	7.39	1.74	0.00	10.98	18.10	0.00
		020B1R2	7.66	3.40	3.59	11.35	79.78	3.41
		070B1R2	7.47	4.23	1.02	16.57	23.24	50.96
		110B1R2	7.46	4.11	0.91	11.34	96.35	3.33
<b>T09</b> 		010B1R2	7.53	3.70	0.00	10.65	14.54	0.00
		020B1R2	7.66	3.40	1.62	10.51	66.50	-1.25
		070B1R2	7.48	4.46	-0.67	15.40	14.48	44.59
		110B1R2	7.48	4.46	-0.67	12.87	122.75	20.86
<b>T10</b> 		010B1R2	7.73	6.37	0.00	9.80	5.44	0.00
		020B1R2	7.91	6.79	2.33	10.0	58.31	2.00
		070B1R2	7.73	7.98	0.11	17.16	27.57	75.04
		110B1R2	7.67	7.04	-0.76	11.39	97.17	16.22

## 4.3 Classification Experiments and Results

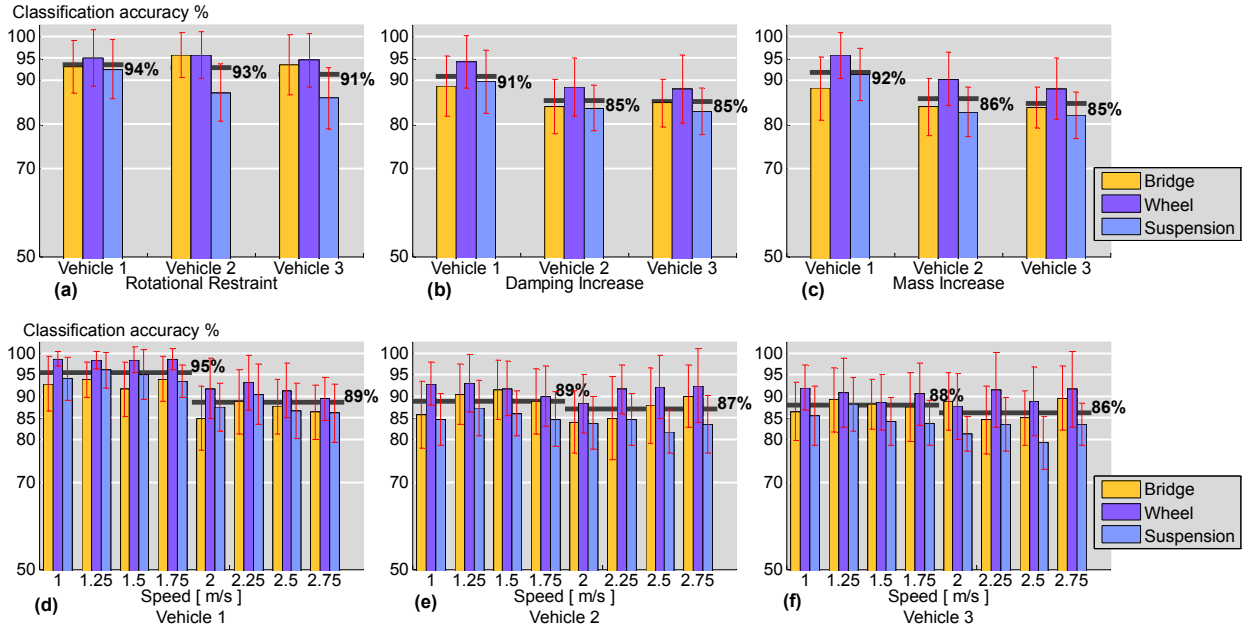
### 4.3.1 Effect on Classification Accuracy of Variations of Vehicles, Bridges, Vehicle Speeds and Severity of Change

The signal processing described in Section 3.3 was used for damage detection and severity identification. The damage detection is a two class experiment (i.e., damaged or undamaged) while the severity classification is a four class experiment (i.e., 020BiR1-050BiR1). We now describe both cases in detail.

**Damage detection.** The first class in this two label experiment, *undamaged*, is associated with pristine condition represented by any scenario labeled as SC010BiR1 in Table 17. Scenarios labeled SC020BiR1-SC0130BiR1 were associated with the second class, *damaged*. We thus obtained,  $7 \text{ (sensors)} \times 12 \text{ (scenarios)} \times 8 \text{ (speeds)} \times 3 \text{ (Vehicles)} \times 2 \text{ (Bridges)} = 4032$  separate assessments of classification accuracy. The classification accuracy is the proportion of true estimated results (both true positives and true negatives) in the population and is a very good indicator of the effectiveness of correctly classifying new incoming data. The results are presented for each bridge separately in Figure 30 - Figure 33.

Figure 30 show the results associated with Bridge 1. Three separate bars are used to associate the sensors to their respective location (Bridge, Wheel or Suspension). The separation of the results by location of bridge sensor allows for a comparison between the *direct* and *indirect* approach. The vertical bars represent the standard deviation associated with of the averaged results of 288 experiments for the bridge sensors  $3 \text{ (sensors)} \times 12 \text{ (scenarios)} \times 8 \text{ (speeds)} = 288$  (detection experiments), and 192 detection experiments for the wheel and suspension sensors  $2 \text{ (sensors)} \times 12 \text{ (scenarios)} \times 8 \text{ (speeds)} = 192$  detection experiments). At the top of each bar the standard deviation is shown. The average accuracy obtained for all the sensors is shown with a black line behind the bar graphs with numeric value of average

included. Figure 30a shows the classification accuracy relative to the rotational restraints as determined using each of the three vehicles. In the framework of the binary classification performed here, an accuracy of 50% represents the probability of randomly assigning a label to one of the two classes. Overall the performance of the sensors mounted on the wheel is comparable to the direct monitoring, and superior to the accelerometers mounted on the suspensions. There is not a significant difference between Vehicle 1 and Vehicle 3 in Figure 30a. Similarly Figure 30b and 6c show the results associated with the damping and the mass increases, respectively. In Figure 30b and 6c there is a 5% to 6% decrease in accuracy between Vehicle 1 and Vehicles 2 and 3. The rotational restraints scenarios are less sensitive to vehicle changes than the damping increase or the mass increase scenarios. The consistent results of the rotational restraint can be attributed to % change in the natural frequency of the rotational restraint scenarios being more significant than the damping or mass increase scenarios (see Table 17). The fundamental frequency of the rotational restraint scenarios vary up to 18% for Bridge 1 and 23.7% for Bridge 2 while the mass and damping increase scenarios vary less than 4%. Figure 30a - c suggest that: 1) the increase of the vehicle mass has a detrimental impact on the classification accuracy that is more significant for slight changes in the bridge; and 2) the sensors at the wheel level outperform all other sensors.



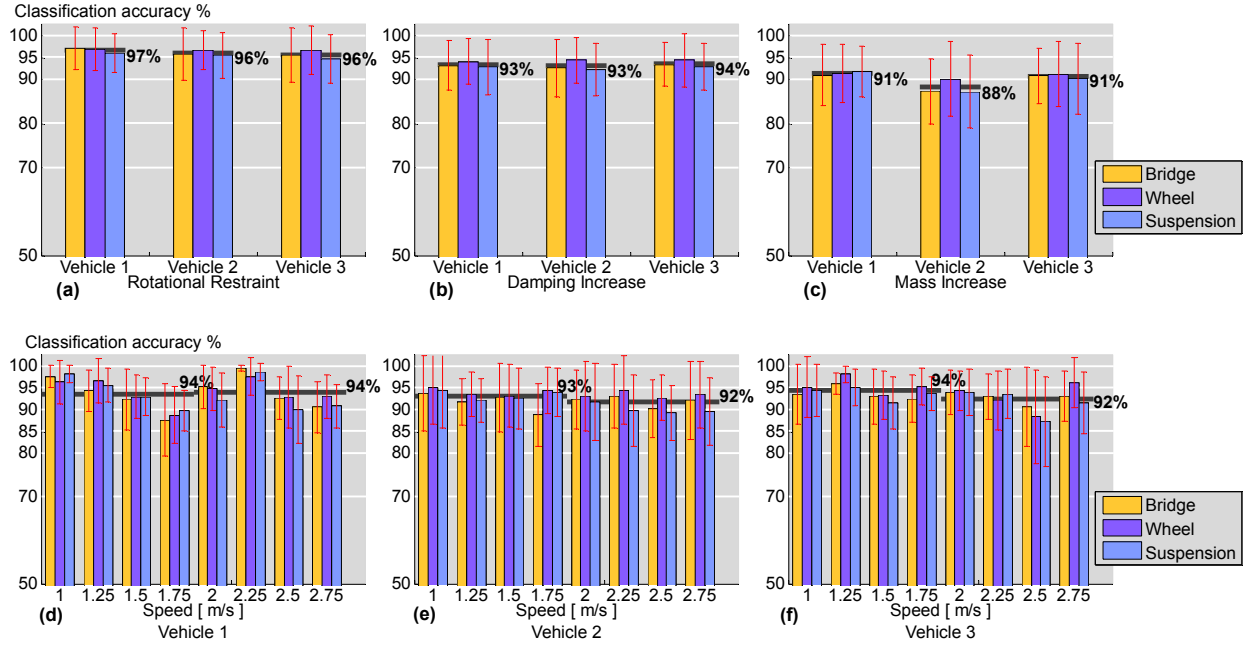
**Figure 30: Bridge 1: (a-c) Damage detection accuracy for different vehicles averaged across different speeds and severity scenarios of the same damage type: (a) Rotational Restraint; (b) Damping Increase and (c) Mass Increase. (d-f) Damage detection accuracy for different speeds averaged across the different damage scenarios of the same vehicle: (d) Vehicle 1; (e) Vehicle 2 and (f) Vehicle 3.**

The effect of the vehicle speed on the classification accuracy is shown in Figure 30d-f. An average of the first four speeds and the last four for all the sensors is depicted with a black line behind the bar graphs with an associated numeric value. Figure 30a shows a decrease among the first four and the last four speeds. The other two vehicles, Figure 30b and c are more stable with respect to speed variation.

Similar to Figure 30, Figure 31 reports on the results associated with Bridge 2. Figure 31a-c shows a small change in the average classification results for the different vehicles and better classification accuracy with respect to the results for Bridge 1. Figure 31a shows an average 96% classification accuracy for the Rotational Restraints scenarios. Figure 31b shows an average 93% classification accuracy for the Damping increase scenarios. Figure 31c shows an average 90% classification accuracy for Mass Increase scenarios. Figure 31d-f shows the classification accuracy across the different speeds for Bridge 2. Figure 31d-f shows a steadier trend across the different speeds for all the vehicles for Bridge 2 when compared to Bridge 1 in



Figure 30d-f. The overall average classification accuracy for the three vehicles and different speeds is about 93% for Bridge 2.



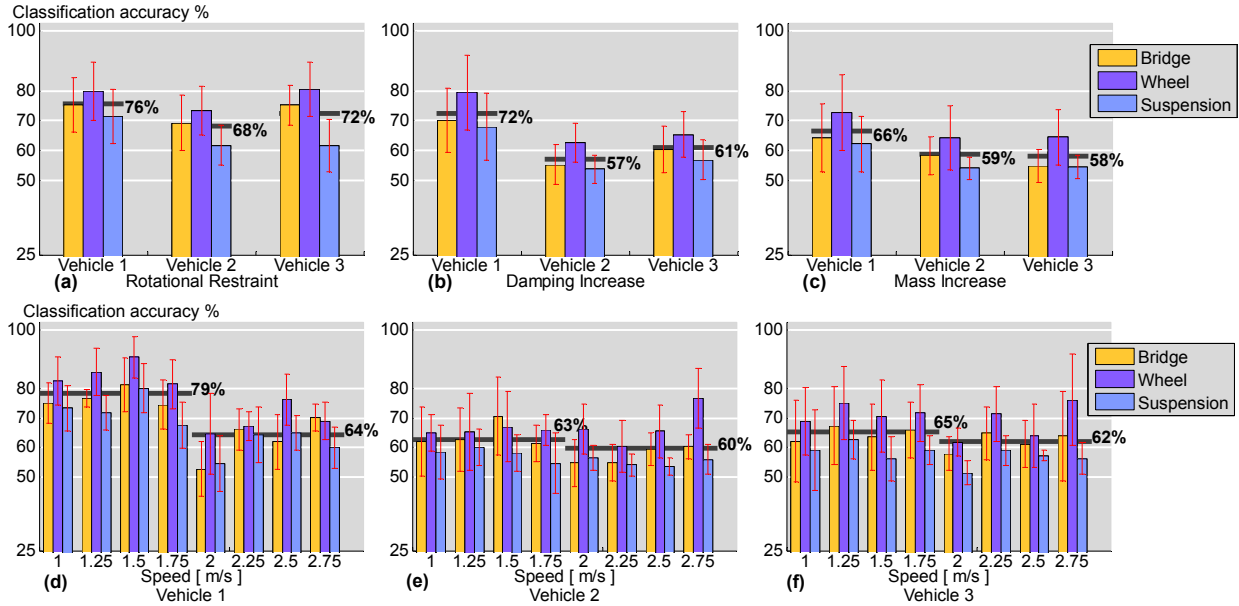
**Figure 31: Bridge 2: (a-c) Damage detection accuracy for different vehicles averaged across different speeds and severity scenario of the same type: (a) Rotational Restraint; (b) Damping Increase; and (c) Mass Increase. (d-f) Damage detection accuracy for different speeds averaged across the different damage scenarios: (a) Vehicle 1; (b) Vehicle 2; and (c) Vehicle 3.**

**Severity classification.** The severity classification experiments were defined as four label classification experiments for each damage type: Rotational Restraints, Damping Increase and Mass Increase. SC020BiR1, SC030BiR1, SC040BiR1 and SC050BiR1 are the four scenarios for the Rotational Restraint damage type as shown in Table 17. The four Damping Increase severity levels were defined by the scenarios: SC060BiR1, SC070BiR1, SC080BiR1 and SC090BiR1. Finally, the four Mass Increase severity levels were defined by the four scenarios: SC100BiR1, SC110BiR1, SC120BiR1 and SC130BiR1. Each of the severity classification experiments considered was run with the corresponding data of the 4 labels, from a particular sensor and for a particular damage type (one of three), vehicle (one of three), vehicle speed (one of eight) and bridge (one of two). We ran, therefore, 1008 total classification experiments 7 (sensors) x 3 (damage types) x 8 (speeds) x 3 (vehicles) x 2 (bridges) = 1008. Just as in the

case of the damage detection experiments, the results are shown for each bridge separately. Results for Bridge 1 are shown in Figure 32 and for Bridge 2 in Figure 33. The three sensor locations (Bridge, Wheel and Suspension) were represented by separate bars in the bar graphs. In Figure 32, the baseline for this case was set at 25%, which is the probability of randomly assigning a label among the four labels,  $P=1/4$ .

Figure 32a-c show the average classification accuracy results for Bridge 1 for each of the three damage types for each of the three different vehicles used (similar to Figure 30a-c and Figure 31a-c). Consistent trends as the ones observed in the two-label detection experiments can be seen in the four-label severity classification experiments. The Rotational Restraint scenarios are on average higher in classification accuracy than the other two damage types because of a more significant shift in the natural frequency of the bridge cause by rotational restraint.

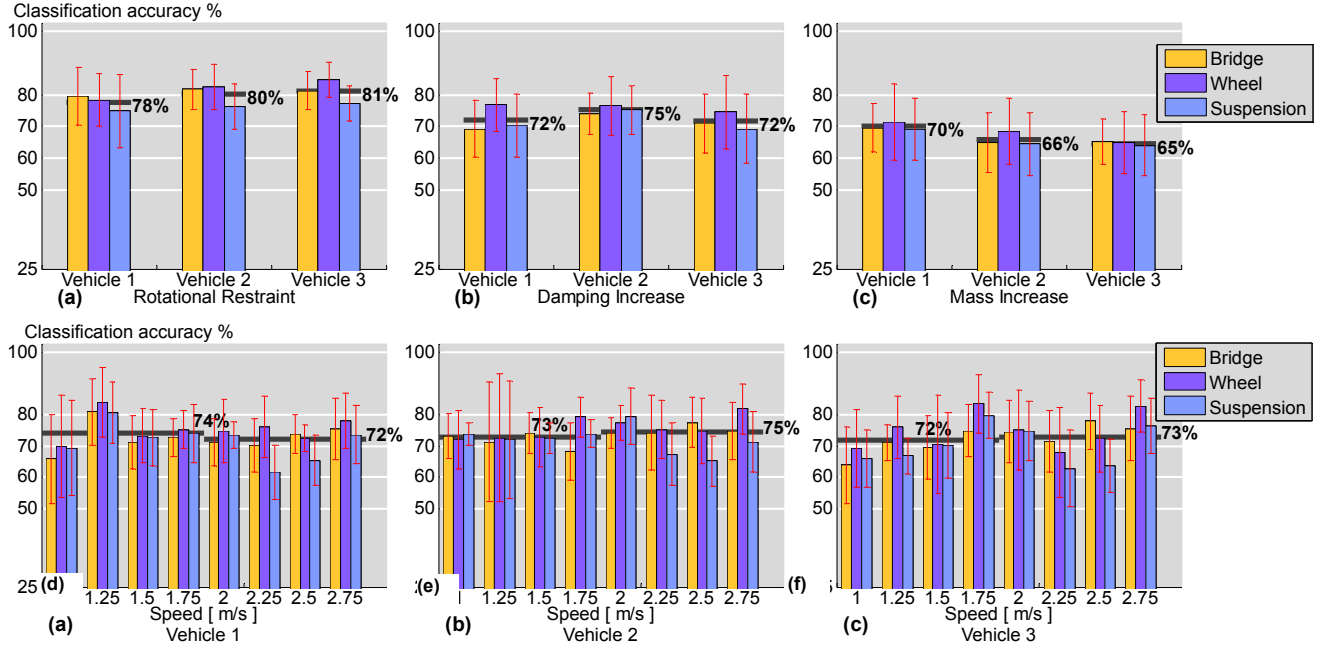
The classification results for the four-label experiments across the different speeds for Bridge 1 are shown in Figure 32d-f. A significant decrease in the average classification accuracy for Bridge 1 occurs for the last four speeds in comparison to the first four speeds for vehicle 1. The classification accuracies for the other two vehicles are less sensitive to a change in speed.



**Figure 32 Bridge 1: (a-c) Damage severity classification accuracy for different vehicles averaged across different speeds and severity scenario of the same damage type: (a) Rotational Restraint; (b) Damping Increase; and (c) Mass Increase. (d-f) Damage severity classification accuracy for different speeds averaged across the different damage scenarios of the same vehicle: (d) Vehicle 1; (e) Vehicle 2; and (f) Vehicle 3.**

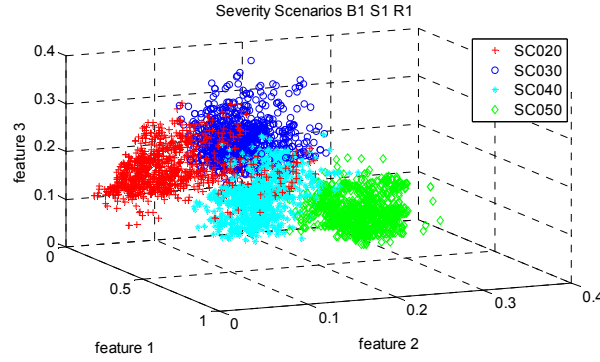
Similarly, Figure 33 presents the classification accuracies for Bridge 2 in the same manner that Figure 32 does for Bridge 1. Figure 33a-c shows better classification accuracy with respect to the results for Bridge 1 shown in Figure 32a-c. An 80% classification accuracy was obtained for the Rotational Restraints scenarios as shown in Figure 33a, a 73% classification accuracy for the Damping increase scenarios is shown in Figure 33b, and a 67% classification accuracy for Mass Increase scenarios is shown in Figure 33c.

Figure 33d-f show the classification accuracy for damage types on Bridge 2 for different vehicle speeds. It shows a steadier trend across the different speeds for all the vehicles for the damage scenarios on Bridge 2 when compared to Bridge 1 in Figure 32d-f. The overall average classification accuracy for the three vehicles and different speeds is about 73% for Bridge 2. Overall the classification results obtained for Bridge 2 were higher than those for Bridge 1 and more stable with respect to the different speeds.



**Figure 33: Bridge 2: (a-c) Damage severity classification accuracy for different vehicles averaged across different speeds and severity scenario of the same damage type: (a) Rotational Restraint; (b) Damping Increase; and (c) Mass Increase. (d-f) Damage severity classification accuracy for different speeds averaged across the different damage scenarios of the same vehicle: (d) Vehicle 1; (e) Vehicle 2; and (f) Vehicle 3.**

The classification results obtained were further inspected by creating cluster plots of the four Rotational Restraint scenarios: SC020B1R1, SC030B1R1, SC040B1R1 and SC050B1R1. Figure 34 shows the cluster plot generated using the first three frequency features for the samples defined for Bridge 1, Vehicle 1, Speed 1 and without additional built-in roughness. The most significant frequencies are used as features for the different scenarios as described in Section 3.3.2. One can see that the high classification accuracy obtained for the rotational restraint scenarios can be well justified when looking at the cluster plots. The four different severity scenarios for the rotational restraints generated distinct clusters that can be distinguished by the naked eye.



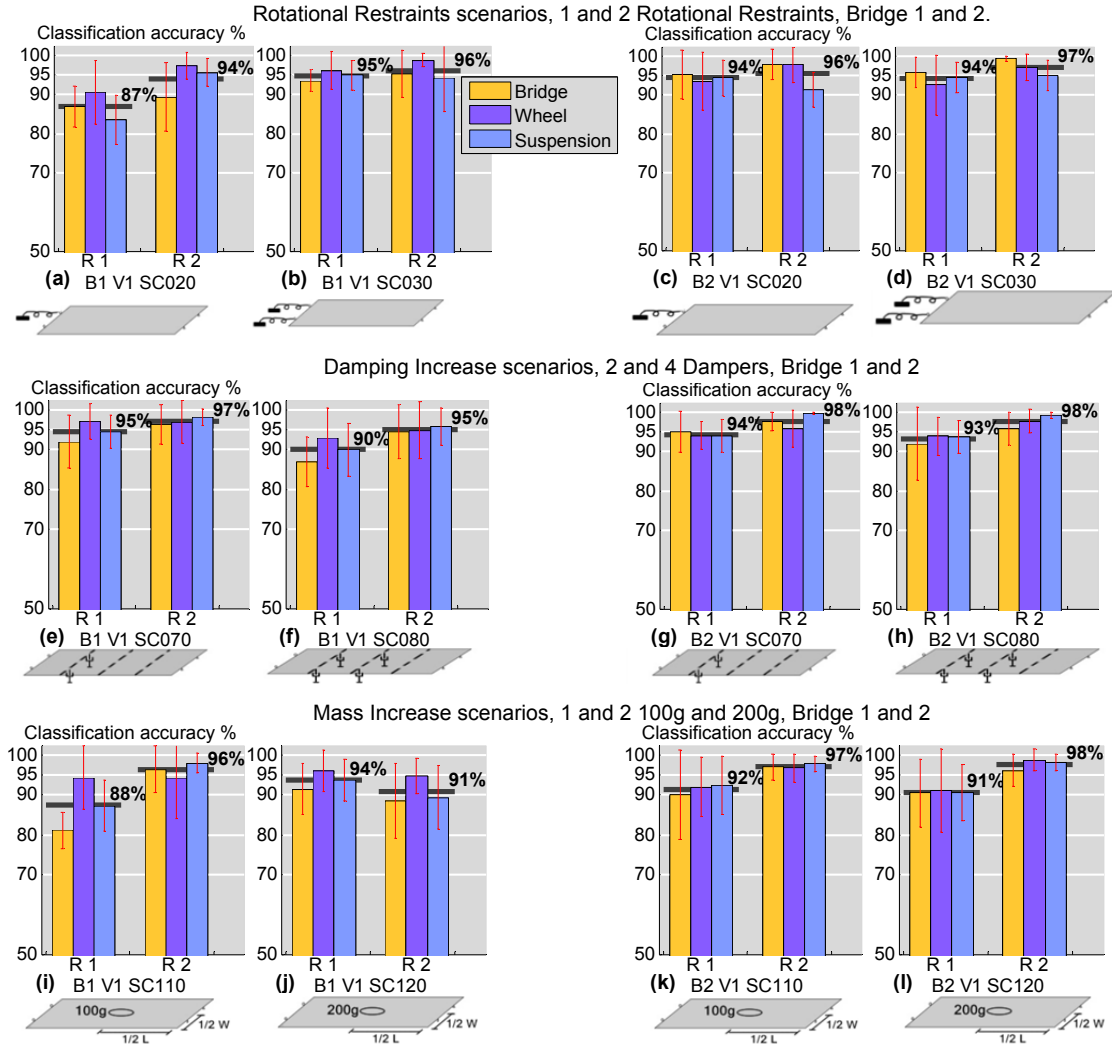
**Figure 34: Rotational restraints scenarios cluster analysis. Vehicle 1, Bridge 1, Speed 1 m/s, R1 (Roughness from accidental imperfections).**

### 4.3.2 Effect of Roughness and Damage Location

Table 18 presented in Section 4.2 showed the second set of scenarios run for determining the effects of roadway roughness on classification accuracy. For this set of experiments, both bridges were modified to include a roadway profile as described in Section 4.2. We compared the damage detection accuracy for two different roughness conditions, R1 and R2.

**Damage detection accuracy for different roughness.** In a second set of experiments, we explored the accuracy of damage detection when a roadway roughness profile exists. The average classification accuracies obtained with and without roughness were plotted in Figure 35. Figure 35 a – d show the cases of the two rotational restraint scenarios Bridges 1 and 2. The caption and the scheme below each plot in Figure 35 identifies the corresponding scenario of one or two rotational restraints. Similarly, schemes and captions identify the corresponding scenario for each plot in Figure 35. Figure 35 e – h show the cases of the two damping increase scenarios in Bridges 1 and 2, and Figure 35i – l show the mass increase scenarios in Bridges 1 and 2. Each graph in Figure 35 shows the average classification accuracy for Vehicle 1 and a specific Bridge (Bridge 1 in Figure 35a,b,e,f,i,j or Bridge 2 in Figure 35b,c,g,h,k,l), using four different vehicle speeds (1.5, 1.75, 2 and 2.25m/s), the different sensor location and the two different roughness profiles (that of the purchased angle referred to as R1 and that of the manufactured roughness referred to as R2, both were discussed in Section 4.2). The baseline

was set to 50% and each bar represents the average results obtained for a particular sensor location as in the previous damage detection graphs.



**Figure 35: Damage detection comparison among bridges with two different roughness profiles. (a-d) two Rotational Restraints scenarios: (a-b) Bridge 1 and (c-d) Bridge 2; (e-h) two Additional Damping scenarios: (e-f) Bridge 1 and (g-h) Bridge 2; (i-l) two Additional Mass scenarios: (i-j) Bridge 1 and (k-l) Bridge 2.**

The comparison presented in Figure 35 shows an increase in the damage detection capability when the bridge had more significant roadway roughness (case R2). These results indicate that roadway roughness may actually contribute to more accurate classification for the indirect approach, which is admittedly counter to what one might expect when adding this variable to the problem. Intuitively, however, we can possibly explain this increase in classification accuracy as a result of the roadway roughness increasing the vibration of the

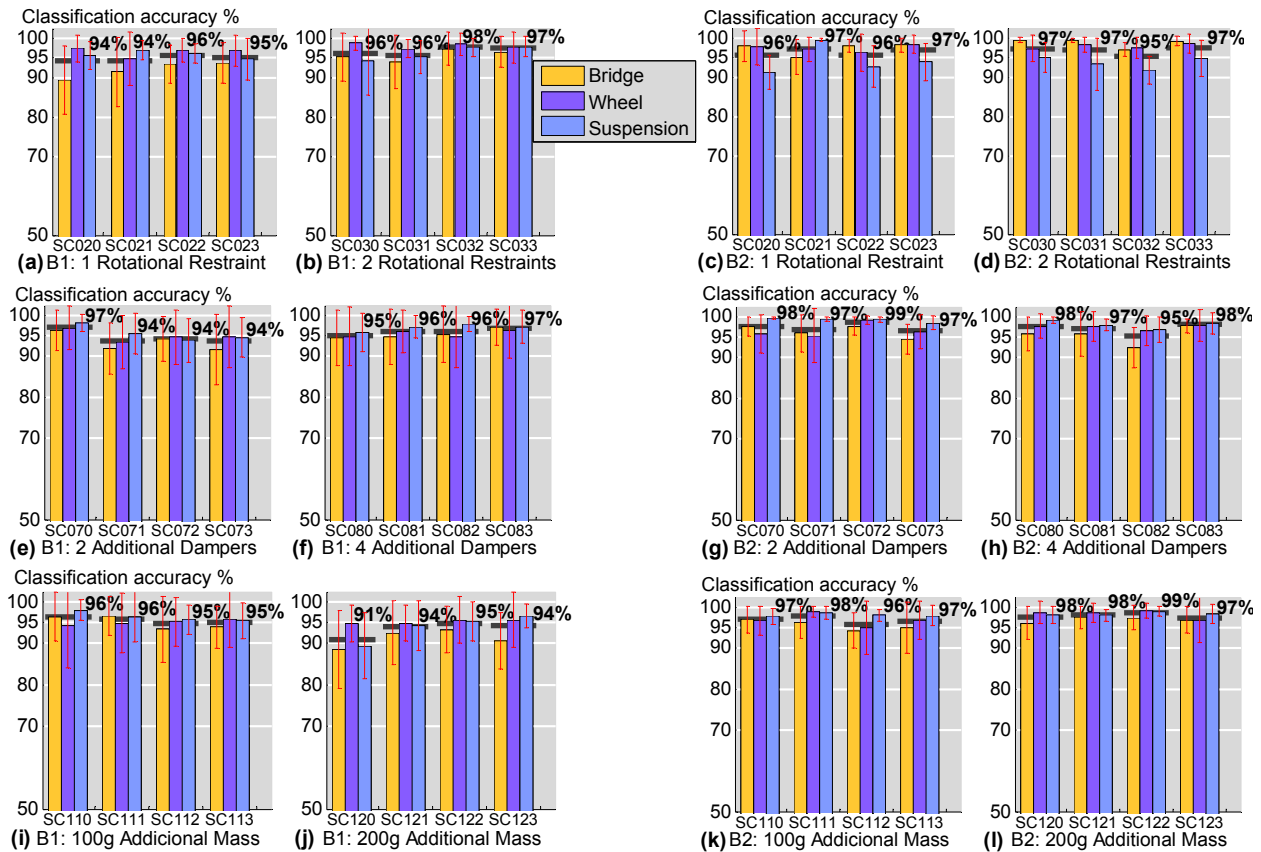
bridge allowing the vehicle to better capture the dynamic characteristics of the bridge structure. However, including the roadway roughness in the manner we did in this experiment (adding an additional portion of the rail) also increased the natural frequency of the undamaged bridge (See Table 18), and the increase in classification accuracy also could be attributed to a different vehicle/bridge frequency ratio. More investigation is necessary on this issue, but the experiment does begin to dispel concerns that adding roadway roughness would make the classification accuracy worse.

### 4.3.3 The Effect of Different Locations of Damage

Using the second set of scenarios shown in Table 18, we setup two types of classification experiments. The first was a set of damage detection experiments for the same amount of damage at different locations, and the second was a set of four label classification experiments where the location was made to be difference among scenarios with the same amounts and type of damaged. These two sets of classification experiments are further described in the following two sub-sections.

**Detection accuracy for damage at different locations.** We explored the accuracy of damage detection for scenarios with the same amount of damage of a certain type at different locations on the bridge structure (see Table 18). In these two-label experiments, we explore the dependence of the accuracy for detecting different types of damage on the location of that damage. As in previous sections, each of the detection experiments considered data from a particular sensor, different damage scenarios, a particular speed, a particular vehicle and a particular bridge. We obtained therefore  $7 \text{ (sensors)} \times 24 \text{ (damage scenarios)} \times 4 \text{ (speeds)} \times 1 \text{ (Vehicle)} \times 2 \text{ (Bridges)} = 1344$  separate assessments of classification accuracy. The corresponding average results shown in Figure 36 are grouped by scenarios of the same damage type and severity level but for different locations. For example, in Figure 36a, SC020 is

the scenario of a single rotational restraint at a particular location and SC021, SC022 and SC023 are also single rotational restraints but at different locations as defined in Table 18.



**Figure 36: Damage detection comparison among scenarios with different damage locations: Bridge 1 (a,b,e,f,i,j), Bridge 2 (c,d,g,h,k,l).**

Figure 36a shows the detection results for different locations of a single rotational restraint for Bridge 1 and Figure 36b shows the average detection results for two rotational restraints at different locations for Bridge 1. Among the scenarios shown in Figure 36b, SC030 and SC031 have both rotational restraints on one side of Bridge 1. The other two scenarios in Figure 36b, SC032 and SC033 had two rotational restraints, one on each side of Bridge 1. Similarly, Figure 36c shows the same scenario for Bridge 2 as that shown for Bridge 1 in Figure 36a. In both bridges, the damage detection accuracy obtained was above 95%. These results suggest that for the damage scenarios modeled, they can be detected with a very high accuracy regardless the location of the applied damage. The same is true for the other scenarios plotted in Figure 36.



**Location classification.** We also performed a four-label classification experiments on the data from the same set of experiments described in Table 18. The four labels were defined as the four possible locations of damage of a particular damage type and severity applied to the bridge. In the caption of Figure 37, we named SC02- the four-label location classification experiment for classifying among the four scenarios in which a single Rotational Restraint is applied (SC020, SC021, SC022 and SC023 for Bridge 1 or 2 and Roughness 2). Similarly, we used SC03-, SC07-, SC08-, SC11- and SC12- in Figure 37 for naming the four-label location classification experiments corresponding to scenarios that vary the locations of scenarios SC030, SC070, SC080, SC110 and SC120, respectively as defined in Table 18. Each four-label location classification experiment was run for a specific sensor, scenario type and severity, speed and bridge. We ran therefore 7 (sensors) x 6 (scenario types and severity) x 4 (speeds) x 1 (vehicle) x 2 (bridges) = 336 four-label location classification experiments. As in previous figures, we plot the different bridge results separately; Figure 37a plots the results for Bridge 1 and Figure 37b plots the results for Bridge 2. The baseline of Figure 37 was set at 25%,  $P=1/4$  ( $P$ =direct probability).

In Figure 37a, the lowest classification accuracy obtained was 67% for SC08-, which suggests a small difference among the scenarios with four dampers. We can confirm this small variation by looking at Table 18. SC080 through SC083 in Table 18 share the same two middle dampers and show small variation in the fundamental frequencies. They would be therefore hard to classify by using the simple frequency-based features that we have used in this study. SC11- and SC12-, which group the location variation for a 100g and a 200g increase as defined in Table 18, also show small or no variation of the natural frequency. However, even for this challenging case an average classification of over 70% was achieved. In Figure 37b, corresponding to Bridge 2, the lowest classification accuracies obtained were for scenarios SC08- and SC11- (four dampers and a 100g increase at different locations accordingly) there the classification accuracies for both scenarios was over 60%.

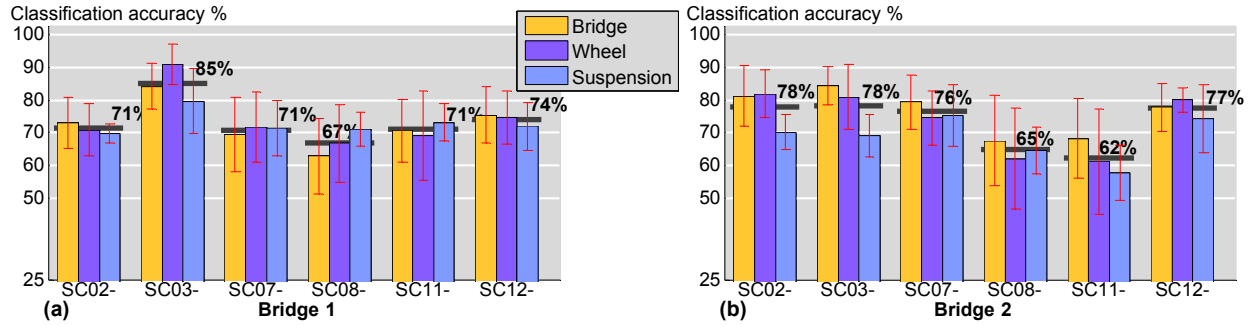


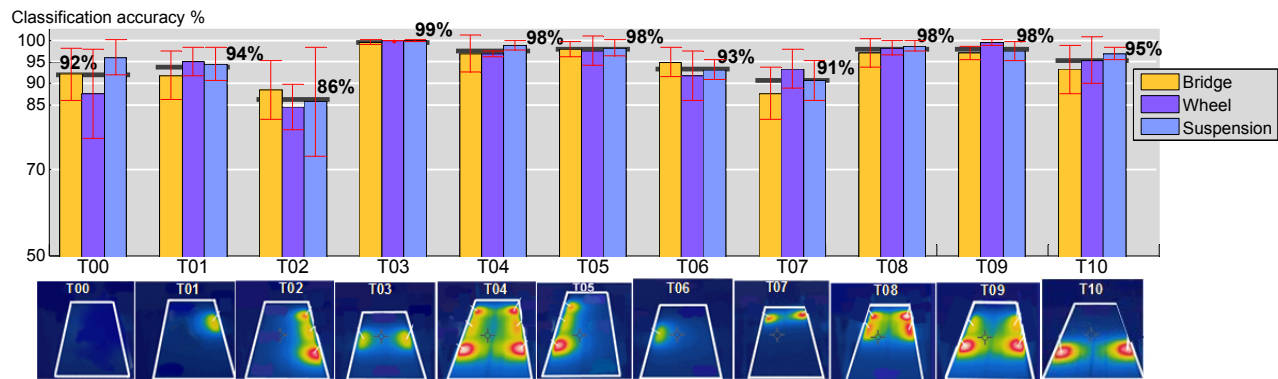
Figure 37: Location classification comparison among scenarios with different damage location: (a) Bridge 1, (b) Bridge 2.

#### 4.3.4 Effect of Temperature gradient scenarios.

We now consider the third data set obtained when the thermal conditions were varied, which was described in Table 19. We ran two different classification experiments using the same signal processing and classifications approach as presented in Section .3.3.. The first classification experiment was a damage detection experiment assuming the temperature scenario to be known, and the second classification experiment was a damage detection experiment assuming the temperature scenarios to be unknown. In this second classification experiment, the data from the 11 different temperature gradients for a particular bridge damage scenario is used to define a label. The next two subsections describe the obtained results.

**Damage detection within same temperature scenario.** As shown in Table 19, four different bridge scenarios: SC010B1R2 (Undamaged), SC020B1R2, SC070B1R2 and SC110B1R2, were run under each specific temperature gradient scenario. We performed damage detection experiments (two labels: Undamaged vs Damaged) for each of the three damage scenarios: SC020B1R2, SC070B1R2 and SC110B1R2 at a particular temperature scenario. In other words, each damage scenario is defined by the corresponding experimental iterations that were conducted for the given temperature scenario that consist of 1 (temperature gradient scenario) x 1 (bridge damage scenario) x 1(speed) x 1 (vehicle)x 1 (bridge) x 32( runs) = 32 iterations to define a particular damage scenario. Figure 38 shows the average and standard deviation of the classification accuracy obtained for the damage detection experiment for each the three

damage scenarios under a specific temperature gradient conditions. That is the average of  $3(\text{damage scenarios}) \times 4 (\text{speeds}) = 12$  classification accuracy experiments. In all these experiments Vehicle 1 was used and the speeds ranged from 1.5 to 2.25m/s at 0.25 m/s increments. The baseline of the graph was set to 50% as in all the previous two-label damage detection graphs. The obtained results show that the average classification accuracy might vary by as much as 15% for the different temperature scenarios (see the results for T02 and T03). This variation suggests that some temperature scenarios might be more favorable for damage detection than others. The results obtained from the bridge sensors and from the vehicle sensors achieved roughly the same classification accuracy.



**Figure 38: Classification accuracy of damage scenarios for specific temperature gradient scenario.**

**Damage detection without considering temperature information.** The second classification experiment conducted considered a particular bridge condition to define a particular bridge damaged label with all the temperature variations. That is, SC01 is now defined by the 32 runs at each of the 11 different temperature conditions. So is the same for the other 3 bridge scenarios as defined in Table 19: SC020, SC070 and SC110. In this case we are treating the temperature condition as an embedded variable in the data. Figure 39 shows the average classification results obtained for the detection experiments. The overall results show an interesting average classification accuracy among the three damage scenarios. The average classification results decrease with respect to the previous experiments shown in Figure 38,

where the temperature was considered a known variable. This decrease was expected as this is a more challenging experiment where the embedded variable can mask the damage changes made to the bridge structure. Figure 39 shows the results for this experiment. In general terms, it can be seen that the Wheel and Suspension sensors achieved classification accuracies similar to or better than those using the sensor located on the bridge structure.

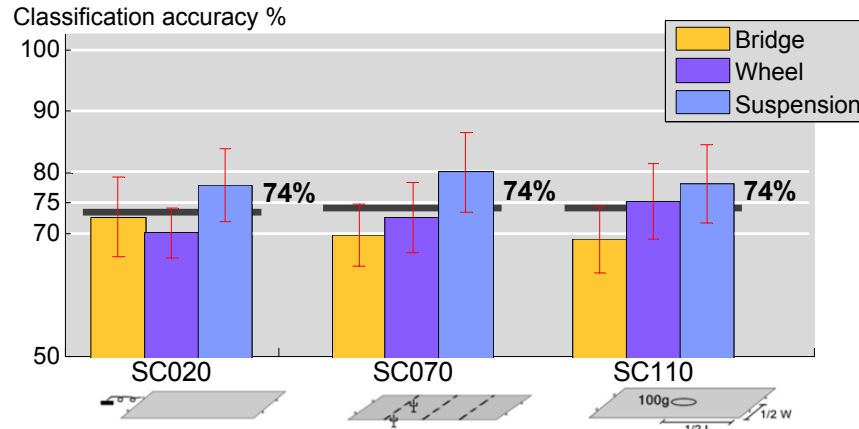


Figure 39: Classification accuracy of damage scenarios regardless temperature scenario for training and testing.

## 4.4 Discussion

In this chapter, we further validated an *indirect* bridge SHM approach based on vibration data collected from a vehicle as it traverses over the bridge structure and compared the results with the traditional *direct* monitoring approach that uses sensors placed on the bridge structure. We built and automated a laboratory scale experimental setup that allowed for data acquisition and accurate control of the speed of the vehicle, accurately known modifications to the bridge, and multiple repetitions. We used a simple feature extraction and classification approach to perform several classification experiments on the collected data. We explored the space of possible variations to the vehicle-bridge interaction system to test the robustness of the indirect monitoring approach versus the direct monitoring approach. The variations considered two different bridges, eight different vehicle speeds, three different masses of vehicle, two roughness scenarios, 11 different temperature gradients, and three different types of damage

made to the bridge (rotational restraints, additional damping and an additional mass). The different types of damage were explored in terms of detecting the existence of the damage and also classifying among scenarios with different damage locations and different levels of damage severity.

For the vehicle variation, the introduction of a higher mass to the vehicle chassis decreased the average classification accuracy for the mass increase and damping increase scenarios in Bridge 1 by about 6%, and showed no significant difference for Bridge 2. The detection classification results for the sensors located at the wheel level and at the suspension system of the moving vehicle (*indirect monitoring*) were comparable with the results obtained with sensors located on the bridge structure (*direct monitoring*).

For the different vehicle speeds, the Bridge 1-Vehicle 1 combination showed a 6% decrease in the damage detection classification accuracy between speeds of 1.75 m/s and 2m/s, however, all other Bridge-Vehicle combinations showed low dependency with respect to speed. The detection results obtained using the indirect or direct monitoring approach were similar. The severity classification results show similar trends to the damage detection classification accuracy for Bridges 1 and 2, but about 20% lower than those for damage detection. The decrease is attributed to the increase of the number of labels from two label in the detection experiments to four labels in the severity classification experiments.

The inclusion of roadway roughness increased the detection rate for almost all the damage scenarios compared. The indirect and direct monitoring approaches showed comparable results for all cases.

Different locations of the same magnitude of damage showed similar average damage detection classification accuracy for both bridge structures. The location classification accuracy, a four label classification task, showed variations from 85% to 67% for Bridge 1 and from 78% to 62% for Bridge 2. This variation can be attributed to the choice of scenarios implemented.

Some scenarios were very similar to others they were being classified against. The indirect and direct monitoring approaches showed comparable results for all location classification cases.

Two types of damage detection experiments were conducted regarding various temperature gradient conditions. The first damage detection experiment compared damage scenarios within the same temperature gradient conditions. The variation of the detection accuracy of about 15% suggests that there are temperature gradient conditions more favorable than others for detecting damage scenarios. The second damage detection experiments assumed that there was no information about the temperature gradients and treated it as an embedded variable in the data. The classification results for the three scenarios explored on this case showed remarkable consistency for the three scenarios explored of about 74%. Once again the sensors considered as indirect performed just as well as those sensors located on the bridge structure.

The results showed in this chapter match, in most cases, the intuition about the behavior of the vehicle-bridge interaction systems with the obtained trends in terms of the classification accuracies. That is, scenarios that had a greater variation of the dynamic characteristics identified by free-vibration experiments had also higher detection accuracy.

The signal processing methodology used in this work was based on a frequency based features and a standard classification algorithm. The numerical classification results could be greatly improved by exploring other feature space representations and other classification algorithms.

Further research is needed to validate the indirect versus the direct approach for bridge SHM. The results presented in this paper are constrained to the corresponding experimental setup. However, the variable space explored does not preclude the indirect monitoring approach and encourages the authors to further explore this line of research.

## **Chapter 5: Summary, Contributions and Future Work**

This chapter presents a summary of the research described in this dissertation, the contributions of this research, a discussion of the results and lessons learned along the course of this work, and possible research topics for future work.

### **5.1 Summary**

In this dissertation, an indirect approach was presented for determining the condition of bridges based on data collected from instrumented vehicles that traverse the structure. This bridge structural health monitoring (SHM) approach shows promise for wide, yet cost-effective, coverage of a bridge stock.

First, the feasibility of the indirect SHM approach was assessed by means of 1D and 3D mathematical models. A multiresolution classification algorithm was employed to detect the existence, severity, and location of changes in the bridge structure. Such changes consisted of modifications of the stiffness at particular locations within the structure. The classification was performed by comparing the full-waveform of the transient response of the bridge in its modified state, as recorded by the moving vehicles, against that of the structure in its pristine condition. Two-label classification experiments (i.e., classifying between Undamaged and Damaged) with the indirect approach were performed with the 1D and the 3D models data from varying vehicle models. The classification accuracy achieved was in the order of 95 percent for the 1D models and of 90 percent for the 3D models, with little dependence on the vehicle parameters. The accuracy, however, varied with the particular experiment and the extent of information desired (e.g., global change vs. no change, or detection of structural change at a particular location). Overall, the results of this study made it desirable to explore the possibility of extending the approach to more realistic structures.

The detection capability of the approach was tested using a laboratory setup to which three different types of change (referred to as damage scenarios) were applied: changing support conditions (rotational restraint), adding more damping to the bridge, and adding mass at the midspan. A set of features based on discriminant frequencies were extracted from the energy spectrum of the signal samples. The features were used in conjunction with a support vector machine classifier on data measured from a passing vehicle at the wheel and suspension levels, and directly from the bridge structure for comparison. For each type of damage, four levels of severity were explored. The results show that for each damage scenario, the classification accuracy based on data measured from the passing vehicle is, on average, as good as or better than that based on data measured from the bridge. Classification accuracy showed a steady trend for low (1-1.75 m/s) and high (2-2.75 m/s) vehicle speeds, with a decrease in accuracy of about 7% for the latter. These results showed promise for a highly mobile structural health bridge monitoring system for wide and cost-effective bridge stock coverage, but the approach needed to be further tested for robustness when varying some interaction parameters and other boundary conditions.

The space of possible variations of the interaction conditions was further explored. The bridge was subjected to various scenarios in order to simulate damage and environmental variations. The data were then processed with the same signal processing and classification methods as in the previous cases. The results showed little influence of the vehicle variations and the vehicle speed on the classification accuracy for all three types of changes made to the bridge structure. The results also showed consistency between two bridges with similar structural configuration but different dynamic properties. The effect on classification accuracy of roadway roughness was also explored. Better classification accuracy was obtained when roughness was introduced on the two bridge structures studied. The introduction of atmospheric variations was also explored by producing temperature gradients on the model bridge deck. The average classification accuracy obtained for damage scenarios within one particular



temperature gradient was up to 15 % lower compared to that achieved for other temperature gradient scenarios, suggesting that it might be easier to detect damage under some temperature gradients than others.

Across all the different vehicle, speed, roughness and temperature variations, it can be concluded that in general terms, the indirect data obtained from sensors at the wheel level or at the suspension level performed just as well or better than the data from sensors on the bridge in terms of the classification accuracy obtained.

## **5.2 Contributions of this research**

In general terms, the contributions of this work relate to extending the idea of an indirect approach for measuring the fundamental frequency of a bridge as an indicator of stiffness change (Yang et al 2004, Lin and Yang 2005) into an approach for indirect *monitoring* of a bridge using enhanced signal processing and machine learning techniques for classification of large sets of vehicle response data. Three main contributions emerged from this research: 1) exploring and further defining the indirect approach for SHM based on data from many passing vehicles and extracting the bridge information by means of signal processing and pattern recognition techniques. This was first explored based on numerical simulations and the use of a multiresolution classifier; 2) validating the indirect approach for bridge monitoring based on laboratory model data and developing a signal processing and classification procedure for 1D vehicle response signals; and 3) expanding the validation of the indirect approach based on the laboratory model data to determine the effects on classification accuracy from vehicle and bridge variations, roadway roughness, and temperature gradients. These three main contributions were described in detail in Chapters 2-4 of this dissertation and are summarized in the following paragraphs of this section.

Exploring the indirect approach for bridge monitoring was first done in this research by means of simulated data and the use of a multiresolution classifier. Previous researchers have

worked on the idea of measuring bridge fundamental frequency or other parameters based on vehicle vibration (Yang et al. 2004, Yang and Chang 2009 Law and Zhu 2004, 2005). Others reported the dynamic response of damaged beams subjected to moving masses (Mahmoud and Abou Zaid 2002, Bilello and Bergman 2004). Bu et al 2006 proposed the use of data from a passing vehicle as a condition assessment approach by optimizing a damage index vector based on a model bridge stiffness change. Most recently, McGetrick et al 2009, showed that variations on the bridge damping could be picked up by a passing vehicle and also suggested that this could be an efficient way to monitor short to medium span bridges. Other researchers have proposed the use of an instrumented city bus for monitoring bridges (Yabe and Miyamoto 2010, Miyamoto and Yabe 2011). Recently, Miyamoto and Yabe (2011) explored variations of a characteristic deflection for damage detection considering simulations at different speeds and roadway roughness. Though these previous research findings suggest the idea of using vehicle data for monitoring bridge structures, they reported detecting some features and damage indicators. However, to make a structural assessment, following the extraction of features, the classification of a damage scenario is needed. In this dissertation, all the results are presented in terms of the classification accuracy for different classification experiments. The classification accuracy is a more comprehensive statistic for predicting the expected classifier performance for new incoming data for which the classifier has not been trained. It is therefore a better parameter for decision making.

This dissertation has taken previous and on-going research on the indirect monitoring approach a step forward by performing classification experiments for damage detection, severity and location of damage scenarios, exploring and validating the indirect approach for structural health monitoring. This validation was made possible by considering the use of large vehicle-data sets from which to extract vehicle-response patterns, and using advanced classification algorithms, so as to determine the classification accuracy of a particular classification experiment. In most cases, above 90% damage detection accuracy was achieved for inertia

reduction of the simulated bridge structures from Chapter 2. Classification experiments considering the location, severity of damage or both were also performed.

This dissertation demonstrated that the multiresolution classification algorithm developed by Kovačević et al for biological image analysis can be applied to the problem of bridge health monitoring. The multiresolution classifier (Chebira et al. 2007), instead of working on the original signal, passes it first through a multiresolution decomposition block generating a number of smaller-sized signals, called subbands, in different subspaces. One possible characterization of multiresolution transforms is in terms of whether they represent the signal in a nonredundant or a redundant fashion. Redundancy often leads to increased accuracy, as has been found in a host of bioimaging problems (see Chebira & Kovačević 2008). Collaboration with Kovačević's lab allowed for further expanding the field of applications for the multiresolution classifier to SHM and therefore extending its generality as an image classifier. The classifier was used for testing the indirect monitoring approach with vehicle interaction data compiled into an image representation for a particular bridge structural condition.

This work also represents a contribution in terms of validating the indirect approach for bridge monitoring based on laboratory model data and a developed signal processing procedure. Moreover, the application of the indirect approach was extended for different types of damage scenarios. The ground breaking early work by Yang et al 2004 and Ling and Yang 2005 reported the frequencies obtained in the indirect fashion. Since then, several studies were conducted numerically and experimentally (Yang and Chang 2009; Bu et al. 2006; Kim and Kawatani 2008; McGetrick et al. 2009, 2010; Isemoto et al. 2010; Miyamoto and Yabe 2011; Yin and Tang 2011; Sirigoringo and Fujino 2012). The monitoring of the natural frequency of bridges was one of the main concerns for early research on the indirect approach. The detection of structural damping as an indicator of structural damage by indirect methods has been explored more recently (McGetrick et al. 2009, and McGetrick et al. 2010, González et al. 2012). In this research, a signal processing scheme was developed for unidimensional time response signals.

Chapter 2 describes the details of the signal processing and classification scheme. In general terms, the scheme consists of: 1) denoising by averaging the power spectrum from three vehicle runs; 2) calculating a discriminant power from a damage scenario and the corresponding pristine condition; 3) extracting the five most significant frequencies from the discriminant power; 4) classifying the scenarios with a standard Support Vector Machine classifier. The damage scenarios explored in this research introduced both changes in the natural frequencies and changes in structural damping. The three types of damage scenario designed and analyzed were: 1) variations on the support condition by imposing rotational restraints, 2) increase of damping at different locations, and 3) a mass increase at different locations. The results showed over 90% detection accuracy on average for the three different types of damage. When looking within the damage type, the *severity* of the changes inflicted in the bridge structure was correlated with higher classification accuracy. The detection of the various changes in the bridge structure was quite insensitive to the vehicle *speed*. The *indirect* and *direct* approaches seem to be equally effective for damage detection when applying the proposed signal processing techniques. Of the two sensor locations considered in the *indirect* approach, the wheel level and the suspension level, the sensors at the wheel level performed better than the sensors at the suspension level.

Another significant contribution of this work was to explore the effects of different variations, such as roadway roughness, temperature gradients, etc, on the classification accuracy of damage on a bridge structure. Using direct SHM approaches, environmental and operating conditions have been pointed out in the literature as causing more significant changes in the dynamic properties of a bridge structure than severe damage conditions (Farrar et al. 1998; Peeters and Roeck 2001; Cornwell et al. 1999; Sohn 2007; Meruane and Heylen 2011; Yan et al. 2005, Deraemaeker et al. 2008, Zhu and Rizzo 2011). This research explored the effect of atmospheric conditions on the classification of the indirect SHM approach. It was

shown that the effect of temperature gradients was significant for both direct damage classification and indirect damage classification. Both approaches showed similar results.

The effect of roadway roughness on the classification accuracy of the indirect approach was also explored in this work. The two bridges used in the laboratory were tested under two roughness conditions. The first was the case of accidental imperfections of a nominally smooth guide rail over which the vehicle travels, and the second was an intentionally created roughness profile on the guide rail for a particular bridge. Previous work found that better accuracy was achieved in determining the natural frequency of a bridge at lower speeds and smoother road profiles McGetrick et al. (2009). However, by means of the signal processing and classification methods employed in the indirect approach explored in this research, this work shows that an additional surface roughness is not detrimental and the classification accuracy can be improved by the vibrations induced by roadway roughness.

### ***5.3 Discussion and lessons learned***

This section provides a discussion based on the results obtained in Chapters 2-4 and some additional thoughts based on the experience and intuition gained through the course of this work. The objective of this section is to provide advice for researches further pursuing some of the ideas presented herein.

From the classification experiments performed on simulated data we learned:

- When exploring a complex physical system, it is better to start with the simplest model possible that captures the main physical phenomena. In this work, we first studied 1D simplified mathematical models and then more complex 3D models. Then, we performed physical experiments. We could have performed 3D mathematical experiments directly, but if the results had not been conclusive, it would then have been hard to rule out some possible sources of complexity that are detrimental to the results.

- The results from Chapter 2 show that for different vehicle variations within a 1 Hz frequency range, the classification results were about the same even though the parameters chosen for the simulated vehicle were very different considering very heavy vehicles and light ones.

From building the experimental setup and performing the classification experiments we learned:

- The experimental process is iterative and requires making fast modifications to the experimental setup as the results show new insight. The results shown in this work are only a fraction of the total number of experiments and results obtained by being able to modify the experimental setup. The fast testing and modifications were only possible by having full control of the setup.
- The need for large data sets required an automated motion control system for the vehicle and a synchronized data acquisition for the accelerometers on the setup. It is important to define the amount of data needed and automate the experimental runs, data acquisition and data pre-processing as much as possible.
- The experimental setup was designed with an encoder for recording the position of the vehicle. However, initial measurements showed the need to have redundant methods to accurately locate the vehicle with respect to the bridge. The initial and the final position were marked on the motion path of the experimental setup to produce a distinctive peak on the vertical acceleration signals. The peak of the signals allowed for accurate matching all the acceleration signals at the same starting point relative to the bridge position. Other practical methods can be explored, but special attention should be paid into accurately locating the vehicle with respect to the structure.
- Regarding the definition of experiments, the experiments described in Chapter 3 were implemented with the purpose of validating the expected increment on the classification accuracy with higher levels of damage. The results do not always show this to be true,

but one can identify that most cases of low classification accuracy are for those scenarios with the lowest level of the severity of damage.

- The results from Chapter 3 showed similar average classification accuracy for all speeds below 1.75 and a lower, but consistent, average classification accuracy for speeds above 2 m/s for Vehicle 1. When looking at the disaggregated results, one can see a greater variability at higher speeds. Other results in Chapter 4 with different vehicle-bridge combinations did not show such a step function and remained more consistent in average classification accuracy across speeds. However, there seem to be two effects balancing each other. On the one hand, at lower speeds, the vehicle signal is longer and one can get more distinct features from a longer signal. On the other, at high speeds greater energy is inserted into the system and the vehicle response carries a more significant bridge response.

By varying the experimental interaction parameters and performing experiments with roughness and different temperature conditions we learned:

- Classification results from the two bridges and the different vehicles were very consistent. Damage detection accuracies for the same type of classification experiments were similar and the vehicles showed similar behavior. However, the classification accuracies for Bridge 2 were higher than the ones achieved for Bridge 1. One possible explanation is that the fundamental frequencies for all of the vehicles were closer to the fundamental frequency of Bridge 2. Thus, future validation experiments should first look at similar vehicle-bridge frequencies and then look at other vehicle-bridge combinations.
- The introduction of roughness also modified the fundamental frequency of the bridges (by adding weight to the bridge), thus affecting the results. However, considering the same behavior on both bridges for different types of damage, one possible explanation for this increase being that the introduction of roughness increased the interaction

between the bridge and the vehicle allowing the vehicle to capture more information about the bridge and therefore achieving higher classification accuracy.

- The first classification experiments under different temperature gradient conditions suggest that some temperature gradient scenarios are better for damage detection than others. Considering the temperature gradient scenarios explored, there is no clear evidence as to which of the temperature gradient patterns are better suited for damage detection. Some cases of asymmetric temperature gradients yielded high classification accuracy and some did not. However, all symmetric temperature gradient scenarios yielded average accuracies for damage detection above 90%. For future field experiments, it would be well to document the surface temperature gradient and first look at scenarios with symmetric temperature gradients before considering complex temperature gradient patterns.
- Considering the two classification experiments performed on scenarios with different temperature gradients, the decrease of the average classification accuracy for the three damage scenarios shows evidence of how the different temperature gradients can mask the damage scenarios. Future experiments should first look at damage detection for data collected under similar ambient conditions. After those experiments, additional experiments can be conducted that include data from different temperature gradients, or in a more general case, different ambient conditions.

## **5.4 Future work**

This dissertation presents an initial exploration of the indirect approach. The author wishes to acknowledge that there is much work to be done before this approach is validated and ready to be transferred as a fully operational technology. The following paragraphs describe possible future work in terms of the experimental setup, signal processing and classification and interaction variables to be studied.



Regarding the dynamic vehicle-bridge interaction variations, future work first should consider that the present experimental setup had a high range of vehicle/bridge mass ratio. Future studies could further expand the range with lighter vehicles and study the influence of the vehicle mass/bridge mass ratio on the expected classification accuracy. Second, although the results obtained show that some level of roughness might be beneficial, the way roughness was built slightly modified the fundamental frequency of the bridge and therefore the improvement on the classification accuracy could be attributed to a different vehicle-bridge frequency relationship. Future work could further expand on the expected classification accuracy for different levels of roughness. Third, in the present work a specific bridge configuration was explored. Future work could expand the validation of the approach to different bridge configurations such as arch bridges, or trust bridges. Moreover, it would be interesting to explore the extrapolation of the indirect SHM of a particular bridge, to a family of similar bridges with similar characteristics and therefore reduce the amount of data needed to establish a baseline.

Regarding the influence of ambient conditions and realistic scenarios, further study should be done first on the influence of temperature gradients on the bridge dynamic properties and the effects of these temperature gradients on the classification accuracy. The study presented in this dissertation only explored the influence of some temperature gradient scenarios on the detection accuracy. It would be interesting to explore the evolution of interaction parameters under different temperature gradients in terms of location, variation and temperature range. Second, the current study only considered a single vehicle; future work could study the Influence of several vehicle combinations and also the effects of realistic on-going traffic on the detection capability of a particular instrumented vehicle.

Regarding the signal processing and machine learning algorithms, preliminary results, not presented in this document, showed significant improvement in the classification accuracy by using sparse representation feature extraction (Wright et al. 2010). It would be very valuable

to explore the use of other features for signal processing and re-run some of the classification experiments presented. Second, the present study was performed with significant amounts of data for characterizing the different scenarios, but future studies could look at the minimum number of data samples needed in the data set for characterizing a particular scenario. Third, a future study could also compare the use of different classification algorithms with the same minimal data sets.

Regarding implementation challenges for the indirect bridge SHM, future work could study the minimum vehicle instrumentation needed for data acquisition and data transmission (In collaboration with robotics). Also, explore the use of readily available equipment on newer vehicle models, such as pressure sensors on tires or accelerometers for active suspension control. Third, future work could explore the prediction of the detection capability of different vehicles for a specific bridge. Another research project could build a real-time demonstration for the laboratory scale bridge by integrating the data acquisition and processing into a common environment as a preparation for full-scale deployment.

The ultimate goal of the indirect approach will be to extract damage sensitive features and develop comprehensive models that relate the condition and reliability of a particular bridge structure (or set of structures) with the evolution of those features. Monitoring those damage features would allow having an accurate diagnostic of the structure and making a prognosis about the expected life of the structure without intervention. Based on degradation models one could plan different intervention strategies to optimize budget allocation at a bridge and at a network level.

## References

- Alippi, C., and Galperti, C. 2008: "An Adaptive System for Optimal Solar Energy Harvesting in Wireless Sensor Network Nodes." *Circuits and Systems I: Regular Papers, IEEE Transactions On* 55, no. 6: 1742–1750.
- Akinci, B., Hendrickson, C., and Karaesmen, I. 2003. "Exploiting Motor Vehicle Information and Communications Technology for Transportation Engineering." *Journal of Transportation Engineering* 129, no. 5: 469–474.
- Beeby, S. P., Tudor, M. J. and White, N. M. 2006 "Energy Harvesting Vibration Sources for Microsystems Applications." *Measurement Science and Technology* 17, no. 12: R175–R195.
- Bilello, C., and Bergman L. A. 2004. Vibration of damaged beams under a moving mass: theory and experimental validation. *Journal of Sound Vibration* 274 (Jul 1): 567-582.
- Brownjohn, J.M.W. 2007. Structural health monitoring of civil infrastructure. *Philosophical Transactions of the Royal Society A: Mathematical, Physical and Engineering Sciences* 365, no. 1851 (February 15): 589-622.
- Bu, J. Q., Law, S. S. and Zhu, X. Q. 2006. "Innovative Bridge Condition Assessment from Dynamic Response of a Passing Vehicle." *Journal of Engineering Mechanics* 132 (12) (December): 1372–1379.
- Carden, E. P., and Fanning, P. 2004. "Vibration Based Condition Monitoring: A Review." *Structural Health Monitoring* 3 (4) (December 1): 355–377.
- Casciati, F., and Giordano, M. 2010. *Structural Health Monitoring 2010: Proceedings of the Fifth European Workshop on Structural Health Monitoring Held at Sorrento, Naples, Italy, June 28-july 4, 2010.*
- Cerda, F., Garrett, J., Bielak, J., Bhagavatula, R., and Kovačević. J. 2010. "Exploring Indirect Vehicle-bridge Interaction for Bridge SHM." *Bridge Maintenance, Safety, Management*

- and Life-Cycle Optimization - Proceedings of the 5th International Conference on Bridge Maintenance, Safety and Management: 708–715.*
- Cerda, F., Chen, S, Bielak, J, Garrett, J, Rizzo, P, Kovačević, J. 2012 “*Indirect structural health monitoring of a simplified laboratory-scale bridge model*”. Submitted to Smart Structures and Systems (Special Issue).
- Chebira, A., and Kovačević, J. 2008. “Frames in Bioimaging.” *Proc. CISS, Princeton, NJ, Mar. 2008*.
- Chebira, A., Barbotin, Y., Jackson, C., Merryman, T., Srinivasa, G., Murphy, R., and Kovačević, J. 2007. “A Multiresolution Approach to Automated Classification of Protein Subcellular Location Images.” *BMC Bioinformatics* 8 (1): 210.
- Cornwell, P., Farrar, C. R. Doebling, S. W. and Sohn, H. 1999. “Environmental Variability of Modal Properties.” *Experimental Techniques* 23 (6): 45–48.
- Daubechies, I. 1992. *Ten Lectures on Wavelets*. Society for Industrial and Applied Mathematics. <http://portal.acm.org/citation.cfm?id=130655>.
- Deraemaeker, A., Reynders, E., De Roeck, G., and Kullaa, J. 2008. “Vibration-based Structural Health Monitoring Using Output-only Measurements Under Changing Environment.” *Mechanical Systems and Signal Processing* 22, no. 1: 34–56.
- Doebling, S. W., Farrar, C. R., and Prime, M. B. 1998. “A Summary Review of Vibration-based Damage Identification Methods.” *Identification Methods,” The Shock and Vibration Digest* 30: 91–105.
- Duda, R., Hart, P., and Stork, D. 2000. *Pattern Classification (2nd Edition)*. Wiley-Interscience.
- FHWA 2001. Reliability of Visual Inspection for Highway Bridges - FHWA-RD-01-020 <http://www.fhwa.dot.gov/publications/research/nde/01020.cfm>
- Farhey, D. 2005. “Bridge Instrumentation and Monitoring for Structural Diagnostics.” *Structural Health Monitoring* 4 (4) (December 1): 301–318.

----2007. "Quantitative Assessment and Forecast for Structurally Deficient Bridge Diagnostics."

*Structural Health Monitoring* 6 (1) (March 1): 39–48.

Farrar, C. R., and Jauregui, D.. 1998. "Comparative Study of Damage Identification Algorithms Applied to a Bridge: I. Experiment." *Smart Materials and Structures* 7 (5) (October 1): 704–719.

Farrar, C. R., and Worden, K. 2007. "An Introduction to Structural Health Monitoring."

*Philosophical Transactions of the Royal Society A: Mathematical, Physical and Engineering Sciences* 365 (1851) (February 15): 303–315.

Frangopol, D. M., Strauss, A., and Kim, S. 2008. "Bridge Reliability Assessment Based on Monitoring." *Journal of Bridge Engineering* 13 (3) (May): 258–270.

Frangopol, D.M., Sause, R., and Kusko, C. eds. 2010. *Bridge Maintenance, Safety and Management - IABMAS'10: Proceedings of the Fifth International IABMAS Conference, Philadelphia, USA, 11-15 July 2010*. 1st ed. CRC Press.

Friswell, M. I. 2007. Damage identification using inverse methods. *Philosophical Transactions of the Royal Society A: Mathematical, Physical and Engineering Sciences* 365, no. 1851 (February 15): 393-410.

Fugate, M. L., Sohn H., & Farrar C. R. 2000. Unsupervised learning methods for vibration-based damage detection. Presented at IMAC, San Antonio, Texas. February 7-10.

Haralick, R.M, Shanmugan, K., and Dinstein, I. (1973). "Textural Features for Image Classification." *IEEE Trans. on Systems, Man, and Cybernetics* 3 (6): 610–621.

Ikenaga, S., Lewis, F.L., Campos, J., and Davis, L. 2000. "Active Suspension Control of Ground Vehicle Based on a Full-vehicle Model." *Proceedings American Control Conference, 2000. Proceedings of the 2000*. Vol 6:4019–4024 vol.6.

- Isemoto, R., Kim, C.W., and Sugiura, K. 2010. "Abnormal Diagnosis of Bridges Using Traffic-induced Vibration Measurements." *The Twenty-Third KKCNN Symposium on Civil Engineering*, Taipei, Taiwan: 189-192.
- Kellogg, R.A., Chebira, A., Goyal, A., Cuadra, P.A., Zappe, S.F., Minden, J.S., and Kovačević, J. 2007. "Towards an Image Analysis Toolbox for High-throughput Drosophila Embryo RNAi Screens." *Proc. IEEE Intl. Symp. Biomed. Imaging, Arlington, VA*,: 288-291.
- Kim, C.W., and Kawatani, M. 2008. "Pseudo-static Approach for Damage Identification of Bridges Based on Coupling Vibration with a Moving Vehicle." *Structure and Infrastructure Engineering* 4 (5): 371–379.
- Kim, C.W., Kawatani, M., and Fujimoto, T. 2010. "Identifying Bending Stiffness Change of a Beam Under a Moving Vehicle." *Bridge Maintenance, Safety, Management and Life-Cycle Optimization - Proceedings of the 5th International Conference on Bridge Maintenance, Safety and Management*, 180–180.
- Kullback, S., and Leibler, R.A. 1951. "On Information and Sufficiency." *Ann. Math. Statist* 22: 79–86.
- Law, S. S., and Zhu X. Q. 2004. Dynamic behavior of damaged concrete bridge structures under moving vehicular loads. *Engineering Structures* 26, no. 9 (July): 1279-1293.
- Law, S. S., and Zhu. X. Q. 2005. Nonlinear characteristics of damaged concrete structures under vehicular load. *Journal of Structural Engineering-ASCE* 131, no. 8 (August): 1277-1285.
- Li, H., Wekezer, J. and Kwasniewski, L. 2008. "Dynamic Response of a Highway Bridge Subjected to Moving Vehicles." *Journal of Bridge Engineering* 13 (5): 439–448.
- Lin, C.W., and Yang, Y.B. 2005. "Use of a Passing Vehicle to Scan the Fundamental Bridge Frequencies: An Experimental Verification." *Engineering Structures* 27 (13) (November): 1865–1878.

- Lynch, J. P. 2007. An overview of wireless structural health monitoring for civil structures. *Philosophical Transactions of the Royal Society A: Mathematical, Physical and Engineering Sciences* 365, no. 1851 (February 15): 345-372.
- Mahmoud, M. A., and Abou Zaid, M. A.. 2002. Dynamic response of a beam with a crack subject to a moving mass. *Journal of Sound and Vibration* 256, no. 4 (September 26): 591-603.
- Mal, A., Ricci, F., Banerjee, S., and Shih, F. 2005. "A Conceptual Structural Health Monitoring System Based on Vibration and Wave Propagation." *Structural Health Monitoring* 4, no. 3: 283–293.
- Mallat, S. 1999. *A Wavelet Tour of Signal Processing*. 2nd ed. Academic Press.
- McGetrick, P.J., González, A., and O'Brien, E.J. 2009. "Theoretical Investigation of the Use of a Moving Vehicle to Identify Bridge Dynamic Parameters." *Insight: Non-Destructive Testing and Condition Monitoring* 51 (8): 433–438.
- McGetrick, P.J., Kim, C.W., and O'Brien, E.J. 2010. "Experimental Investigation of the Detection of Bridge Dynamic Parameters Using a Moving Vehicle." *The Twenty-Third KKCNN Symposium on Civil Engineering*, Taipei, Taiwan:177-180.
- Melhem, H., and Kim, H. 2003. "Damage Detection in Concrete by Fourier and Wavelet Analyses." *Journal of Engineering Mechanics* 129 (5) (May): 571–577.
- Meruane, V., and Heylen, W. 2012. "Structural damage assessment under varying temperature conditions." *Structural Health Monitoring-an International Journal* 11 (3) (May): 345–357.
- Peeters, B., and De Roeck, G. 2000 . "One Year Monitoring of the Z24-bridge : Environmental Influences Versus Damage Events." In *SPIE Proceedings Series*, 1570–1576. Society of Photo-Optical Instrumentation Engineers.

- Miyamoto, A., and Yabe, A. 2011. "Bridge Condition Assessment Based on Vibration Responses of Passenger Vehicle." *Journal of Physics: Conference Series* 305 (July 19): 012103.
- Reda Taha, M. M., Nouredin, A., Lucero, J. L. and Baca, T. J. 2006. "Wavelet Transform for Structural Health Monitoring: A Compendium of Uses and Features." *Structural Health Monitoring* 5 (3) (September 1): 267–295.
- Rytter, A. (1993). "Vibration Based Inspection of Civil Engineering Structures". Denmark: Department of Building Technology and Structural engineering, Aalborg University.
- Serker Kamrujjaman, N. H. M., Wu, Z. and Li, S. 2010. "A Nonphysics-based Approach for Vibration-based Structural Health Monitoring Under Changing Environmental Conditions." *Structural Health Monitoring* 9 (2) (March 1): 145–158.
- Siringoringo, D.M., and Fujino, Y. 2012. "Estimating Bridge Fundamental Frequency from Vibration Response of Instrumented Passing Vehicle: Analytical and Experimental Study." *Advances in Structural Engineering* 15 (3): 417–433.
- Sohn, H. 2007. "Effects of Environmental and Operational Variability on Structural Health Monitoring." *Philosophical Transactions of the Royal Society A: Mathematical, Physical and Engineering Sciences* 365 (1851) (February 15): 539–560.
- Toshinami, T., Kawatani, M. and Kim, C.W. 2010. "Feasibility Investigation for Identifying Bridge's Fundamental Frequencies from Vehicle Vibrations." In *Bridge Maintenance, Safety, Management and Life-Cycle Optimization - Proceedings of the 5th International Conference on Bridge Maintenance, Safety and Management*, 329–334.
- Van der Auweraer, H., and Peeters B. 2003. International Research Projects on Structural Health Monitoring: An Overview. *Structural Health Monitoring* 2, no. 4 (December 1): 341–358.



- Vetterli, M and Kovačević, J. 1995. *Wavelets and Subband Coding*. Signal Processing. Prentice Hall PTR. <http://waveletsandsubbandcoding.org>.
- Worden, K., & Dulieu-Barton J. M. 2004. An Overview of Intelligent Fault Detection in Systems and Structures. *Structural Health Monitoring* 3, no. 1 (March 1): 85-98.
- Worden, K., & Manson G. 2007. The application of machine learning to structural health monitoring. *Philosophical Transactions of the Royal Society A: Mathematical, Physical and Engineering Sciences* 365, no. 1851 (Feb. 15): 515-537.
- Wright, J., Yi Ma, Mairal, J., Sapiro, G., Huang, T.S., and Shuicheng Yan. "Sparse Representation for Computer Vision and Pattern Recognition." *Proceedings of the IEEE* 98, no. 6 (June 2010): 1031 –1044.
- Yan, A.-M., G. Kerschen, P. de Boe, and J.-C. Golinval. 2005a "Structural Damage Diagnosis Under Varying Environmental conditions---Part I: A Linear Analysis." *Mechanical Systems and Signal Processing* 19: 847–864.
- 2005b. "Structural Damage Diagnosis Under Varying Environmental Conditions---part II: Local PCA for Non-linear Cases." *Mechanical Systems and Signal Processing* 19: 865–880.
- Yabe, A and Miyamoto, A. 2010. "Development of a bridge condition assessment system by using city bus." *Bridge Maintenance, Safety, Management and Life-Cycle Optimization - Proceedings of the 5th International Conference on Bridge Maintenance, Safety and Management*. 2056–2063.
- Yang, Y.B., and Chang, K.C. 2009. "Extraction of Bridge Frequencies from the Dynamic Response of a Passing Vehicle Enhanced by the EMD Technique." *Journal of Sound and Vibration* 322 (4-5): 718–739.
- Yang, Y. B., Lin, C.W., and Yau, J. D. 2004. "Extracting Bridge Frequencies from the Dynamic Response of a Passing Vehicle." *Journal of Sound and Vibration* 272 (3-5) (May 6): 471–493.

- Yang, Y.B., and Lin, C.W. 2005. "Vehicle-bridge Interaction Dynamics and Potential Applications." *Journal of Sound and Vibration* 284 (1-2) (June 7): 205–226.
- Yin, S.H., and Tang, C.Y. 2011. "Identifying Cable Tension Loss and Deck Damage in a Cable-Stayed Bridge Using a Moving Vehicle." *Journal of Vibration and Acoustics* 133 (2): 021007.
- Zhu, X.Q., and Law, S.S. (2006). "Wavelet-based Crack Identification of Bridge Beam from Operational Deflection Time History." *International Journal of Solids and Structures* 43 (7-8) (April): 2299–2317.
- Zhu, X., and Rizzo, P. (2011). "Guided Waves for the Health Monitoring of Sign Support Structures Under Varying Environmental Conditions," *Structural Control and Health Monitoring*, Available online: 21 AUG 2011 .